Max-Planck-Institut für Metallforschung
Stuttgart

Characterization of the Electronic Conduction Parameter of Cation Conducting Solid Electrolytes

Krenar Shqau

Dissertation
an der
Universität Stuttgart

Bericht Nr. 141
November 2003

Characterization of the electronic conduction parameter of cation conducting solid electrolytes

Dissertation

Von der Fakultät Chemie der Universität Stuttgart

zur Erlangung der Würde eines

Doktors der Naturwissenschaften (Dr. rer. nat.)

vorgelegt von

Krenar SHQAU

Tirana, Albanien

Hauptberichter: **Prof. Dr. rer. nat. F. Aldinger**

Mitberichter: **Prof. Dr. rer. nat. Dr. hc. mult. G. Petzow**

Tag der mündlichen Prüfung: 10. November 2003

Institut für Nichtmetallische Anorganische Materialien der Universität Stuttgart

Max-Planck-Institut für Metallforschung, Stuttgart

Pulvermetallurgisches Laboratorium

2003

"Many of life's failures are those people who did not realize how close they were to success when they gave up!"

Monit

Acknowledgements

This work was done from November 1999 to July 2003 in Max-Planck Institute for Metal Research, Stuttgart, supported by a Max-Planck-Society Scholarship.

I wish to express my deep gratitude to my advisor Prof. Fritz Aldinger for giving me the opportunity to realize this thesis in his laboratory. He encouraged and supported me with much kindness throughout this work. In particular, I wish to thank him for the opportunity to present my results at international conferences all over the world.

I wish to express my sincere appreciation to Dr. Näfe for the initiation and subject of this work, the excellent scientific support, lively discussions and assistance during the whole period.

Prof. G. Petzow is gratefully acknowledged for being co-examiner of the thesis. I also want to thank Prof. E. J. Mittemeijer for giving consent to examine my thesis.

Special thanks to Mrs. Gisela Feldhofer, the good soul of the Functional Ceramics Working Group, for her technical support of the experimental work and also for her encouragement during the difficult times.

Furthermore, I am deep in debt to many present and former colleagues in Powder Metallurgical Laboratory, in particular; to Dr. S. Raghavan who introduced me into the mysteries of solid state electrochemistry and the electrode processes; the permanent staff, Mrs. S. Paulsen and Mrs. J. W. Bock for administrative work; Mr. Kozmon, Mr. Zeindelmeier, Mr. Eckstein, Mr, Bruckner, Miss. Martina, Mr. Hammoud for technical assistant; to Mr. Labitzke and Mr. Kaiser for all their advice with regard to SEM and chemical analyzes; and to all the members of the soccer dream team: who made my working and living easier and full of fun.

I would like to thank my friends from Functional Ceramics Working Group: Bogdan, Vladimir, Amin, Ezzat, Gautam, Steffi and also Matovic, Biswas, Ravi, Carsten, Dirk, Manga, Nana, Datta, Lee, Jung, Ahn, Sandra, Stefanie, Aleksander, Marija, Zaklina, Dragan, Jia, Andre who not only helped me from being engulfed by frustration at times but also made my days at PML memorable.

I would like to thank also Dr. G. M. Kale from Leeds University for explaining some dark secrets of material science.

I would like to remember the affection of my mother who always helped me remaining behind the curtain. Without her encouragement, I would not have become what I am today.

Contents

List of figures

List of Tables

Abstract

The thesis aims at the characterization of the p-electronic conduction parameter of cation conducting solid electrolytes. For this purpose potentiometric as well as thermoelectric measurements were carried out. The investigations have been done on commercially available potassium and sodium beta alumina as well as on laboratory-prepared samples of NASICON.

The information about the p-electronic conduction parameter of K-beta-Al_2O_3 was obtained by evaluating the voltage of various galvanic cells using two different reference electrodes under variable measuring conditions, i.e. temperature (593 to 893 K) and potassium chemical potential of the electrodes. Under isothermal condition, a non-linear chemical potential dependence of the voltage response of galvanic cell is obtained. From the results obtained it is evident that the p-electronic conduction parameter of the solid electrolyte is not a constant but adapts to the potassium chemical potential in the surroundings which confirms previous findings on sodium beta alumina.

Using the same technique the electronic conduction parameter of NASICON was characterized as a function of the sodium chemical potential at the measuring electrode as well as of the temperature.

To prove the consistency of electronic conduction properties obtained from potentiometric methods on sodium beta alumina, another independent technique without employing a secondary electrode i.e. thermoelectric power measurement, was performed. The p-electronic conduction parameters obtained from thermoelectric power and potentiometric methods are in excellent agreement with each other.

In addition, the impact of the electronic conduction on the behaviour of potentiometric cells was evident by evaluating thermodynamic data on the system pyrochlore-$NaSbO_3$. As a consequence, the thermodynamic stability obtained from these measurements proves to be much higher compared to that reported in the literature, thereby again confirming the non-conventional properties of the electronic conductivity of beta alumina.

1. Introduction

The ionic conductivity of the solid electrolyte Na-beta-Al_2O_3 (NBA) has been studied since a long time, whereas its electronic conductivity was not mentioned in the literature until it become relevant to the development of the thermoelectric converters [1] and in connection with investigations on sodium sulfur batteries, when De Jonghe [2, 3] and Virkar [4] supposed a possible impact of n-type electronic conductivity.
In the meantime NBA was intensively been studied (see Table 1-1) but nothing is known about the electronic conduction properties of other cation conductors like K-beta-Al_2O_3 or NASICON.

Table 1-1. Previous measurements on partial electronic conductivities of Na-beta-Al_2O_3

Author	**Method**	**Cell construction**
Weber [1]	AMTEC	(–) Na | NBA | Na (+)
Sun [5]	HW	(–) Na | NBA | C (+)
Takikawa [6]	HW	(–) Na | NBA | Ni (+)
Fritz [7]	Hebb-Wagner polarization	(–) Na | NBA | Mo (+)
Steinbrück [8]	Permeation	(–) Na | NBA | Na (+)
Näfe [9]	Potentiometric measurement	CO_2,O_2,Na_2CO_3|NBA|Na
Näfe [10]	Hebb-Wagner polarization	(–) Na | NBA | Mo (+)
Näfe [11]	Hebb-Wagner polarization	(–) Na | NBA | Mo (+)
Näfe [12]	Evaluation of data	CO_2,O_2,Na_2CO_2|NBA|$Na_2Ti_2O_6$,TiO_2,O_2
Näfe [13]	Potentiometric measurement	CO_2,O_2,Na_2CO_2|NBA|NiO/$FeO_{(glass)}$ |FeNi(48)

It was shown [14] that the electronic conductivity may have a substantial influence on NBA used as a solid electrolyte in potentiometric gas sensors. The situation is, however, more complex. On the one hand, there are examples showing that such galvanic cells work quite well [15-19], and on the other hand, it follows from the data on the p-electronic conduction parameter of sodium beta alumina [10-14] that the performance of such cells will be interfered by a non-negligible electronic transference number.

As a possible interpretation for this apparent contradiction as suspected [9], [14] and later proved [13] that the p-electronic conduction parameter of NBA is a function of the chemical potential of the neutral species in the surroundings.

In view of this the question to be clarified is, to what extent the findings on NBA are valid for other cation conductors and could be confirmed by other experimental approaches.

If the above conclusion was generally valid independent of the conductor under consideration a revision of the conventional defect-chemical views would be necessary.

The aim of the present work is the characterization of the p-electronic conduction parameter ($a_{\oplus}$) of K-beta-Al_2O_3, NBA and NASICON in particular and to establish further proofs for the role of the electronic conduction in electrochemical applications of these solid electrolytes.

The parameter $a_{\oplus}$ has to be evaluated using various techniques like potentiometry, thermoelectric power and thermodynamic measurements. These techniques have to be employed to eliminate or minimize the drawback of one technique so as to have a precise knowledge about the p-electronic conduction parameter.

The measurements are performed not only as a function of temperature but especially as a function of the activity of the mobile species, giving better insight into the particular properties of the p-electronic parameter.

2. Theoretical background

2.1 Structure of solid electrolyte

The crystal structure of the Na- and K-beta-Al_2O_3 and NASICON provides an essential rigid framework with channels along which one of the ionic species of the solid can migrate. Ion transport involves hopping from site to site along these channels. Hence, for better understanding of the properties of material the structure of solid electrolytes under investigation is discussed.

2.1.1 Structure of NASICON

NASICON, the acronym for Na superionic conductor, is a non-stoichiometric framework of zirconophosphosilicate [20]. It is primarily a solid solution between $NaZr_2(PO_4)_3$ and $Na_4Zr_2(SiO_4)_3$, in which the phosphor may be partially replaced by silicon, resulting in a solid solution $Na_{1+x}Zr_2P_{3-x}Si_xO_{12}$ in the range of 0< x < 3.

All structures are rhombohedral $R\bar{3}c$, except in the range 1.8 <x< 2.2 where distortion to the monoclinic C2/c space group is found at room temperature [20]. In the $(Zr_2P_{3-x}Si_xO_{12})^{(1+x)-}$ skeleton, each Zr^{4+} octahedron shares its six corners with tetrahedral, and each tetrahedron shares its four corners with octahedral sites (Fig. 2-1).

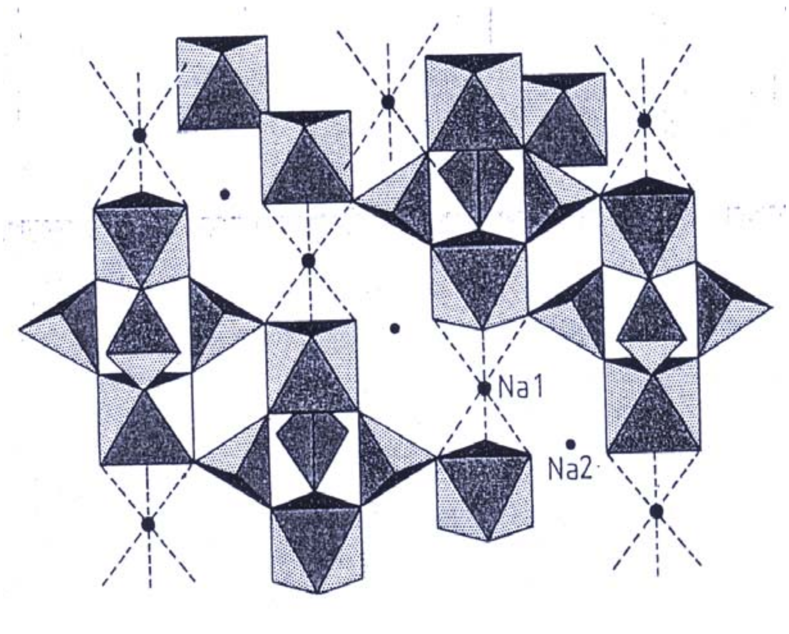

Fig. 2-1 View of rhombahedral $R\bar{3}c$ structure of NASICON showing the $(ZrP_3O_{12})^-$ units parallel to c_r and Na^+ ions in Na1 positions octahedrally coordinated by O^{2-} ions. The Na1 positions are also octahedrally coordinated by empty Na2 positions in the same basal planes as the nearest-neighbour O^{2-} ions.

Thus each anion bonds strongly to a tetrahedral and an octahedral cation of the skeleton. In the rhombohedral phase, two Na^+-ion sites are distinguishable in the interstitial space: close-packed-hexagonal Na2 layers in the basal plane connected by one-third as many Na1 sites between the Na2 layers.

In the compound $NaZr_2P_3O_{12}$, Na1 sites are filled and the Na2 sites are empty. Substitution of Si for P is charge compensated by the introduction of Na^+ ions on Na2 sites, which are linked to one another via Na1 sites. Therefore, so long as the Na1 sites remain occupied, Na^+ ion conductivity requires a correlated ionic motion:

$Na^+_2 + Na^+_1 + \square_2 \rightarrow \square_2 + Na^+_1 + Na^+_2$

where the subscripts refer to sites Na1 and Na2 and $\square$ represent an empty site.

The specific resistivity due to Na^+ ion mobility passes through a minimum at intermediate x~2 (Fig 2-2) [21]. This fact occurs if the rhombohedral axis c_r and cell volume are maximum [21] suggests that Na^+-Na^+ electrostatic interactions reduce the Na1-site preference energy with increasing x.

For x > 2, both Na1 and Na2 vacancies must coexist. The fact that crystal cell volume reaches a maximum with increasing x suggests that the electrostatic forces between Na ions at adjacent Na1 and Na2 sites may displace Na ions towards bottleneck position between Na1 and Na2 sites which will correspond to a high resistivity.

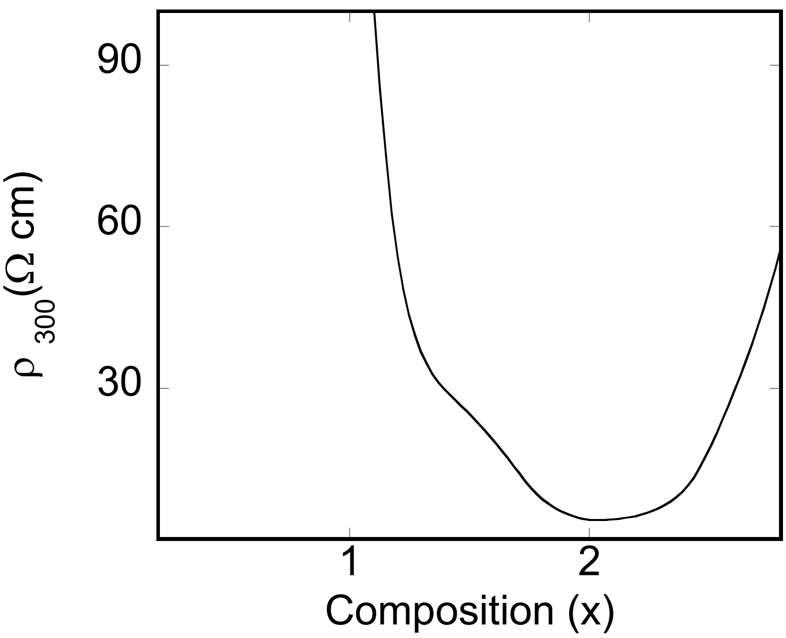

Fig. 2-2 Composition dependence of specific resistivity of dense ceramic NASICON with graphite electrodes at higher frequencies [21]

2.1.2 Structure of beta alumina

Most of the information concerning the structure of alkali beta-Al_2O_3 has been obtained from x-ray diffraction, although in recent years several other experimental techniques have been applied to determine details of the structure and the properties resulting from it, e.g. conduction properties. The basic crystal structure was revealed by Beevers and Ross [22] in 1937. The structure of Na- or K-beta-Al_2O_3 is shown in Fig. 2-3. The block of Al^{3+} and O^{2-} are packed in the same fashion as in a spinel, $MgAl_2O_4$. They are usually called "spinel block". Al^{3+} ions occupy the octahedral sites; the tetrahedral sites are occupied by Mg^{2+} ions. The spinel-type blocks are separated from each other by a loosely packed plane containing Na^+ (or K^+) and O^{2-}.

Because of the loose packing, space is avaible for movement of the alkali ions leading to a high ionic conductivity. However, the conductivity is limited to this plane only and movement along the c axis is exceedingly difficult. The material, therefore, is highly anisotropic.

The conduction plane of β-Al_2O_3 is a mirror plane, with face centred cubic packing arrangement of oxide ions in the ambience shown in Fig. 2-4. This packing arrangement is

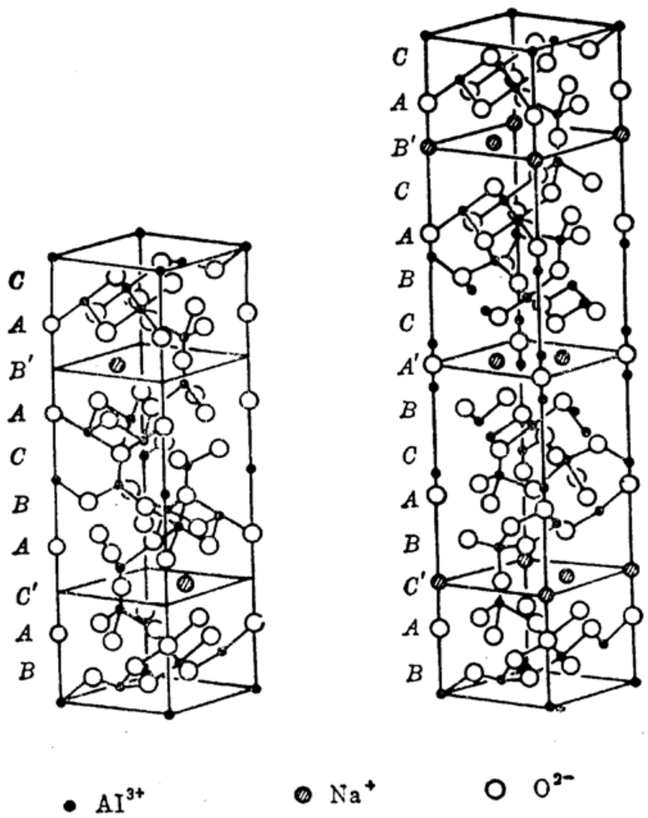

Fig. 2-3 Structure of Na-β-Al_2O_3 (left) and Na-β"-Al_2O_3 (right)

slightly different in β"-Al_2O_3 since the conduction plane is not a mirror plane. As can be seen in Fig. 2-3, it takes three spinel-type blocks before the stacking arrangement is repeated, and for this reason, β"-Al_2O_3 is called "3-block" material while the β-Al_2O_3 is called "2-block".

Although spinel is cubic, the additional conduction planes lead to a hexagonal crystal structure for β-alumina and a rhombohedral structure for β"-alumina. The lattice constants are a = 0.559 nm, c = 2.253 nm and a = 0.559 nm, c = 3.423 nm for β- and β"-Al_2O_3, respectively. Other modifications of the spinel block stacking arrangement have been reported [23] and given the names β''' and β''''-Al_2O_3.

These modifications contain six oxide ion layers in each spinel-type block and therefore the c axis is larger than in β-Al_2O_3. The most probable position of Na in the Na-β-Al_2O_3 determined by Beevers and Ross [22] is shown in Fig. 2-5 and is called BR ("Beevers Ross") position.

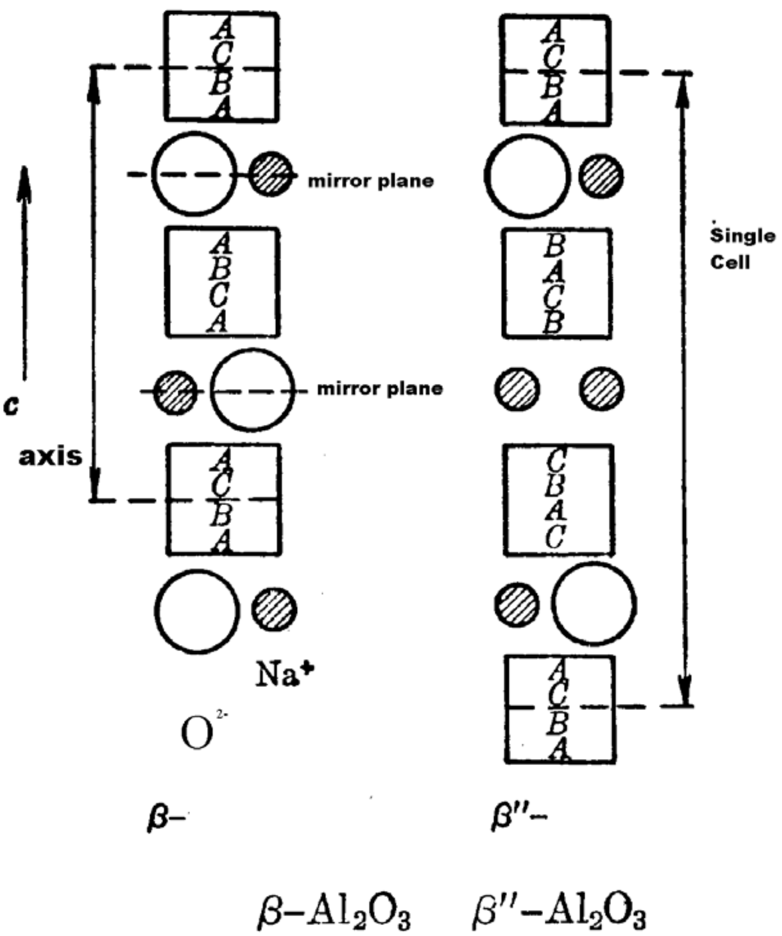

Figure 2-4 Oxide ion packing arrangement in β-Al_2O_3 (left) and β"-Al_2O_3 (right) (letters refer to stacking arrangement where ABC represent face-centered cubic packing while ABAB represents hexagonal packing)

All these sites would ordinarily be filled in the stoichiometric $NaAl_{11}O_{17}$ material. However, Felsche [24] found using three-dimensional refinement method that the sodium sites are only partially occupied. Peters et al. [25] studied typical crystals containing 29% excess sodium and concluded that the sodium was smeared out from the conduction plane. They postulated that the excess sodium is charge compensated by aluminium vacancies so that the formula could be written more accurately as $Na_{1+x}Al_{11-x/3}O_{17}$ where x is usually 0.15-0.30. Two possible positions for the excess sodium are shown in Figure 2-5. The sites labelled aBR refer to "anti Beevers-Ross" positions since Beevers and Ross rejected this type of site. The other positions lie between the oxide ions and are labelled mO for "mid-oxygen".

Peters et al. [25] measured the electron density due to Na^+ and found that the BR sites were only 75 % occupied. No electron density due to Na^+ was found at aBR sites and remaining Na^+ electron density was found in a diffuse fashion around the mO sites.

A similar single crystal x-ray diffraction study of K^+-β-Al_2O_3 and cobalt doped K^+-β-Al_2O_3 was carried out by Derier and Remeika [26]. They showed that potassium behaved in a similar fashion to sodium in occupying BR and mO sites with no occupation of aBR sites.

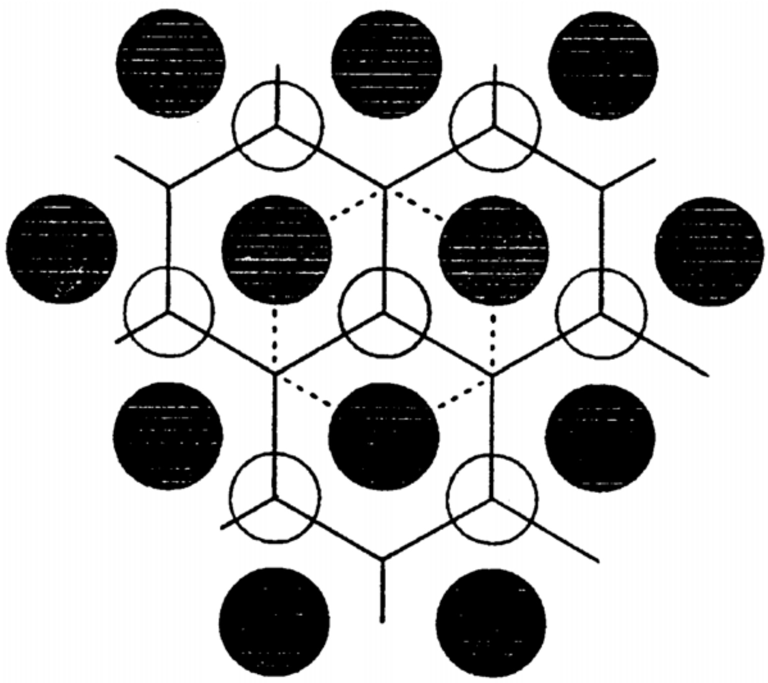

Fig. 2-5 Ideal structure of the conducting plane of beta alumina. Solid circles are column oxygen ions; open circles are mobile cations on BR sites; unoccupied hexagon vertices are aBR sites; and sites between neighbouring BR and aBR are mO sites. A mobile cation in ideal structure is in a deep potential well indicated by dotted lines.

They also found that the cobalt resided exclusively in a tetrahedral site normally occupied by aluminium. For the K^+-β-Al_2O_3 this tetrahedral site was probably occupied and may be reflecting an aluminium ion deficiency to account for charge compensation. The different sites occupied by Na^+ and K^+ in β-Al_2O_3 compared to Ag^+ and Tl^+ are shown in Table 2-1.

Table 2-1 Occupation of various sites by mobile ions in β-Al_2O_3

Compound	**Relative percentage occupation in site**			**Ref.**
	BR	aBR	mO	
Na-β-Al_2O_3	59	0	41	[25, 27]
K-β-Al_2O_3	54	0	46	[26]
Ag-β-Al_2O_3	66	34	0	[28]
	53	34	13	[27]
Tl-β-Al_2O_3	70	30	0	[27]

2.2 Defect Chemistry

In 1956 Kröger and Vink [29, 30] proposed the commonly used nomenclature for the description of defects. The point defects are considered as dilute species and the solid as the solvent. Several analogies can be found between intrinsic defect formation and self-dissociation of water:

1. A pair of charge defects is formed, which are responsible for electrical conduction;
2. A mass action law constant using defect activities (or concentration for dilute species) describes the defect equilibrium; and
3. Defect concentrations are normally thermally activated.

In the Kröger-Vink notation, the subscript shows the site of a defect. For instance, the subscript *i* represents an interstitial site. The effective defect charge is written as a superscript, relative to the ideal lattice: a dot ($^\bullet$) represents a positive and a prime (') a negative charge. In K-beta-Al_2O_3 for example, $K^\bullet_i$ represents an interstitial potassium ion and V'_K a single negatively charged potassium vacancy. Bulk defect chemical reactions must obey mass balance, charge balance (global electrical neutrality), and lattice-site balance.

There are essentially three ways of establishment of equilibrium of defects in ionic crystals.

(i) Intrinsic defect; i.e. the defect present in the bulk of a crystal is in thermodynamic equilibrium. This includes the Frenkel and Schottky defects.

(ii) Defect doping; i.e. the intentional manipulation of defect types and concentration by incorporation of specific impurities into the bulk of the crystal.

(iii) Defect reactions at interface, e.g. the incorporation of the neutral species from the "outside" into the crystal via defect or the opposite, the loss of crystal atoms to the ambience generating defects in crystal.

In cation conductors, like beta-Al_2O_3 and NASICON lattice disorder occurs predominantly in the cation sublattice. The intrinsic lattice defects are Frenkel pairs [14, 31], i.e. metal interstitials and metal vacancies, $M^{\bullet}_i$ and V_M, respectively, while the anions are immobile.
In the following, the discussion will be focused on K-beta-Al_2O_3 as solid electrolyte but also valid for other mono-valent cation conductors. The charged potassium defects may be compensated by electronic carries, such as electrons e', and holes, $h^{\bullet}$, or by charged ionic defects. We shall assume here that the concentration of interstitial potassium ions is much larger than those of electrons and defect electrons.
The relevant defect formation reactions in K-beta-Al_2O_3, along with their mass action relations, assuming dilute solution, are given in Table 2-2.

Table 2-2 Defect formation reactions along with mass action law

Type of reaction	Reaction	Law of mass action	Eq.
Intrinsic defect formation	$K_K + V_i \leftrightarrow K_i^{\bullet} + V_K'$	$K_F = \frac{[K_i^{\bullet}]\cdot[V_K']}{[K_K]\cdot[V_i]}$	2-1
Interaction with the surroundings	$K_K \leftrightarrow K + V_K' + h^{\bullet}$	$K_p = \frac{[V_K']\cdot[h^{\bullet}]}{[K_K]} a_K$	2-2a
	$K + V_K' \leftrightarrow K_K + e'$	$K_n = \frac{[K_K]\cdot[e']}{[V_K']} a^{-1}{}_K$	2-2b
Electron-hole generation-recombination	$0 \leftrightarrow e' + h^{\bullet}$	$K_e = [e']\cdot[h^{\bullet}]$	2-3

a_K is potassium activity in the surroundings, V_i and V_K are the interstitial and potassium vacancies, respectively, h is electron hole, e is excess electron, [ ] denote concentration of ion or electron defect and K_F, K_R, K_p and K_n are the constants of above equilibriums, having the form

$$K(T) = K_0 \exp\left(-\frac{\Delta H}{RT}\right),$$ Eq. 2-4

where K_0 includes the entropy term, ΔH is the reaction enthalpy, T is the absolute temperature and R is the gas constant.

In addition, the electro-neutrality condition has to be taken into account

$$[V_K'] + [e'] = [h^\bullet] + [K_i^\bullet].$$ Eq. 2-5

Eq. 2-1, 2-2, 2-3 and 2-5 allow to calculate the defect concentration as a function of the potassium chemical potential and temperature.

The defect concentration in solid electrolyte as a function of the chemical potential of the neutral species in the ambience of solid electrolyte is represented with the so called Brouwer diagram.

Fig. 2-6 represents the Brouwer diagram for K-beta-Al_2O_3.The Brouwer diagram can be divided into three different regions. In each of them, one of the defects on either side of Eq. 2-5 controls the neutrality equation, and thus, the potassium activity dependence of the defects involved.

At relatively low chemical potential of potassium, the excess electron concentration ([e']) becomes negligible while the level of the hole concentration becomes comparable to that of the potassium vacancy concentration.

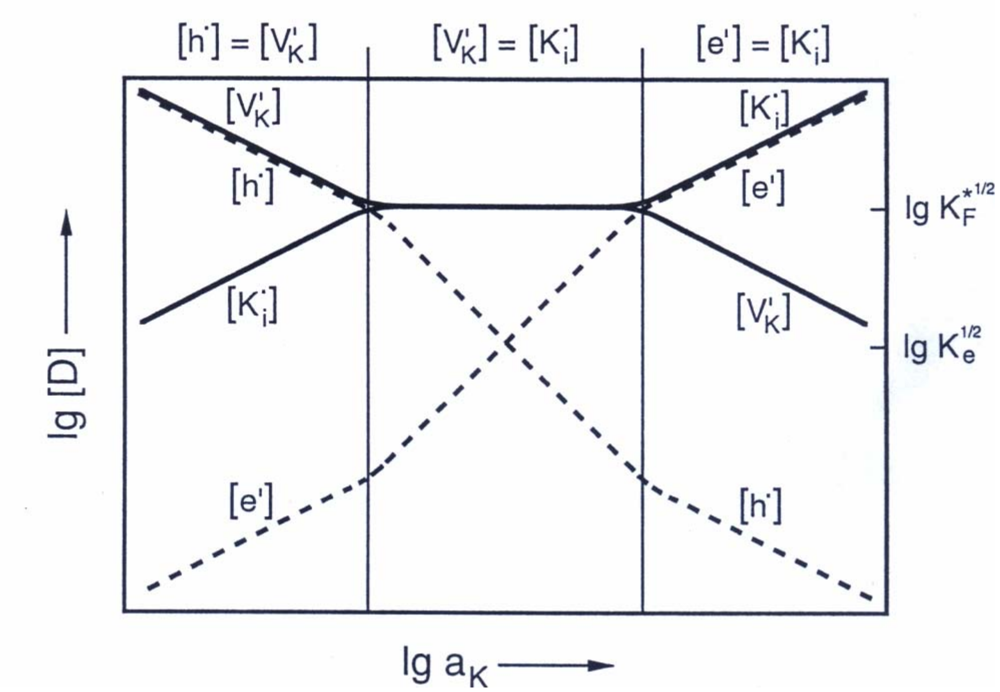

Figure 2-6 Brouwer diagram for undoped K-beta-Al_2O_3

Due to the interaction with the surrounding charge neutrality is maintained by decreasing the negatively charged potassium vacancies (Eq. 2-2b) and increasing the positively charged potassium interstitial (Eq. 2-2a). In the extreme case considering

$$[h^{\bullet}] = [V_K'] \qquad \text{Eq. 2-6}$$

for charge neutrality.

Inserting the new neutrality condition into the mass action Eqs. 2-1, 2-2 and 2-3, the defect concentration in the solid electrolyte can be calculated. Since the concentration of potassium ions on potassium sites is assumed to be constant, the concentration of hole electrons is proportional to the second root of the potassium chemical potential with which potassium beta alumina is in equilibrium.

In the vicinity of the stoichiometric point, the concentrations of potassium ions on interstitial sites and vacancies are much larger than the concentrations of electrons and defect electrons, the relative changes in the concentrations of electronic charge carriers are much larger than that of the interstitial ions ($K_i^{\bullet}$) and the vacancies (range II in Fig. 2-6). Hence the concentrations of potassium ion vacancies and potassium ions in the interstitial site may be considered as virtually being constant:

$$[V_K'] = [K_i^{\bullet}] \cong \text{const.} \qquad \text{Eq. 2-7}$$

Applying the law of mass action to Eq. 2-2a and taking Eq. 2-7 into consideration we obtain the relation

$$[h^{\bullet}] \propto a_K^{-1}, \qquad \text{Eq. 2-8}$$

i.e., the concentration of electron defects is proportional to the inverse of the potassium activity in the surroundings.

Proceeding in a similar fashion the expression for the concentration of the electrons in this range can be obtained by incorporating Eq. 2-2b

$$[e'] \propto a_K. \qquad \text{Eq. 2-9}$$

The situation is totally different for large deviations from ideal stoichiometry. If the chemical potential of potassium is very low, the concentration of the holes and potassium ions on interstitial sites may be neglected, hence the electroneutrality condition 2-5 reduces to:

$$[e'] = [K_i^{\bullet}]. \qquad \text{Eq. 2-10}$$

Applying the law of mass action to Eq. 2-2b and taking into account the above relation one obtains

$$[e'] \propto a_K^{1/2}, \qquad \text{Eq. 2-11}$$

i.e., the concentration of excess electrons, now equal to the concentration of interstitial ions, is proportional to the square root of the potassium activity.

These results based on the considerations stated above are summarized in Table 2-3 and shown schematically in Fig. 2-6. In case of doped material like MgO doped Na-beta-alumina, the concentration of charge species in different regions of the Brouwer diagram is shown in Table 2-4 and plotted in Fig. 2-7.

Table 2-3 Potassium chemical potential dependence of the concentration of charge species in different regions of Brouwer diagram for un-doped K-beta-Al_2O_3

Electro-neutrality condition (limit case)	a_K	$[V_K']$	$[K_i^\bullet]$	$[h^\bullet]$	$[e']$
$[h^\bullet]=[V_K']$	low	$\propto a_K^{-1/2}$	$\propto a_K^{1/2}$	$\propto a_K^{-1/2}$	$\propto a_K^{1/2}$
$[V_K']=[K_i^\bullet]$	middle	$\cong$ const	$\cong$ const	$\propto 1/a_K$	$\propto a_K$
$[e']=[K_i^\bullet]$	high	$\propto a_K^{-1/2}$	$\propto a_K^{1/2}$	$\propto a_K^{-1/2}$	$\propto a_K^{1/2}$

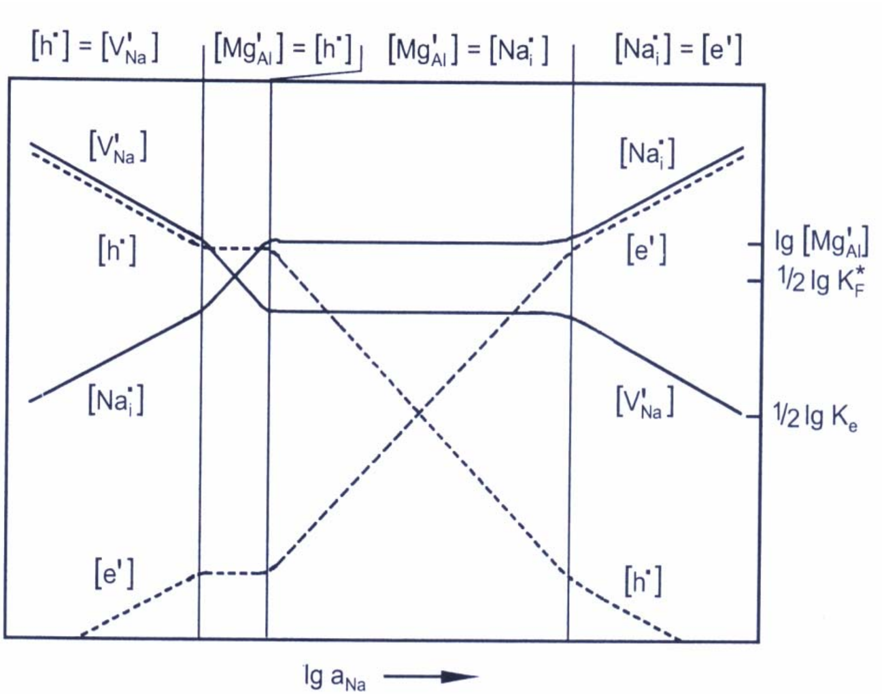

Fig. 2-7 Brouwer diagram for Mg doped Na-beta-Al_2O_3

Table 2-4 Sodium activity dependence of the concentration of charge species in different regions of the Brouwer diagram for Mg-doped Na-beta-Al_2O_3

Electro-neutrality condition	a_{Na}	$[V'_{Na}]$	$[Na_i^\bullet]$	$[h^\bullet]$	$[e']$
$[h^\bullet]=[V'_{Na}]$	low	$\propto a_{Na}^{-1/2}$	$\propto a_{Na}^{1/2}$	$\propto a_{Na}^{-1/2}$	$\propto a_{Na}^{1/2}$
$[Mg'_{Al}]=[h^\bullet]$	middle	$\propto a_{Na}^{-1}$	$\propto a_{Na}$	$\cong$ const	$\cong$ const
$[Mg'_{Al}]=[Na_i^\bullet]$	middle	$\cong$ const	$\cong$ const	$\propto a_{Na}^{-1}$	$\propto a_{Na}$
$[e']=[Na_i^\bullet]$	high	$\propto a_{Na}^{-1/2}$	$\propto a_{Na}^{1/2}$	$\propto a_{Na}^{-1/2}$	$\propto a_{Na}^{1/2}$

2.3 Conductivity

For a material to behave as a solid electrolyte a number of ions should not be restricted to normal lattice positions. They must be free to move from one position to another after application of an electric field (migration), as in an oxygen pump, or under a concentration gradient (diffusion), as in the case of a sensor. In the solid electrolyte, movement differs from the gas or liquid phase in that only one type of ions is free to move. For Na-beta-Al_2O_3 the Na^+ ions are moving with the Al^{3+} and O^{2-} are fixed.

Though many conduction mechanisms can be produced only three are regarded as likely in ionic conductors, these are interstitial, interstitialcy and vacancy diffusion. The vacancy mechanism for transport of ions is illustrated in Fig. 2-8. The two dimensional representation of interstitial motion shown in Fig. 2-9 looks very overcrowded, a three dimensional model for the same motion shows the motion to be quite energetically favorable. The third type of motion involves a possible combination of vacancy and interstitial mechanisms, as shown in Fig. 2-10.

If the mobile ions simply exchange places with a near neighbour then no net ion flow is observed or detected. A detectable flow only occurs when a series of ionic movements occur that produces a net change in charge or mass over the material. This movement of ions or atoms is usually modelled as a process of discrete jumps over energy barriers in which one sublattice acts as a liquid like component while the other remains rigid.

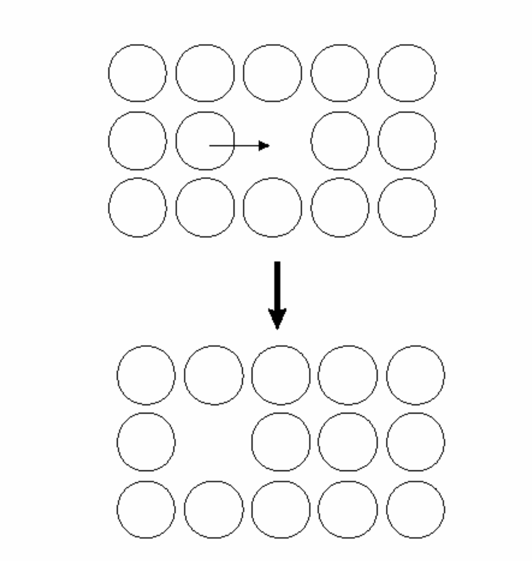

Fig. 2-8 Vacancy mechanism for transport of ions.

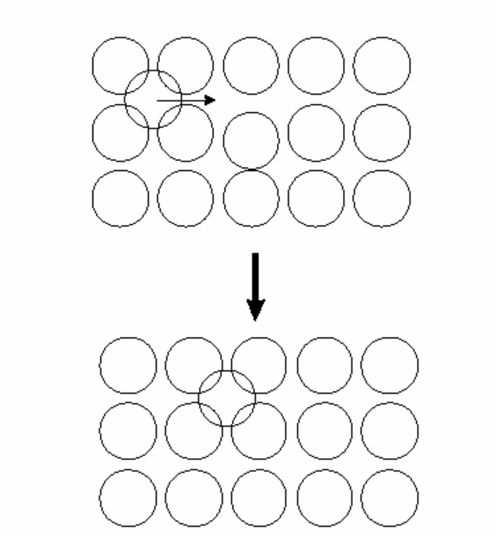

Fig. 2-9 Interstitial mechanism for transport of ions.

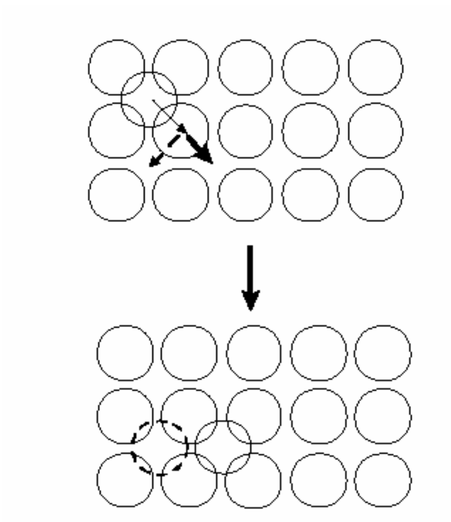

Fig. 2-10 Interstitialcy mechanism showing the two possible locations of ions after movement.

Electronic defects can be formed by thermal excitation of electrons from the valence band to the conduction band. Equilibrium between free electrons (e') in the conduction band and electron holes ($h^{\bullet}$) in the valence band can be expressed by Eq. 2-3. The expression for thermal equilibrium of electrons and holes leads to the equation [32]:

$$np = N_c N_v \exp\left(-\frac{E_g}{kT}\right), \qquad \text{Eq. 2-12}$$

where n and p denote the concentrations of electrons and electron holes, respectively, E_g is the energy difference between valence and the conduction band (bandgap energy) N_v is the effective density of valence band energy levels and N_c is the effective density of conduction band levels.

Concentrations of ionic and electronic defects discussed in chapter 2.2 are important because electrical charge is transported by movement of these defects. The electrical conductivity (σ) of a solid is related to its defect concentration by [33]

$$\sigma = \sum_i c_i z_i q u_i + nq_e u_e + pq_h u_h, \qquad \text{Eq. 2-13}$$

where c_i, n and p are the ionic, electron and hole concentration, q is the charge, u is the mobility (i.e., the mean particle velocity per unit potential gradient), and subscripts i, e and h denotes ions, electrons and electron holes, respectively.

The mobility of an electronic carrier is usually significantly larger than that of an ion. This means that ionic motion will only predominate if the concentration of electron holes is considerably smaller than the concentration of ionic defects.

2.3.1 Ionic conductivity of the beta alumina

The ionic conductivity of highly conducting solids like beta-Al_2O_3 is difficult to measure accurately because of the problem of having at one's disposal reversible electrodes. An alternative approach to the use of the reversible electrodes is the use of non-reversible electrodes at high frequency with a frequency range where the conductivity is independent of frequency. Conductivity data for single crystals of potassium beta alumina has been reported by Briant and Farrington [34] and Roth et al. [35] using blocking electrodes and in the range of 0.1 – 10 MHz. The conductivity of K- and Na-beta-Al_2O_3 at certain temperature has been listed in Table 2.5. Fig. 2-11 shows the temperature dependence of the conductivity reported in literature for polycrystalline K-beta-Al_2O_3.
As it is assumed that the β''-phase exhibits a higher conductivity and can be stabilized by adding large amounts of K_2O to Al_2O_3 and further by doping with suitable oxides such as MgO and Li_2O, it is possible to optimize the conductivity as a function of composition, and also as a function of the way of the fabrication of potassium beta alumina [36, 37].
The ionic conductivity of Na-beta-Al_2O_3 at room temperature may reach values of about 0.3 S cm^{-1}. The mobile potassium ions are incorporated into the lattice sheets located between non-conducting spinel blocks. Hence, the movements of these ions are only possible in two dimensions. Polycrystalline material must therefore be used to obtain a three-dimensional conductor. Nevertheless the structure of the material plays a vital role for giving high transport property.

Table 2-5 Conductivity of polycrystalline K- and Na-beta-Al_2O_3

Electrolyte	σ (S cm^{-1}) 300 °C	E_{act} (eV)	Ref.
K-β-Al_2O_3	$1.7*10^{-3}$	1.92	[37]
K-β-Al_2O_3	$1*10^{-3}$	1.86	[37]
K-β-Al_2O_3	$0.05*10^{-3}$	2.8	[36]
K-β"-Al_2O_3	0.05	1.58	[39]
K-β- Al_2O_3	$4.1*10^{-3}$	0.91	[40]
Na-β- Al_2O_3	0.27	0.14	[41]
Na-β”-Al_2O_3	1.00	0.33	[41]

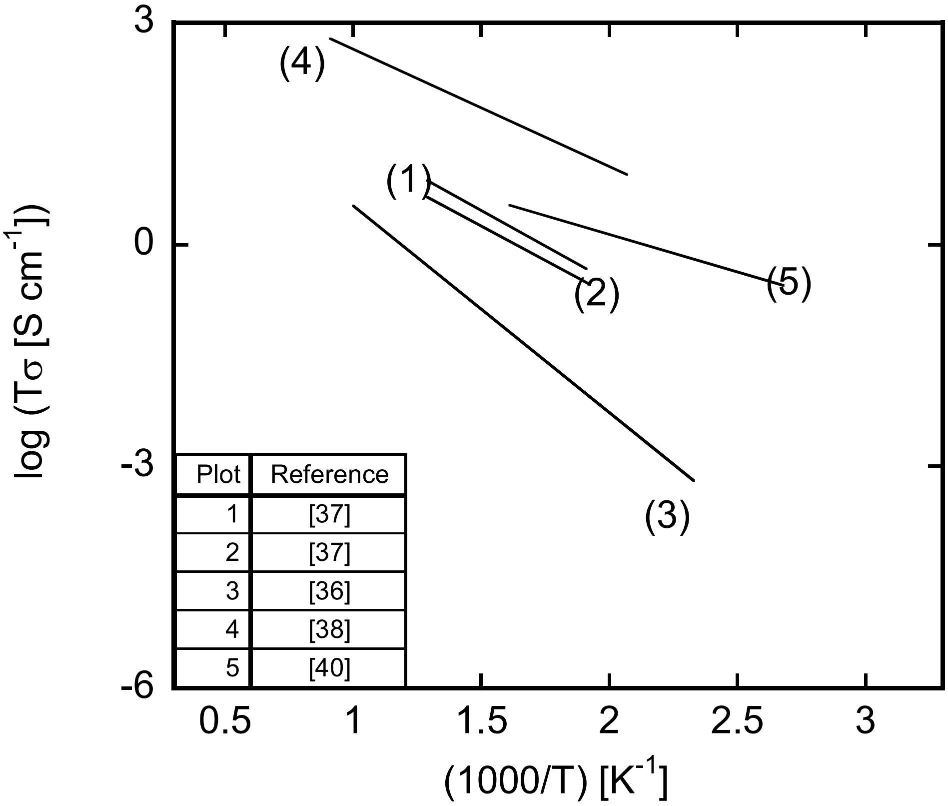

Fig. 2-11 Temperature dependence of the conductivity for polycrystalline K-beta-Al_2O_3

2.3.1.1 Influence of dopands on conductivity

According to Eq. (2-13) the conductivity of solid electrolyte (beta alumina) depends on the concentration of mobile ion. Charge balance in undoped beta alumina has been attributed to Al^{3+} vacancies and O^{2-} interstitials in the conduction plane. If a metal ion Mg^{2+} having a charge less than +3 replaces an aluminium ion [35, 45], additional potassium ions could be incorporated for charge balance. By introducing such metal ions as a dopand, e.g. Mg^{2+}, which substitutes for Al^{3+} in the spinel block, will affect the conductivity [43, 44]. The relation between the sodium content and the conductivity were studied as a function of MgO doping level by Kennedy and Sammells [45]. It was found [45] that the optimum concentration of sodium (minimum resistivity) depended on MgO content and that the optimum sodium content increased as the MgO content increased. The optimum of sodium content could be predicted by assuming that each Mg^{2+} added leads to the incorporation of one extra Na^+ compared to the undoped material. However, the effects are smaller than the prediction. There is some evidence [46] that +2 metal ions can exchange with Na^+ in the conduction plane and this role would be expected to decrease the conductivity. Calcium decreases conductivity of beta alumina drastically with a 1% addition causing a 50-100 fold decrease [43, 44, 47]. De Jounghe [47] attributed this to calcium accumulation in the grain boundary region. Mössbauer [48] and diffusion [49] measurements have indicated that Eu^{2+} may reside in both the conduction plane and spinel block. Lithium is another element which has been shown by NMR line narrowing studies [50] to reside in both conduction plane and spinel block. When a +2 metal ion such as Mg^{2+} substitutes for Al^{3+} it can cause at least three effect:

1. Incorporation of additional Na^+ ions, according to this defect reaction:
   $$O \rightarrow xNa_i^{\bullet} + xMg'_{Al}$$
2. Removal of interstitial O^{2-} which block Na^+ conduction according to
   $$xNa_i^{\bullet} + \frac{x}{2}O_i'' \rightarrow xNa_i^{\bullet} + xMg'_{Al}$$
3. Removal of Al^{3+} vacancies which hold Na^+ electrostatically according to the defect reaction
   $$xNa_i^{\bullet} + \frac{x}{3}V_{Al}''' \rightarrow xNa_i^{\bullet} + xMg'_{Al}$$

2.3.2 Electronic conductivity

Supposing the mobility of the ionic and electronic defects is independent of their concentration, and also taking into account the defect chemistry consideration (cf. Fig. 2-6 and 2-7) it holds that

$$\sigma_{M^+} = \text{const.}, \qquad \text{Eq. 2-14}$$

$\sigma_p \propto (a_M)^{-1}$ and Eq. 2-15

$\sigma_n \propto (a_M)$ Eq. 2-16

These results based on the considerations of section 2.1.2 are shown schematically in Fig. 2.12 and 2.13 for K-beta-Al_2O_3 (undoped) and MgO-doped Na-beta-Al_2O_3, respectively. The electronic conduction parameters $a_\oplus$ and $a_\ominus$ denote the metal (K or Na) activity at which the electronic conductivities σ_p and σ_n, respectively, are equal to the ionic conductivity σ_{M^+} (cf. Fig. 2-12 and 2-13). Thus, the electronic conduction parameters characterize the limit of the ionic and electronic domain of the electrolyte.

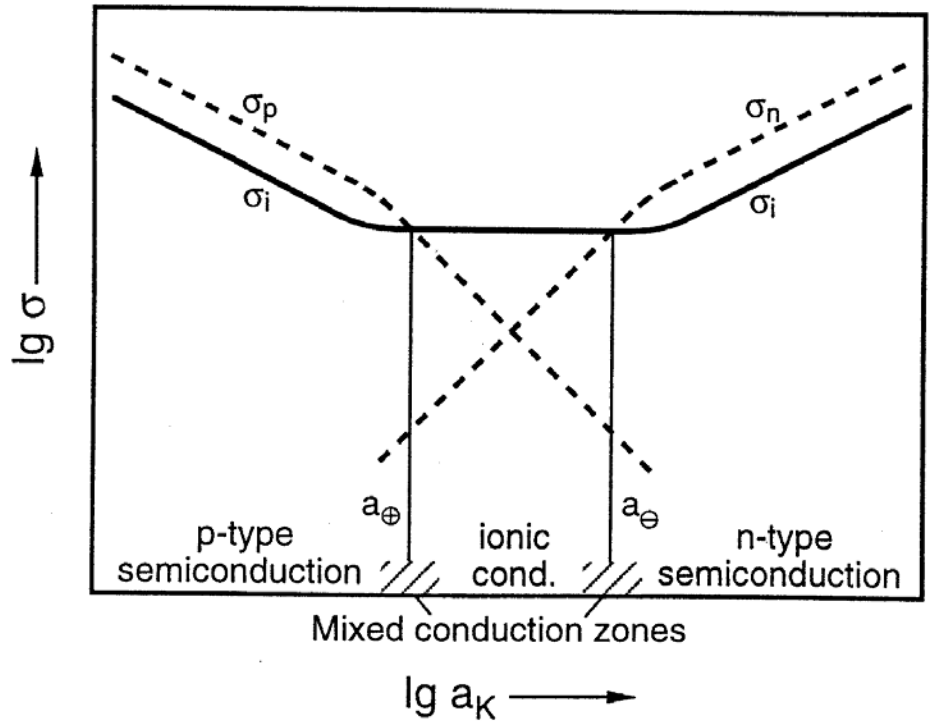

Fig. 2-12 Conductivity diagram of undoped K-beta-Al_2O_3

Taking into consideration Eq. 2-12 and 2-13, the partial conductivities at two different metal (M= Na, K) activities (a'_M and a''_M) can be rewritten in the following form

$$\sigma'_p = \sigma''_p \left(\frac{a'_M}{a''_M} \right)^{-1}$$ Eq. 2-17

and

$$\sigma'_n = \sigma'_n \left(\frac{a'_M}{a''_M} \right).$$ Eq. 2-18

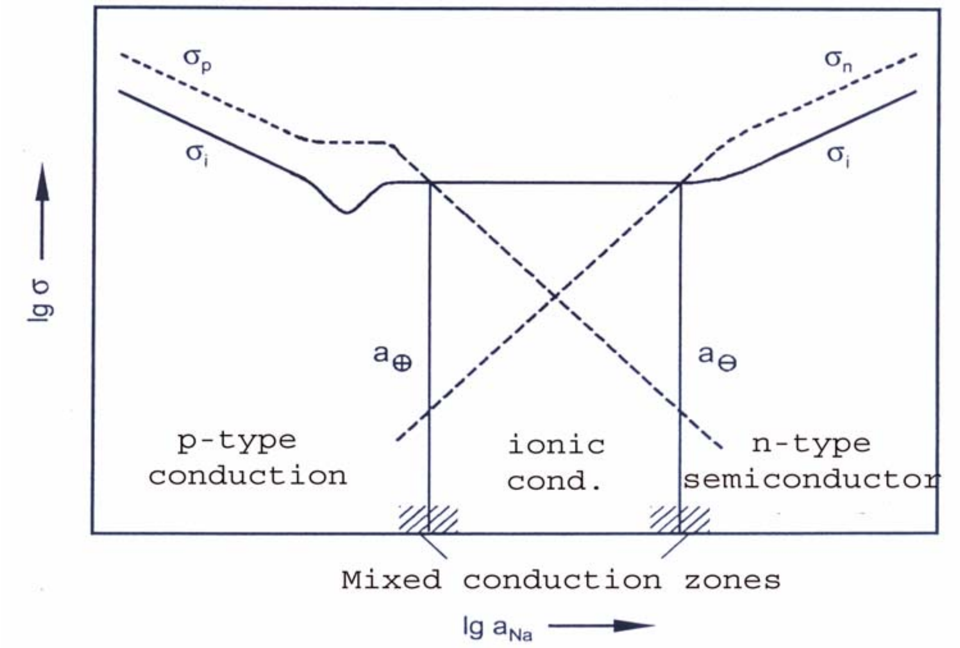

Fig. 2-13 Conductivity diagram of Mg doped Na-beta-Al_2O_3

The electronic transference number denotes the contribution of the electronic conductivity to the total electrical conductivity of the solid electrolyte and can be represented as follows:

$$t_e = 1 - t_{M^+},$$ Eq. 2-19

where $t_{M^+} = \dfrac{1}{1 + \dfrac{\sigma_n}{\sigma_{M^+}} + \dfrac{\sigma_p}{\sigma_{M^+}}}$ represents the ionic transference number.

The definition of the ionic transference number requires the knowledge of the ratio between the electronic and the ionic conductivities of the electrolyte.

Using the conduction parameter the partial electronic conductivities can be represented as

$$\sigma_p = \sigma_{M^+}\left(\frac{a_\oplus}{a_M}\right)$$ Eq. 2-20

and

$$\sigma_n = \sigma_{M^+}\left(\frac{a_M}{a_\ominus}\right).$$ Eq. 2-21

According to the Eq. 2-20 and 2-21, the ionic transference number can be represented in terms of the electronic conduction parameters ($a_\oplus$, $a_\ominus$) as

$$t_{M^+} = \frac{1}{1 + \dfrac{a_\oplus}{a} + \dfrac{a}{a_\ominus}}$$ Eq. 2-22

2.4 The cell voltage according to Wagner

If conduction takes place by electrons in the solid electrolyte in addition to ionic conduction, potassium or sodium ions flow through the electrolyte from the electrode with higher metal chemical potential to that with lower one. The electrical partial current density i_k for each type of particle k is given by the equation according to the principles of irreversible thermodynamics [51]

$$i_k = -\frac{\sigma_k}{z_k F}\left(\frac{d\eta_k}{dx}\right), \qquad \text{Eq. 2-23}$$

where σ_k is the partial conductivity, z_k is the charge of the particle species k and η_k is its electrochemical potential, which can be expressed in terms of the chemical potential μ_k and the electrical potential φ:

$$\eta_k = \mu_k + z_k F \varphi . \qquad \text{Eq. 2-24}$$

Under open circuit condition, the partial current densities of alkali ions (M^+; z = 1) i_{M^+} and electrons i_{e^-} must, for electrical neutrality reason, be equal:

$$i_{M^+} = -i_e . \qquad \text{Eq. 2-25}$$

Thus, using Eq. 2-23, it follows that

$$d\eta_{M^+} = -\frac{\sigma_e}{\sigma_{K^+}} d\eta_e . \qquad \text{Eq. 2-26}$$

A local equilibrium can be assumed to exist between alkali ions (M^+ =Na^+ or K^+), electrons and the neutral metals (M = Na or K).

$$M^+ + e' \leftrightarrow M \qquad \text{Eq. 2-27}$$

Accordingly, the electrochemical potential of the alkali ions is related to the metal chemical potential and that of the electrons, as follows

$$d\eta_{M^+} + d\eta_e = -d\mu_M . \qquad \text{Eq. 2-28}$$

Eqs. 2-26 and 2-28 lead to the expression

$$d\eta_e = t_{M^+} d\mu_M . \qquad \text{Eq. 2-29}$$

Integrating Eq. 2-29 over the thickness of the electrolyte gives

$$\eta_e'' - \eta_e' = \int_{x'=0}^{x''=L} t_{M^+} d\mu_M(x), \qquad \text{Eq. 2-30}$$

where η_e'', η_e' denote the electrochemical potential of the electrons of the electrolyte at both electrodes and L is the thickness of the solid electrolyte (see Fig. 2-14).

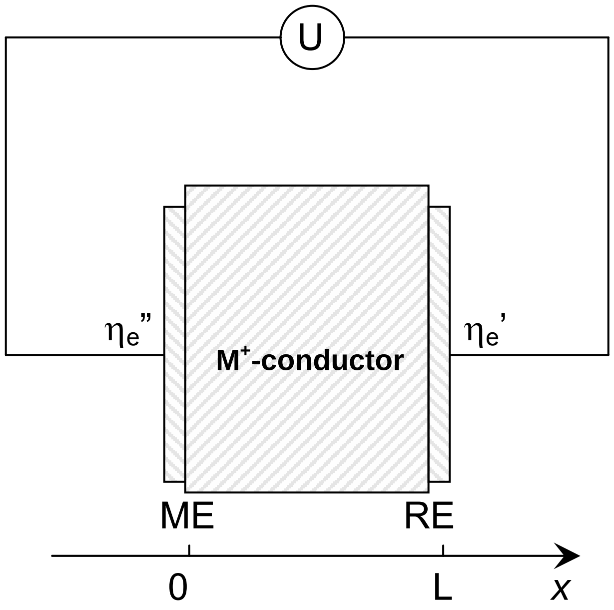

Fig. 2-14 Schematic representation of M^+-conductor exposed to an external chemical potential of metal (M)

Let μ_M' and μ_M'' be the chemical potential of the metal (Na or K) at the reference (RE) and measuring (ME) electrode (Fig. 2-14), respectively. Hence, the Eq. 2-30 can be written in terms of chemical potential as

$$\eta_e'' - \eta_e' = \int_{\mu_K'}^{\mu_K''} t_{M^+} d\mu_M \,. \qquad \text{Eq. 2-31}$$

Since the difference in the electrochemical potential of the electrons itself is related to the measurable galvanic cell voltage by the equation

$$\eta_e'' - \eta_e' = -UF \,, \qquad \text{Eq. 2-32}$$

Eqs. 2-31 and 2-32 yield

$$U = -\frac{1}{F}\int_{\mu_M'}^{\mu_M''} t_{M^+} d\mu_M \,. \qquad \text{Eq. 2-33}$$

Using the definition of the chemical potential of the metal

$$\mu_M = \mu^\circ{}_M + RT\ln a_M \qquad \text{Eq. 2-34}$$

the integral over the transference number can be represented as

$$U = -\frac{RT}{F}\int_{a_M'}^{a_M''} t_{M^+} d(\ln a_M). \qquad \text{Eq. 2-35}$$

Hence, it is possible in principle to use the measured value of the voltage to obtain information about the ionic transference number. Working with Eq. 2-33 it must, however, be noticed that the transference number is not constant but a function of the metal chemical potential. This dependence, which follows from Eq. 2-22, must be included in the evaluation to be carried out.

For mathematical reasons, under the condition that

$$\left(\frac{a_\oplus}{a_\ominus}\right) \ll \frac{1}{4} \qquad \text{Eq. 2-36}$$

the integration yields [12]:

$$U = -\frac{RT}{F}\ln\left[\frac{(a''_M + a_\oplus)(a'_M + a_\ominus)}{(a''_M + a_\ominus)(a'_M + a_\oplus)}\right]. \qquad \text{Eq. 2-37}$$

Eq. 2-37 is the general form of the integrated Wagner equation for a galvanic cell where a cation conductor is used as a solid electrolyte. It quantitatively takes the fact into account that the partial internal short-circuit due to electronic conduction results in a voltage decay along the internal resistance of the electrolyte. Eq. 2-37 holds in the whole range of the chemical potential of the metal in the ambience in which Eq. 2-36, 2-20 and 2-21 are fulfilled. The restrictive condition of Eq. 2-36 means that the electronic conduction parameters have to differ by several orders of magnitude implying a sufficiently large width of the ionic domain. This in any case is the prerequisite a solid electrolyte does satisfy.

If the electrolyte has an infinitely extended width of the ionic domain, that means

$$a_\oplus \rightarrow 0 \text{ and } a_\ominus \rightarrow \infty \qquad \text{Eq. 2-38}$$

Eq. 2-37 results in the relationship for the Nernst equilibrium cell voltage (U_{eq}):

$$U_{eq} = -\frac{RT}{F}\ln\frac{a''_M}{a'_M}. \qquad \text{Eq. 2-39}$$

Depending on the magnitudes of the metal activities (a''_M and a'_M) in comparison with the electronic conduction parameters ($a_\oplus$ and $a_\ominus$) Eq. 2-37 takes various forms [12].

The following cases will be discussed below:

Case (i): $a''_M \gg a_\oplus;\ a'_M \ll a_\ominus$ Eq. 2-40

This means, each of the electrodes lies in one of the mixed conduction regions of the electrolyte with the measuring electrode being exclusively affected by n-type and the reference electrode by p-type electron conduction. With the limiting condition of Eq. 2-40, the cell voltage according to Eq. 2-37 changes into

$$U = \frac{RT}{F}\left[\ln\left(a''^{-1}_{M} + a_{\ominus}^{-1}\right) + \ln\left(a'_{M} + a_{\oplus}\right)\right].$$ Eq. 2-41

Case (ii): $a''_M \gg a_\oplus$; $a_\oplus \ll a'_M \ll a_\ominus$ Eq. 2-42

Eq. 2-42 describes the situation that n-type electronic conductivity exclusively occurs at the measuring electrode of the galvanic cell whilst the reference electrode is chosen such that it lies within the ionic domain of the electrolyte. Then the cell voltage equation takes the form

$$U = \frac{RT}{F}\left[\ln\left(a''^{-1}_{M} + a_{\ominus}^{-1}\right) + \ln\left(a'_{M}\right)\right].$$ Eq. 2-43

Case (iii): $a''_M \ll a_\ominus$; $a_\oplus \ll a'_M \ll a_\ominus$ Eq. 2-44

According to Eq. 2-44 the situation is the same as in the foregoing case, except that p-type instead of n-type conduction prevails. The cell voltage is calculated as follows:

$$U = -\frac{RT}{F}\ln\frac{a_M'' + a_\oplus}{a'_M}.$$ Eq. 2-45

Case (iv): $a''_M \ll a_\ominus$; $a'_M \ll a_\ominus$ Eq. 2-46

The limiting condition of Eq. 2-46 describes the circumstances under which both of the electrodes are exclusively affected by p-electron conduction. Thus, the cell voltage yields:

$$U = -\frac{RT}{F}\ln\frac{a''_M + a_\oplus}{a'_M + a_\oplus}.$$ Eq. 2-47

2.5 Cell voltage under non-isothermal conditions

The thermo cell having following configuration has been studied

$$Pt \underset{\phi(\beta)}{\overset{T}{|}} Pt, CO_2, O_2, Na_2CO_3(Pt) \overset{T+\Delta T}{|} NBA \overset{T}{|} Na_2CO_3(Pt), CO_2, O_2, Pt \underset{\phi(\alpha)}{\overset{T}{|}} Pt\ ,$$ (IV)

where Na-beta-Al_2O_3 (NBA) is the solid electrolyte, Na_2CO_3, CO_2, O_2, Pt are the electrodes and Pt serves as the leads for electrical connection.

The thermoelectric power of the cell (IV) can be defined as

$$\varepsilon = \lim_{\Delta T \to 0}\frac{\Delta\phi}{\Delta T} = \frac{d\left(\phi^{(\alpha)} - \phi^{(\beta)}\right)}{dT}.$$ Eq. 2-48

$\Delta\phi$ is the electrical potential difference of electrons in the platinum and ΔT is the temperature gradient across the cell. Where $\phi^{(\alpha)}$ $\phi^{(\beta)}$ are the electrical potential of the electrons in the Pt leads at the terminals α and β, respectively.

From the definition of the electrochemical potential of electrons in equation,

$$\eta_e = \mu_e - \phi_e F\,, \qquad \text{Eq. 2-49}$$

it follows that the potential difference between α and β terminals of thermo-cell equals

$$\phi^{(\beta)} - \phi^{(\alpha)} = -\frac{\left[\eta_e^{(Pt,\beta)} - \eta_e^{(Pt,\alpha)}\right]}{F}. \qquad \text{Eq. 2-50}$$

In the case of local equilibrium at a phase boundary, the electrochemical potential η_e is the same at the two sides of the interface. Thus the right side of Eq. 2-50 is determined by the local difference of η_e within the phases NBA and Pt involving temperature gradients.

Hence, the thermoelectric power is given as follows

$$\varepsilon = \frac{d\left[\phi^{(\beta)} - \phi^{(\alpha)}\right]}{dT} = -\frac{1}{F}\left[\frac{d\eta_e^{(NBA)}}{dT} - \frac{d\eta_e^{(Pt)}}{dT}\right]. \qquad \text{Eq. 2-51}$$

According to Eq. 2-51 the total thermoelectric power is equal to the difference of thermoelectric power of the solid electrolyte (NBA) and the leads (Pt):

$$\varepsilon = \varepsilon^{(NBA)} - \varepsilon^{(Pt)}. \qquad \text{Eq. 2-52}$$

To obtain the thermoelectric power of solid electrolyte (NBA), one has to invoke the phenomenological equations for flux of charge carrier (J) under the temperature gradient according to irreversible thermodynamic [51].

The flux of charge particle "k" in a temperature gradient is given as

$$J_k = -\frac{\sigma_k}{z_k^2 F^2}\left[\frac{d\eta_k}{dx} + \left(\overline{S_k} + \frac{Q_k{}^*}{T}\right)\frac{dT}{dx}\right] \qquad \text{Eq. 2-53}$$

where σ_k is the conductivity;

$\overline{S}_k$ and Q^* the molar entropy and heat of transfer for particle “k”, respectively,

x the distance two electrodes and

$\overline{\overline{S_k}} = \left(\overline{S_k} + \frac{Q_k{}^*}{T}\right)$ the transport entropy.

Under the steady state the fluxes of the Na^+ ions (J_{Na^+}) and electrons (J_e) must be equivalent, as each volume element of the solid electrolyte must remain electrically neutral:

$$J_e = J_{Na^+} .$$ Eq. 2-54

Furthermore, from Eq. 2-53 in the case of virtually independent movement of species one may write

$$\sigma_{Na^+}\left[\frac{d\eta_{Na^+}}{dx} + \left(\bar{S}_{Na^+} + \frac{Q^*_{Na+}}{T}\right)\frac{dT}{dx}\right] = \sigma_e\left[\frac{d\eta_e}{dx} + \left(\bar{S}_e + \frac{Q^*_e}{T}\right)\frac{dT}{dx}\right],$$ Eq. 2-55

where the symbol has meaning described above for the respective species.

An electrochemical equilibrium can be assumed to exist inside the solid electrolyte between Na^+ ions, electrons and neutral Na atoms without ambiguity. According to definition of the electrochemical potential

$$\eta_{Na^+} + \eta_e = \mu_{Na^+} + \mu_e = \mu_{Na},$$ Eq. 2-56

where μ_{Na} is the chemical potential of neutral sodium atoms.

According to the above equation, one has

$$\frac{d\eta_{Na^+}}{dx} = \frac{d\eta_{Na^+}}{dT}\frac{dT}{dx} = \left(\frac{d\mu_{Na}}{dT} - \frac{d\eta_e}{dT}\right)\frac{dT}{dx}.$$ Eq. 2-57

Furthermore, one may write

$$\frac{d\eta_e}{dx} = \frac{d\eta_e}{dT}\frac{dT}{dx}.$$ Eq. 2-58

Substituting Eqs. 2-57 and 2-58 in Eq.2-55 and solving for $d\eta_e/dT$, one obtains

$$\varepsilon^{(NBA)} = \frac{1}{F}\left[\frac{\sigma_{Na^+}}{\sigma_{Na^+} + \sigma_e}\left(-\frac{d\mu_{Na}}{dT} - \bar{S}_{Na^+} - \frac{Q^*_{Na+}}{T}\right) + \frac{\sigma_{Na^+}}{\sigma_{Na^+} + \sigma_e}\left(\bar{S}_e + \frac{Q^*_e}{T}\right)\right].$$ Eq. 2-59

When both of the electrodes are exclusively affected by p-electron conductivity, the thermoelectric power of the solid electrolyte (Eq. 2-59) change into

$$\varepsilon = \frac{1}{F}\left[\frac{\sigma_{Na^+}}{\sigma_{Na^+} + \sigma_p}\left(-\frac{d\mu_{Na}}{dT} - \bar{S}_{Na^+} - \frac{Q^*_{Na+}}{T}\right) + \left(\frac{\sigma_p}{\sigma_{Na^+} + \sigma_p}\right)\left(\bar{S}_p + \frac{Q^*_p}{T}\right)\right].$$ Eq. 2-60-a

According to eq. 2-52 and eq. 2-20, the thermo power for the cell IV can be given by

$$\varepsilon = \frac{1}{F}\left[\left(1 + \frac{a_\oplus}{a_{Na}}\right)^{-1}\left(-\frac{d\mu_{Na}}{dT} - \bar{S}_{Na^+} - \frac{Q^*_{Na+}}{T}\right) + \left(1 + \frac{a_{Na}}{a_\oplus}\right)^{-1}\left(\bar{S}_p + \frac{Q^*_p}{T}\right)\right] - \varepsilon^{(Pt)}$$ Eq. 2-60-b

The above equation represents the thermoelectric power developed in cell IV exposed to a temperature gradient and a gradient of chemical potential.

Depending on the magnitude of sodium chemical potential in comparison with the p-electronic conduction parameter ($a_{\oplus}$) two different limit cases can be distinguished:

Case (i): $a_{\oplus} \rightarrow 0$ Eq. 2-61

This means, the solid electrolyte infinitely lies in the ionic conduction region. With the above limiting condition, the thermoelectric power Eq. 2-60 transforms into:

$$\varepsilon = \frac{1}{F}\left[\left(-\frac{d\mu_{Na}}{dT} - \overline{S}_{Na^+} - \frac{Q^*_{Na+}}{T}\right)\right] - \varepsilon^{(Pt)} \qquad \text{Eq. 2-62}$$

Hence, the thermoelectric power vs. lg a_{Na} is a straight line with slope equal –R/F.

Case (ii): $a_{\oplus} \rightarrow \infty$ Eq. 2-63

The limit case eq. 2-63 describes the situation under which the solid electrolyte behaves like a p-semiconductor material. Thus, the thermoelectric power yields:

$$\varepsilon = \frac{1}{F}\left[\left(\overline{S}_p + \frac{Q^*_p}{T}\right)\right] - \varepsilon^{(Pt)}. \qquad \text{Eq. 2-64}$$

According to the theory of the defect chemistry (cf. section 2.2), the molar entropy of the hole electrons can be represent as

$$\overline{S}_p = \overline{S}^0_p - R\ln a_{Na}. \qquad \text{Eq. 2-65}$$

Hence, the sodium activity dependence of thermoelectric power is straight line with slope equal –R/F and intercept equal to the transport entropy.

Using the eq. 2-60, the $a_{\oplus}$ can be quantitatively evaluated from the field of data on thermo power under various activities.

2.6 Electrochemical determination of a_{Na_2O} in $NaSb_{1.67}O_{4.67}$ - $NaSbO_3$ phases

Galvanic cells are often used to obtain the thermodynamic data of phases. Until now mostly the thermodynamic stability of binary phases of Na-M-O (where M = Mo, Sb, Cr, Al) has been determined exclusively by measuring the voltage on appropriate solid electrolyte galvanic cell using cation conductor and evaluating the data according the Nernst equation [52-75]. Only few authors have used an oxygen conductor as a solid electrolyte [76, 77]. In this study the impact of the electronic conduction transference on thermodynamic stability data reported [72] will be investigated.

Table 2-6 Previous measurements on thermodynamic stability of binary phase

Solid electrolyte (SE)	Binary phase under investigation	Reference
NASICON	Na_2MoO_4-$Na_2Mo_2O_7$	[71]
NASICON	NiO-Na_2NiO_2	[71]
Na-β-Al_2O_3	BaO-Al_2O_3	[73]
Na-β-Al_2O_3	Na_2ZrO_3-ZrO_2	[75]
K-β-Al_2O_3	α/ K-β-Al_2O_3	[65]
Na-β-Al_2O_3	Na-Fe-O	[74]
Na-β-Al_2O_3	Na-Fe-O	[70]
Na-β-Al_2O_3	Na-Fe-O	[64]
NASICON	α/ Na-β-Al_2O_3	[59]
Na-β-Al_2O_3	Na-Fe-O	[60]
Na-β-Al_2O_3	Na-Sb-O	[72]

The galvanic cells used for the thermodynamic stability measurements of two-phase, Pyrochlore-Ilmenite, (cf. Fig. 2-15) in present study, is represented as follows

$$\mathrm{Pt}\left|\ \mathrm{CO_2, O_2, Na_2CO_3 (Au)}\right|\mathrm{NaSb_{1.67}O_{4.33} - NaSbO_3}\ \underset{a'', p''_{O_2}}{\Big|}\ \mathrm{YSZ}\ \underset{p'_{O_2}}{\Big|}\ \mathrm{O_2}\ \Big|\ \mathrm{Pt} \qquad \text{(V)}$$

where YSZ is used as a solid electrolyte.

The data resulting from present galvanic cell are unaffected by any electronic transference due to electronic short-circuit [78].

The galvanic cell voltage can be calculated according to the Nernst equation

$$U = \frac{RT}{4F} \ln\left(\frac{p''_{O_2}}{p'_{O_2}}\right), \qquad \text{Eq. 2-66}$$

where p''_{O_2} and p'_{O_2} represents oxygen partial pressure, respectively, at left and right side of the electrolyte.

The oxygen partial pressure at the left side of YSZ results from the equilibrium between the $NaSb_{1.67}O_{4.33}$, $NaSbO_3$ and sodium according to

$$3\mathrm{NaSb_{1.67}O_{4.33}} + 2\mathrm{Na} + \frac{1}{2}\mathrm{O_2} \leftrightarrow 5\mathrm{NaSbO_3}. \qquad \text{Eq. 2-67}$$

In equilibrium condition the oxygen chemical potential can be expressed by

$$\ln p''_{O_2} = \frac{2\left(3\Delta G^\circ_{\mathrm{NaSb_{1.67}O_{4.67}}} - 5\Delta G^\circ_{\mathrm{NaSbO_3}}\right)}{RT} - 2\left[\ln\frac{a^3_{\mathrm{NaSb_{1.67}O_{4.33}}}}{a^5_{\mathrm{NaSbO_3}}} - 2\ln a_{\mathrm{Na}}\right]. \qquad \text{Eq. 2-68}$$

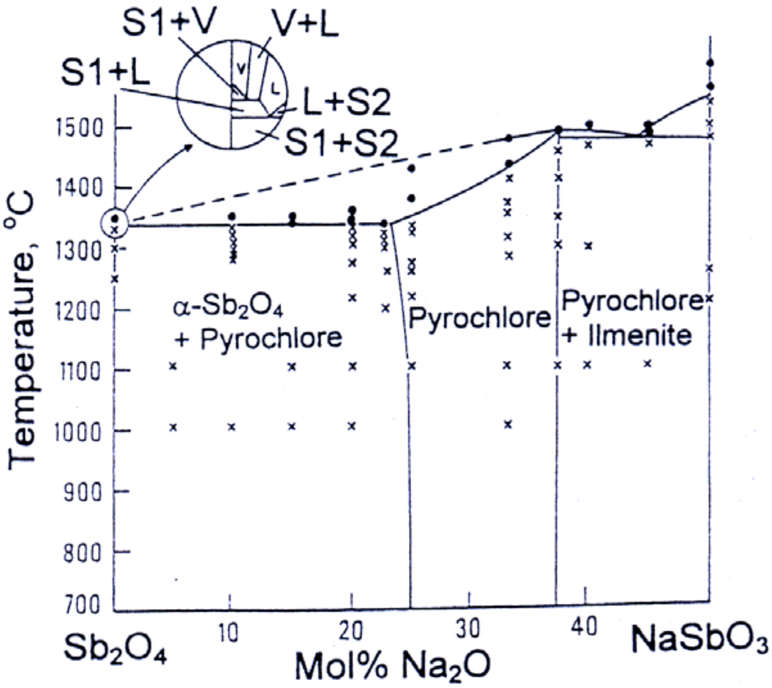

Fig. 2-15 Phase diagram of the Sb_2O_4-$NaSbO_3$ pseudo binary system [86]

The magnitude of sodium activity at the measuring electrode (a''_{Na}) is established by using CO_2, O_2 gas mixture with know composition in contact with the carbonate system (see section 2.7.1).

The equilibrium as described by Eq. 2-67 can alternatively be understood as establishing the sodium oxide activity (a_{Na_2O}) dissolved in the solid $NaSb_{1.67}O_{4.33}$ -$NaSbO_3$ phases as

$$3NaSb_{1.67}O_{4.33} + Na_2O \leftrightarrow 5NaSbO_3 . \qquad \text{Eq. 2-69}$$

Accordingly, it holds that:

$$\ln a_{Na_2O} = \frac{\left(5\Delta G^\circ{}_{NaSbO_3} - 3\Delta G^\circ{}_{NaSb_{1.67}O_{4.33}} - \Delta G^\circ{}_{Na_2O}\right)}{RT} - \left[\ln \frac{a^3_{NaSb_{1.67}O_{4.33}}}{a^5_{NaSbO_3}}\right]. \qquad \text{Eq. 2-70}$$

The material under investigation consists of a heterogeneous mixture of pure $NaSb_{1.67}O_{4.33}$ (pyrochlore) and $NaSbO_3$ (ilmegnite). Hence, the sodium oxide activity is related to the thermodynamic stability of the phase involved in equilibria ($NaSb_{1.67}O_{4.33}$ -$NaSbO_3$ phases).

Taking Eq. 2-68, 2-70 and 2-75 into consideration, Eq. 2-66 can be rewritten in terms of the metal oxide activity as follows:

$$U = \frac{\left(\Delta_f G^0_{Na_2O} - \Delta_f G^0_{Na_2CO_3} + \Delta_f G^0_{CO_2}\right)}{2F} - \frac{RT}{2F}\left[\ln p_{CO_2} + \ln a_{Na_2O}\right]. \qquad \text{Eq. 2-71}$$

Eq. 2-71 enables sodium oxide activity determined from measuring the galvanic cell voltage at known CO_2 partial pressure of the gas atmosphere.

By inserting the experimental values of voltage obtained along with those of p_{CO_2}, p_{O_2} and the thermodynamic data for Na_2CO_3 and CO_2 which were taken from JANAF [79] in Eq. 2-71, the sodium oxide activity for the $NaSb_{1.67}O_{4.33}$ – $NaSbO_3$ mixture can be derived for different temperatures and varying sodium activity.

2.7 Electrode systems

2.7.1 Chemical potential of carbonate electrodes

The potassium and sodium activity (a''_K and a''_{Na}) of the carbonate electrode used in this study as measuring electrode, i.e. at the interface between the gas sensitive layer and the electrolyte, results from the dissociation of K_2CO_3 or Na_2CO_3 into K / Na and gas components CO_2 and O_2 according to the following equilibria

$$K_2CO_3 = 2K + CO_2 + 1/2\ O_2 \qquad \text{Eq. 2-72}$$

and

$$Na_2CO_3 = 2Na + CO_2 + 1/2\ O_2. \qquad \text{Eq. 2-73}$$

The activities can be calculated according to the relationship:

$$\ln a''_K = \frac{\Delta_f G^\circ_{K_2CO_3} - \Delta_f G^\circ_{CO_2}}{2RT} - \frac{1}{2}\ln p_{CO_2} - \frac{1}{4}\ln p_{O_2} \qquad \text{Eq. 2-74}$$

and for sodium carbonate system as

$$\ln a''_{Na} = \frac{\Delta_f G^\circ_{Na_2CO_3} - \Delta_f G^\circ_{CO_2}}{2RT} - \frac{1}{2}\ln p_{CO_2} - \frac{1}{4}\ln p_{O_2}\,. \qquad \text{Eq. 2-75}$$

where $\Delta_f G^\circ_{K_2CO_2}$ $\Delta_f G^\circ_{Na_2CO_2}$,$\Delta_f G^\circ_{CO_2}$ denote the standard Gibbs energies of formation of K_2CO_3, Na_2CO_3 and CO_2. They were taken from [79]. p_{CO_2} and p_{O_2} are the CO_2 as well as O_2 partial pressure of the gas atmosphere.

2.7.2 Reference electrodes

The selection of the reference electrode used in a galvanic cell is a crucial decision. The reference electrode must produce a stable, reproducible potential, in the desired temperature range. Further criterion is that the reference electrodes must be chemically stable. It is also desirable that reference electrodes must be electrically conducting as this allows the movement of charge away from the surface of the solid electrolyte, thereby reducing or minimizing the polarization effect. The choice of reference electrode is therefore highly specific to each new application. The reference electrodes used in the present study are

Pt; FeNi(48) | $NiO/FeO_{(glass)}$ | K_2O dissolved in KBA, Eq. 2-76

Pt, FeNi(48) | $NiO/FeO_{(glass)}$ | Na_2O dissolved in NASICON and Eq. 2-77

Pt, O_2, KSi_xO_y, SiO_2 | K_2O dissolved in KBA. Eq. 2-78

2.7.2.1 Magnifer electrodes

The potassium chemical potential of the reference electrode (a'_K) expressed by 2-76 is the consequence of an interaction between the FeNi alloy, the oxides of the alloy component and the constituent phases of the heterogeneous mixture of the electrolyte. FeO and NiO that are dissolved in the glass phase establish an oxygen potential by the following equilibrium

$$\mathrm{NiO/FeO_{(glass)}} \leftrightarrow \frac{1}{2}\mathrm{O_2} + \mathrm{Ni/Fe}. \qquad \text{Eq. 2-79}$$

Furthermore, a dissociation equilibrium exists between K, O_2 and the phases of the electrolytes, i.e., K-β-Al_2O_3, corresponding to the ideal formula $KAl_xO_{(3x+1)/2}$ (x≈11), and K-β''-Al_2O_3, corresponding to $KAl_yO_{(3y+1)/2}$ (y≈5):

$$\frac{2y}{x-y}\mathrm{KAl_xO_{(3x+1)/2}} + 2\mathrm{K} + \frac{1}{2}\mathrm{O_2} \leftrightarrow \frac{2x}{x-y}\mathrm{KAl_yO_{(3y+1)/2}}. \qquad \text{Eq. 2-80}$$

The summation of Eq. 2-79 and 2-80 provides the total electrode reaction

$$\frac{2y}{x-y}\mathrm{KAl_xO_{(3x+1)/2}} + 2\mathrm{K} + \mathrm{NiO/FeO_{(glass)}} \leftrightarrow \frac{2x}{x-y}\mathrm{KAl_yO_{(3y+1)/2}} + \mathrm{Ni/Fe} \qquad \text{Eq. 2-81}$$

by means of which a'_K is defined as follows:

$$\ln a'_K = \frac{2x\Delta_f G^\circ_{\beta''} - 2y\Delta_f G^\circ_{\beta} - (x-y)\Delta_f G^\circ_{NiO/FeO}}{2(x-y)RT} + \frac{1}{(x-y)}\ln\frac{a^x_{\beta''}}{a^y_{\beta}} + \frac{1}{2}\ln\frac{a_{Ni/Fe}}{a_{NiO/FeO}}. \qquad \text{Eq. 2-82}$$

In Eq. 2-79 and 2-81 both Ni and Fe as well as NiO and FeO must be considered to be equal reaction partners. There is no reason to assume that one of the Me/MeO equilibria contributes more than the other to the definition of the oxygen potential. Therefore this potential will most likely be a mixed potential. This is expressed by denoting the activities involved by $a_{Ni/Fe}$ and $a_{NiO/FeO}$, and Gibbs energy of formation of involved oxide by $\Delta_f G^\circ_{NiO/FeO}$.

As long as the solid electrolyte represent a two phase mixture of K-β- and K-β”-Al_2O_3, the activities of both of these components are equal to one. Therefore, Eq. 2-82 can be simplified to

$$\ln a'_K = \frac{2x\Delta_f G^\circ_{\beta''} - 2y\Delta_f G^\circ_{\beta} - (x-y)\Delta_f G^\circ_{NiO/FeO}}{2(x-y)RT} + \frac{1}{2}\ln\frac{a_{Ni/Fe}}{a_{NiO/FeO}}\,. \qquad \text{Eq. 2-83}$$

There are three problems that prevent a quantitative evaluation of Eq. 2-83:

- the occurrence of the mixed potential situation as alluded above;
- the uncertainty about the magnitude of the activity of the oxides dissolved in the glass phase, i.e. $a_{NiO/FeO}$ and
- the uncertainty about the magnitude of the metal activity $a_{Ni/Fe}$ in alloy.

Thus, a'_K is not known from a quantitative point of view.

The structure of the reference electrode in the galvanic cell employing NASICON as solid electrolyte (2-77) has the same structure with the one discussed above. As it has been described earlier the oxygen potential is established according to the Eq. 2-79. It is commonly assumed in the literature that Na_2O is present at the interface or dissolved into the NASICON [80-84]. So the following equilibrium can be written, as

$$\frac{1}{2}O_2 + 2Na \leftrightarrow Na_2O_{(NASICON)}\,. \qquad \text{Eq. 2-84}$$

The explanation of the presence of Na_2O in NASICON is based on the change of stoichiometry between phases, for example according to the following reaction [83]:

$$Na_3Zr_2Si_2PO_{12} + Na_3PO_4 \leftrightarrow Na_2Zr_2SiP_2O_{12} + SiO_2 + 4Na + O_2\,. \qquad \text{Eq. 2-85}$$

It must be mentioned that such reaction is only an example, without real experimental foundations and other equilibrium that could be proposed. The summation of Eqs. 2-79 and 2-84 provides the following total electrode reaction:

$$2Na + NiO/FeO_{(glass)} \leftrightarrow Na_2O + Ni/Fe\,. \qquad \text{Eq. 2-86}$$

For the reason of the stoichiometry variation as it is discussed above, the magnitude of a'_{Na} is unknown.

Metal alloy FeNi (48) used as a part of this electrode is known by the name magnifer and henceforth the electrode will be referred as magnifer electrode.

2.7.2.2 Silicate electrode

The silicate electrode is expressed by Eq. 2-78. The potassium chemical potential of this electrode is the consequence of the equilibrium between $KSi_xO_{2x+0.5}$, SiO_2 and the ambient oxygen atmosphere:

$$K + \frac{1}{4}O_2 + xSiO_2 \leftrightarrow KSi_xO_{\left(2x+\frac{1}{2}\right)}. \qquad \text{Eq. 2-87}$$

Therefore, the potassium activity of the silicate electrode can be written as

$$\ln a'_K = \frac{\left(\Delta_f G^\circ_{KSi_xO_{2x+0.5}} - x\Delta_f G^\circ_{SiO_2}\right)}{RT} - \frac{1}{4}\ln pO_2 + \ln\left(\frac{a_{KSi_xO_{\left(2x+\frac{1}{2}\right)}}}{a^x_{SiO_2}}\right), \qquad \text{Eq. 2-88}$$

where $\Delta_f G^\circ_{KSi_xO_{2x+0.5}}$,$\Delta_f G^\circ_{SiO_2}$ $a_{KSi_xO_{\left(2x+\frac{1}{2}\right)}}$ and a_{SiO_2} denotes the standard Gibbs energies of formation and activities of $KSi_xO_{\left(2x+\frac{1}{2}\right)}$ and SiO_2, respectively. In pure compound the values of activities are equal to unity and hence the Eq. 2-88 can be rewritten as

$$\ln a'_K = \frac{\left(\Delta_f G^\circ_{KSi_xO_{2x+0.5}} - x\Delta_f G^\circ_{SiO_2}\right)}{RT} - \frac{1}{4}\ln pO_2. \qquad \text{Eq. 2-89}$$

There are literature data on the standard Gibbs energy of formation of $KSi_xO_{2x+0.5}$ given in [85].

2.8 Measuring principles

2.8.1 Isothermal voltage measurements of $a_\oplus$

In order to obtain the p-electronic conduction parameter on K-β-Al_2O_3 (KBA) and NASICON, cells of the type shown in the Table 2-7 have been investigated.

Table 2-7 Galvanic cell under isothermal condition for evaluation of $a_\oplus$

Cell construction	cell
Pt, O_2, CO_2, K_2CO_3(Au)$_{a''_K}$|KBA|$_{a'_K}$ NiO/FeO_{glass}, FeNi48 (O_2, CO_2) Pt	I
Pt, O_2, CO_2, K_2CO_3(Au) $_{a''_K}$|KBA|$_{a'_K}$ $KSi_{1.5}O_{3.5}$, SiO_2, O_2, (CO_2) Pt	II
Pt, O_2, CO_2, Na_2CO_3(Au) $_{a''_{Na}}$|NASICON|$_{a'_{Na}}$ NiO/FeO_{glass}, FeNi48 (O_2, CO_2) Pt	III

In all experiments reported henceforth, a CO_2, O_2, K_2CO_3 (Au) and CO_2, O_2, Na_2CO_3 (Au) were used as a measuring electrodes on the left-hand side of cells (I), (II) and (III) (see above).

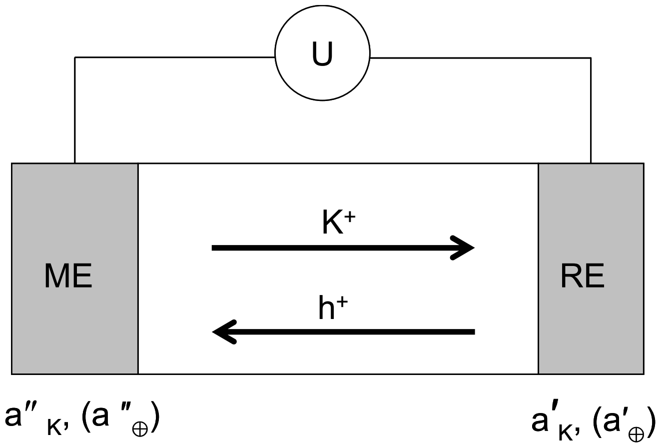

Fig. 2-16 Schematic sketch of galvanic cell

From previous data on $a_{\ominus}$ of sodium beta alumina [8, 12] and from the thermodynamic data on Gibbs energy of phases [79, 85] involved in the establishment of chemical potential of the electrodes it can be estimated that $a'' \ll a_{\ominus}$; $a' \ll a_{\ominus}$.
As consequence it implies that the electronic conductivity in material (K-beta-Al_2O_3 or NASICON), if present, is exclusively due to p-conduction. Hence, the voltage can be represented by Eq. 2-47 (cf. case (iii) in section 2.2). To evaluate the p-electronic conduction parameter two methods were used.

1) The chemical potential of the reference electrode is unknown. Nevertheless, the chemical potential of the magnifer electrode (see chapter 2.7.2) can be assumed to represent a temperature dependence of the following form

$$\lg\ a = A - \frac{B}{T}. \qquad \text{Eq. 2-90}$$

Eq. 2-47 can be evaluated in terms of $a_{\oplus}$ by means of a non-linear regression procedure taking into account the quantitative values of chemical potential at the measuring electrode and a field of experimental data U= (T, a''_M).

2) The second determination of $a_{\oplus}$ is based on the comparison of the cell voltage data influenced by electronic transference with the Nernstian cell voltage without electronic transference. The $a_{\oplus}$ value is calculated by substituting the chemical potential of the measuring electrode (a'') as well as of the reference electrode (a') into Eq. 2-47.

2.8.2 Non-isothermal voltage measurement

To determine the p-electronic conduction parameter of Na-β-Al_2O_3 the thermo cell IV has been studied. In the present work the side whose temperature is maintained constant (see Fig. 2-17), connected to the positive pole of the multimeter. This electrode later will be called as reference electrode. The thermoelectric power is determined as slope of voltage vs. temperature gradient.

A very well defined sodium activity is established by using CO_2 / O_2 gas composition in contact with sodium carbonate. The sodium chemical potential is determined by Eq. 2-75. Hence it follows that

$$\frac{d\mu}{dT} = \left(\frac{d\mu^0_{Na}}{dT} + \frac{d}{dT}(RT\ln a_{Na})\right) = -S^0_{Na} + R\ln a_{Na} + RT\frac{d}{dT}(\ln a_{Na}). \qquad \text{Eq. 2-91}$$

Substituting equation 2-90 in equation 2-59, the thermoelectric power of cell IV in terms of p-electronic ($a_\oplus$) reads as

$$\varepsilon = \frac{1}{F}\left[\left(1+\frac{a_\oplus}{a_{Na}}\right)^{-1}\left(-\left(C_1 + R\ln a_{Na} + RT\frac{\partial}{\partial T}(\ln a_{Na})\right)\right) + \left(1+\frac{a_{Na}}{a_\oplus}\right)^{-1}\left(-R\ln a_{Na^+} + C_2\right)\right] + C_3$$

Eq. 2-92

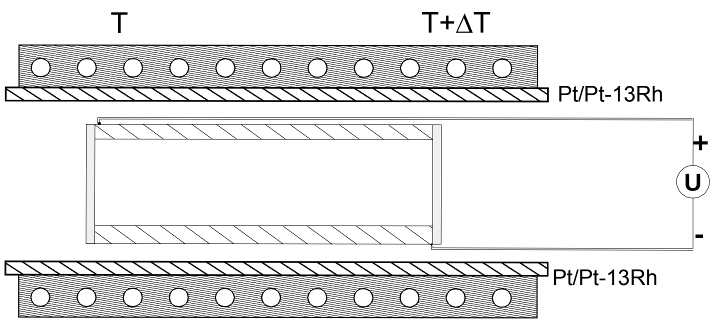

Fig. 2- 17 Schematic diagram of the thermocell

where: $C_1 = \left(-S^0_{Na}\right) + \overline{S}_{Na^+} + \frac{Q^*_{Na+}}{T}$,

$$C_2 = \left(\overline{S^\circ}_e + \frac{Q^*_e}{T}\right)$$

and $C_3 = \varepsilon^{(Pt)}$.

Even though C_1, C_2 are unknowns, Eq. 2-92 can exactly be evaluated in terms of p-electronic conduction parameter ($a_\oplus$) by means of non-linear regression technique taking into account a field of $\varepsilon = f\left(T, p_{CO_2}, p_{O_2}\right)$.

2.8.3 Electrode characterization

The measuring principle is based on a galvanic cell that allows to reproducibly transform the potassium activity into an oxygen chemical potential and to measure that by means of an oxygen ion conducting solid electrolyte, i.e. yttria stabilized zirconia (YSZ). The galvanic cells used to evaluated the chemical potential of the electrodes are shown in Table 2-8.

Table 2-8 Galvanic cells for the determination of the chemical potential of the reference electrodes

Construction of galvanic cell	cell
$\text{Pt}, \mid CO_2, O_2,\ K_2CO_3(\text{Au})_{a''_K} \mid \text{KBA}(\text{Au}) \mid \text{YSZ} \mid \text{KBA}(\text{Au})_{a'_K} \mid \text{NiOFeO}_{(\text{glass})}\text{FeNi48}(\text{Au}) \mid, \text{Pt}$	VI
$\text{Pt}, \mid \text{FeNi48}, \text{NiOFeO}_{(\text{glass})\,a'_K=f(T)} \mid \text{KBA}(\text{Au}) \mid \text{YSZ} \mid \text{KBA}(\text{Au})_{a''_K} \mid KSi_xO_{2x+0.5}, SiO_2, (\text{Au}) \mid O_2, \text{Pt}$	VII

Between the potassium and the oxygen chemical potential, the potassium oxide dissolved in K-(β+β'')-Al_2O_3 (KBA) serves as the connecting link. For that purpose, both electrodes of the cell VI consists of a sintered ceramic pellet of K-(β+β'')-Al_2O_3 that in its turn is in contact with, a pellet of K_2CO_3 on the one electrode side and, on the other electrode side, the heterogeneous phase equilibrium that is to be characterize. The later one comprises of a solid solution of NiO and FeO dissolved in a borate glass [87].

In cell VII the sintered ceramic KBA pellet is in contact with a dehydrated suspension of potassium water glass, i.e. $KSi_xO_{2x+0.5}$ on one side and on the other side of electrode is a solid solution of the metal oxide dissolved in a borate glass.

The cells under investigation (VI and VII) were symmetrical with regard to the arrangement of both the potassium beta alumina (KBA) pellets and the oxygen ion conductor. At each of the interfaces YSZ/KBA the potassium and the oxygen chemical potentials are interrelated to each other by the following equilibrium:

$$K_2O(\beta(\beta'') \leftrightarrow 2K(a_K) + \frac{1}{2}O_2(p_{O_2}). \qquad \text{Eq. 2-93}$$

As a consequence of Eq. 2-93, it follows for the oxygen equilibrium partial pressures p'_{O_2} and p''_{O_2} at both the interfaces KBA/YSZ:

$$\ln p_{O_2} = \frac{2\Delta_f G^\circ_{K_2O}}{RT} - 4\ln a_K + 2\ln a_{K_2O}, \qquad \text{Eq. 2-94}$$

where $\Delta_f G^\circ_{K_2O}$ is the standard Gibbs energy of formation of potassium oxide.

Substituting Eq. 2-94 into Eq. 2-66, the relationship for the cell voltage can be rewritten in terms of potassium and potassium oxide activities at both electrodes:

$$U = -\frac{RT}{F}\ln\frac{a''_K}{a'_K} + \frac{RT}{2F}\ln\frac{a''_{K_2O}}{a'_{K_2O}} \qquad \text{Eq. 2-95}$$

where a''_K, a'_K, a''_{K_2O} and a'_{K_2O} are the potassium and potassium oxide activities, respectively, established at both of the YSZ/KBA interfaces.

The potassium activities in Eq. 2-95 are defined by those phases that are in contact with KBA. The potassium oxide activity in of the KBA pellet adjacent to the electrolyte is fixed by the nature and the thermodynamic stability of the constituent phases of KBA as well as the proportions of those phases. From previous investigations [77], it was found for sodium beta alumina, that sodium oxide at fixed temperature changes with changing sodium activity. Analogically we can deduce that the potassium oxide activity is not constant but is a function of potassium activity in surrounding.

The electronic short-circuit owing to the gold wires within or gold layers outside the sintered bodies of the electrodes guarantees that any potassium potential gradient throughout these pellet (the pellet which participate to the electrodes) is instantaneously balanced out by potassium diffusion. As a result, the potassium activity established at the right KBA/YSZ interface is always identical to the potassium chemical potential of electrode of the right side of the cell and similarly can be conclude also for the left side of the cell.

The fundament measuring principle is based on Eq. 2-95. This equation allows to determine the unknown potassium activity by comparing it with the known potassium activity (a''_K). The result of this comparison is expressed numerically in the voltage as a function of a” for cell VI and as function of p_{O_2} for cell VII. If the potassium activity a'_K to be determined is within the measuring interval, the voltage of cells (cell VI and VII) will reach zero. Then and only then, a'_K is equal to a''_K and a'_{K_2O} as well a''_{K_2O} will be identical and cancels out in Eq. 2-95. Therefore it holds that

$$U = 0 \Rightarrow \ln a''_K = \ln a'_K \ . \qquad \text{Eq. 2-96}$$

By that, the standard Gibbs energy of formation of $KSi_xO_{2x+0.5}$ can be evaluated as

$$\Delta_f G^\circ_{KSi_xO_{2x+0.5}} = RT\left(\ln a''_K + \frac{1}{4}\ln p_{O_2}\right) + x\Delta_f G^\circ_{SiO_2} \ , \qquad \text{Eq. 2-97}$$

where a''_K denote the potassium activity of magnifer electrode which is known from cell VI. Otherwise, if the voltage measured is different from zero, the potassium oxide activities a' and a'' cannot be neglected and have to be taken into account [88].

2.8.3.1 Characterization of K_2O in K-β-β''-Al_2O_3

The principle of evaluation of the potassium oxide as a function of the potassium activity is similar with that discussed for the sodium activity dependence of sodium oxide in $NaSb_{1.67}O_{4.43}$-$NaSbO_3$ binary phase.

The potassium oxide activity in K-β-β''-Al_2O_3 (KBA) was evaluated by using the cell construction type V (see in section 2.6) where the KBA pellet was used instead of the $NaSb_{1.67}O_{4.67}$-$NaSbO_3$ pellet and the cell under investigation can be represented as

$$Pt\,|\,CO_2,O_2 \underset{a'_K}{|} K_2CO_3\,(Au) \underset{a'''_K}{|} KBA(Au) \underset{a''_K,\,p''_{O_2}}{|} YSZ \underset{p'_{O_2}}{|} O_2\,|\,Pt\,. \qquad \text{VIII}$$

The measuring electrode consists of a sintered pellet of K-(β/β'')-Al_2O_3 in contact with a densified disk of K_2CO_3. Both of these are electronically short-circuited using metallic Au so as to transmit the potassium activity established at the $CO_2,O_2|K_2CO_3$ interface to that of $K_2CO_3|KBA$. The potassium activity at the $CO_2,O_2|K_2CO_3$ interface is established according to Eq. 2-73 (see 2.7.1)

The potassium oxide activity a_{K_2O} in a biphasic mixture (β/β'') of KBA has to be unambiguously fixed at a constant temperature and pressure by the Gibbs phase rule. Hence, if the a_{K_2O} is invariant, then the p_{O_2} at the KBA| YSZ interface has to be fixed by the equilibrium between the two existing phases (β/β''). Therefore, the equilibrium can be expressed by Eq. 2-93.

From Eq. 2-93, it follows that the potassium oxide activity in a β/β″ mixture can be expressed by the equation

$$[K_2O]_{\beta\text{-}\beta''} \leftrightarrow 2K + 1/2O_2. \qquad \text{Eq. 2-98}$$

The galvanic cell is a stacked pellet assembly in which both the reference and the measuring electrodes are exposed to the same gas atmosphere, CO_2 + O_2 mixture in this case. Whilst both of the gas components, i.e. CO_2 and O_2 act as the potential determining species at the measuring electrode, only O_2 is the potential determining one at the reference electrode. Hence, the equilibrium existing at the reference electrode may be written as

$1/2O_2 + 2e^-(Pt) \leftrightarrow O^{2-}$ (YSZ). Eq. 2-99

Taking Eq. 2-74 and 2-99 into consideration, Eq. 2-66 can be rewritten in terms of potassium oxide activity as follows

$$\ln a_{K_2O} = \frac{2FU}{RT} - \frac{\Delta_f G^\circ{}_{K_2O} - \Delta_f G^\circ{}_{K_2CO_3} + \Delta_f G^\circ{}_{CO_2}}{RT} - \ln p_{CO_2} \ . \qquad \text{Eq. 2-100}$$

Eq. 2-100 enables the determination of the potassium oxide activity and thus the thermodynamic stability of the β''-phase by measuring the galvanic cell voltage at known CO_2 partial pressure of the gas atmosphere.

3. Experimental

3.1 Techniques to characterize

3.1.1 Chemical Analysis

Potassium, sodium and alumina in Na- and K-beta-Al_2O_3 were analyzed by optical emission and optical absorption spectrometry with inductively plasma excitation (OES-ICP, JY 70 Plus, Instruments S.A., France). Carrier hot gas extraction method was used in a resistance furnace at T $>$ 2500° C, (TC-436 DR, Leco, USA) to determine oxygen contents in K-beta-Al_2O_3, Na-beta-Al_2O_3 and NASICON.

3.1.2 X-ray analysis and scanning electron microscopy

The phase composition was analyzed by X-ray diffractometry (XRD) (Siemens Diffractometer D5000/Kristalloflex) using Cu-Kα_1 radiation (λ = 1.5418Å) and a graphite monochromator. The step size was 0.02°, and the time step was 2 s for phase analysis, the program DIFRACAT was used.

The microstructure and the phase composition of K-beta-Al_2O_3 were investigated by scanning electron microscopy (SEM) (Zeiss DSM982 GEMINI) coupled with EDX (Oxford-Instrument ISIS 300).

3.1.2.1 Ceramographic preparation

The beta aluminates are extremely sensitive to water and even react with moisture in air. Hence preparation of commercially available sodium and potassium beta aluminates were done in complete absence of water and moisture. Between each step in the ceramographic preparation the sample was stored in evacuated desiccators filled with phosphorus pent oxide (P_2O_5) in order to prevent any possible reaction with atmosphere. The polishing procedure of the commercial lapped beta-alumina pellet is outlined in Table 3-1.

Table 3-1 Ceramographic preparation of K- and Na-beta-Al_2O_3

<table>
<tr><th colspan="2">Step</th><th>Substrate</th><th>Diamond spray [µm]</th><th>Lubricant</th><th>Time [min]</th><th>Pressure [N]</th><th>Speed U/min</th></tr>
<tr><td>1</td><td rowspan="3">Polishing</td><td>Texmet (Nylon cloth)</td><td>6</td><td>Butandiol</td><td>20-45</td><td>90</td><td>150</td></tr>
<tr><td>2</td><td>DP-Dac (Nylon cloth)</td><td>3</td><td>Butandiol</td><td>40-60</td><td>90</td><td>150</td></tr>
<tr><td>3</td><td>DP-Dac</td><td>1</td><td>Butandiol</td><td>30-60</td><td>90</td><td>150</td></tr>
</table>

For microstructural analysis, the surface of the K- and Na-beta-Al_2O_3 sample were polished to a 1 μm finish and etched for 20 min at 1693 K.

3.2. Solid electrolytes

The following solid electrolytes (SE) were used to study the p-electronic conduction parameter as depicted in the Table 3-2:

Table 3-2 Solid electrolytes under investigation

SE	Company	Form	Dimension
K-beta-Al_2O_3	Ionotec Inc. UK	Pellet	16 mm * 0.6 mm *)
Na-beta-Al_2O_3	Ceramatec Inc. UK	Tube	20 mm * 25 mm * 0.2 mm**)
NASICON	Laboratory-prepared	Pellet	10 mm * 1.0 mm*)

*) Diameter * Thickness

**) Diameter* Height* Thickness

3.2.1 K-beta-Al_2O_3

The commercial K-beta-Al_2O_3 (KBA) pellet supplied by Ionotec Inc., UK with dimensions 16 mm diameter and thickness 0.6 mm has a chemical composition, corresponding to 11.58 wt% K_2O; 0.73 wt% Li_2O and rest Al_2O_3.

Fig. 3-1 shows the XRD pattern of the K-beta-Al_2O_3 Ionotec Inc., UK. The pattern reveals that the phase composition of the material is a mixture of β- and β''-alumina.

The phase compositions (β and β'') in KBA were calculated using modified method of Jonson et al. [89, 90]. Definition of f(β) as the fraction of β-Al_2O_3 phase in the material, is determined from the normalized intensity (I) values for the characteristic plane (110) β- and (01. 11) β″- diffraction peaks as follows:

$$f(\beta) = \frac{I_\beta}{I_\beta + 1.37\ I_{\beta''}} . \qquad \text{Eq. 3-1}$$

The characteristic peaks of β and β'' occur at 33.3° and 34.4° of 2θ, respectively. The peaks are well separated from each other (Fig. 3-2). The fraction of β-phase present in the commercial K-beta-Al_2O_3 pellet (Ionotec Inc., UK) is 13.8 %.

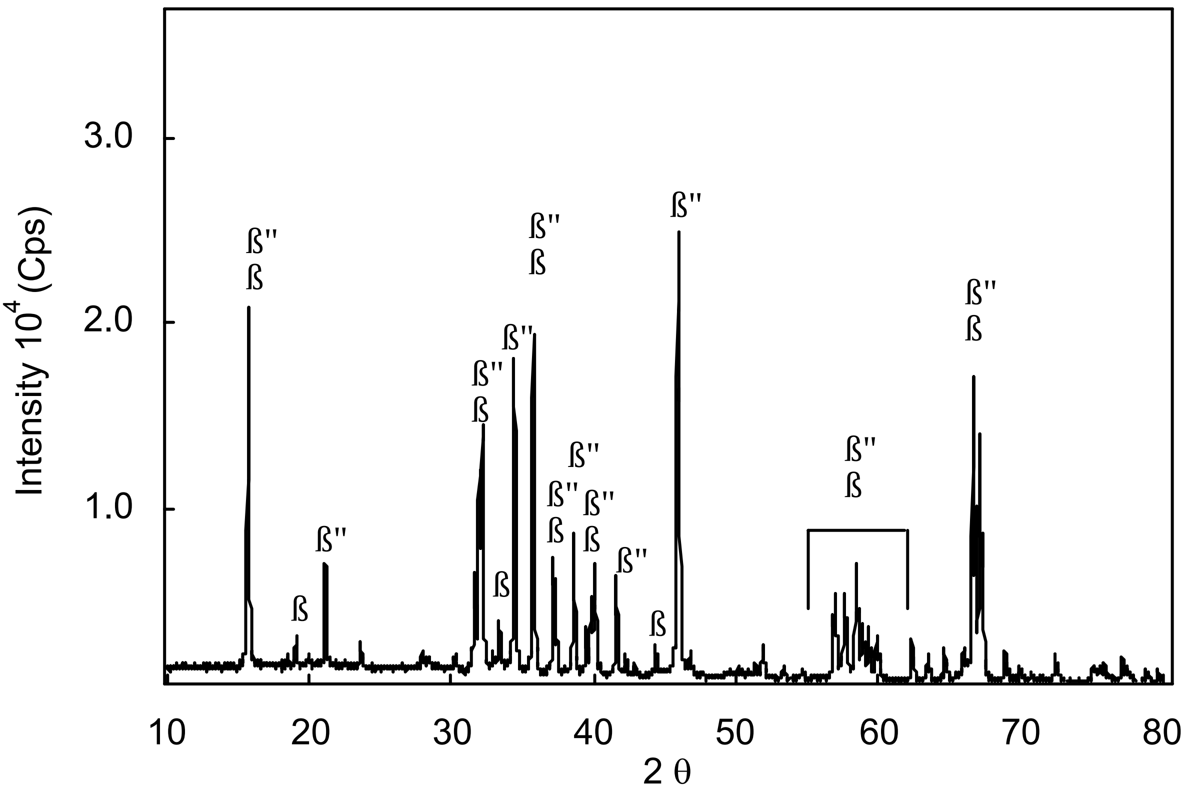

Fig. 3-1 XRD pattern of the commercial K-beta-Al_2O_3 pellet

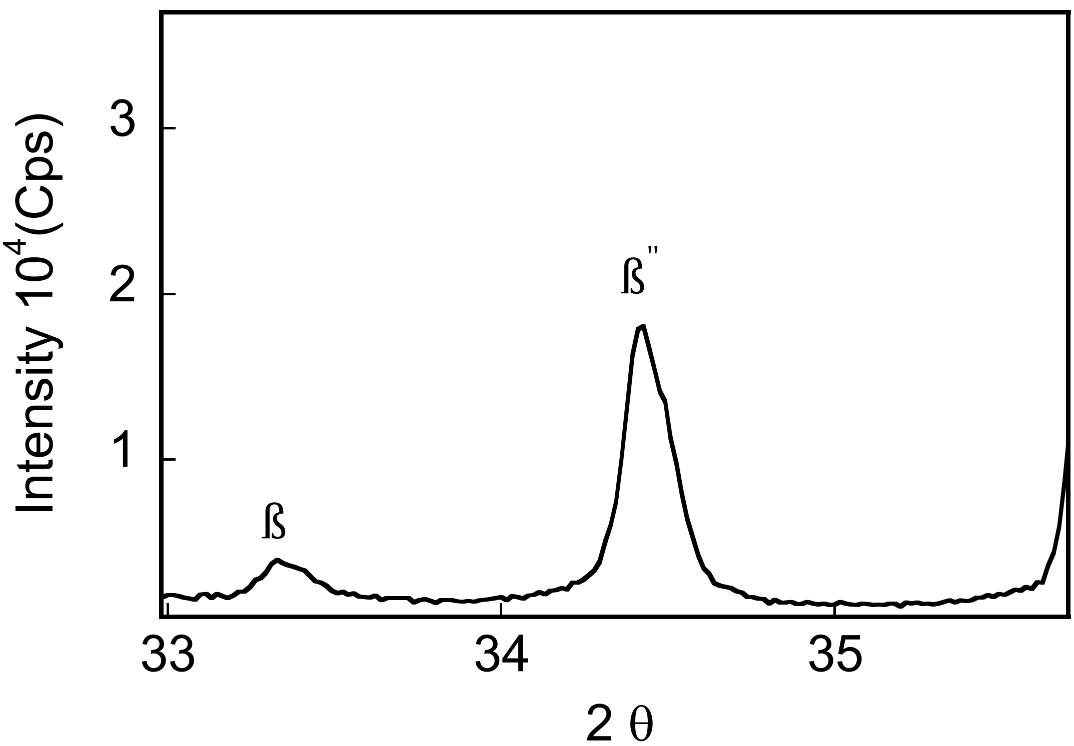

Fig 3-2 Enlargement of XRD pattern of K-beta-Al_2O_3 sample (from 33° to 35.8° of 2θ)

To evaluate the microstructural properties of sintered material (average grain and pore size and the porosity) the Image C Statistic program was used. The microstructure consists of plate-like grains (Fig 3-3) and of large agglomerates made up of micro-sized particles of about 1-10 μm, which is intrinsic characteristic of K-beta-Al_2O_3. The average grain size is 2μm.

The chemical analysis obtained from EDS spectra for K-beta-Al_2O_3 sample (Fig. 3-4) are in agreement with that taken from OES-ICP.

From Fig. 3-5 it is seen that the pores are not connected with each other and the shape of pores is polyhedral. The pore sizes are between 1.5- 5 μm and amount of the porosity of K-beta-Al_2O_3 is 3.6%.

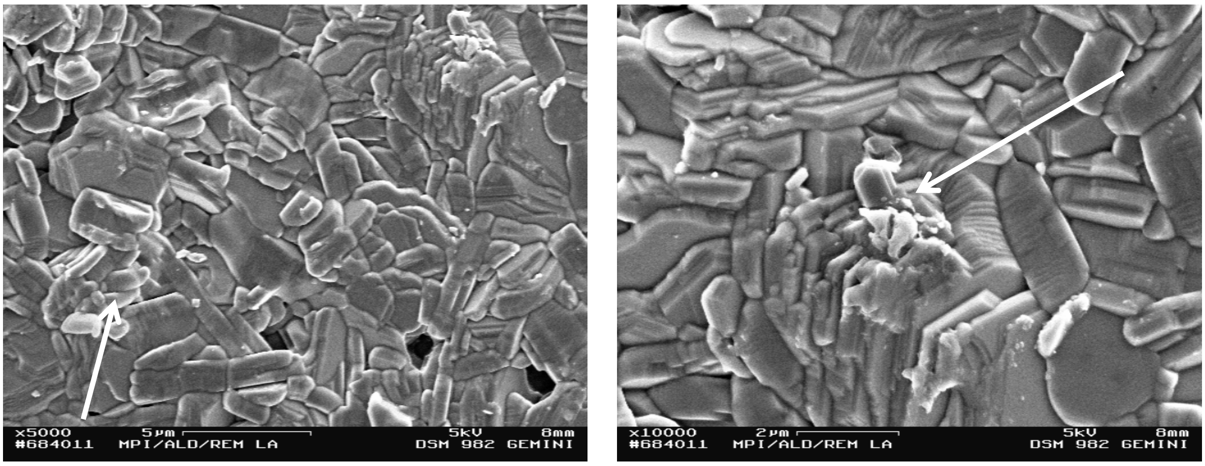

Fig. 3-3 SEM images of K-beta-Al_2O_3 in two different magnifications (Arrow denote the agglomeration)

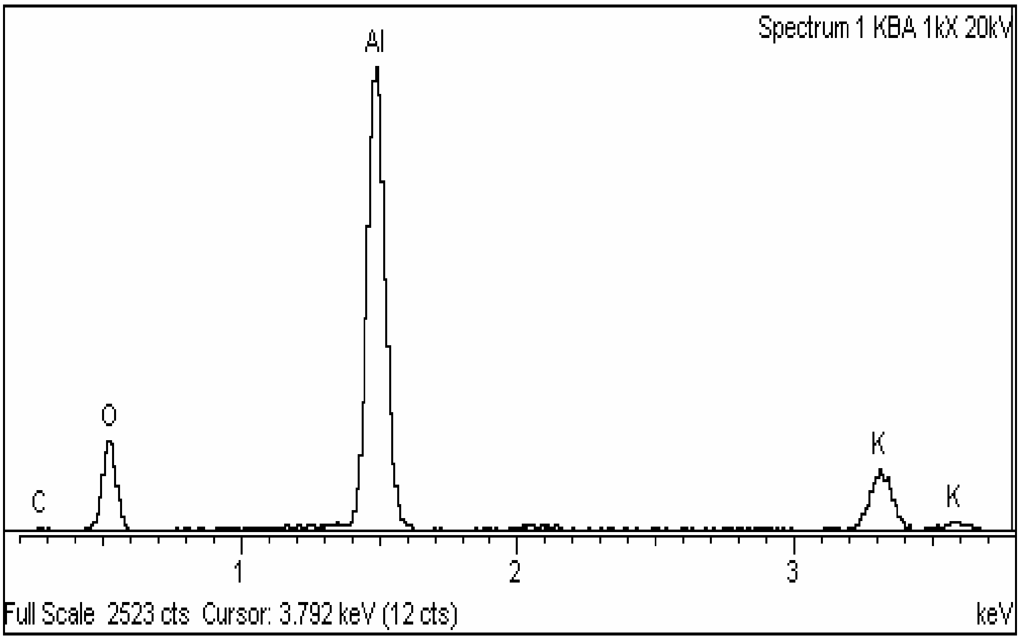

Fig. 3-4 EDS spectra for K-beta-Al_2O_3 material

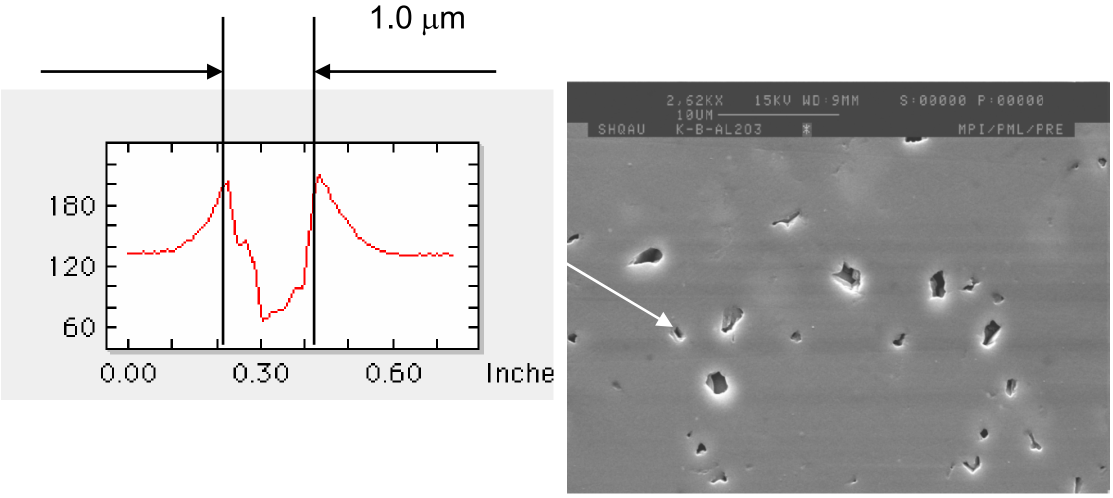

Fig. 3-5 SEM image and the corresponding line profile of a selected area of the surface of K-beta-Al_2O_3.

3.2.2 NASICON

The chemical composition of NASICON prepared by solid state reaction method was analysed using EDX technique. The EDS spectra for NASICON sample is shown in Fig. 3-6. According to the analysis this material has the formula $Na_3Zr_2Si_2PO_{12}$.

3.2.3 Characterization of Na-beta-Al_2O_3

The end closed Na-beta-Al_2O_3 (NBA) tube supplied by Asea Brown Boveri, Germany with internal diameter 25 mm and wall thickness 1 mm used as a solid electrolyte in the thermoelectric power measurement has an elementary composition of 7.2 wt% Na, 1.6 wt% Mg and 46.1 wt% Al (rest O). The material predominantly consisted of the β" phase, which was revealed by the XRD pattern obtained within 5 mass % limit of detection of the β phase.

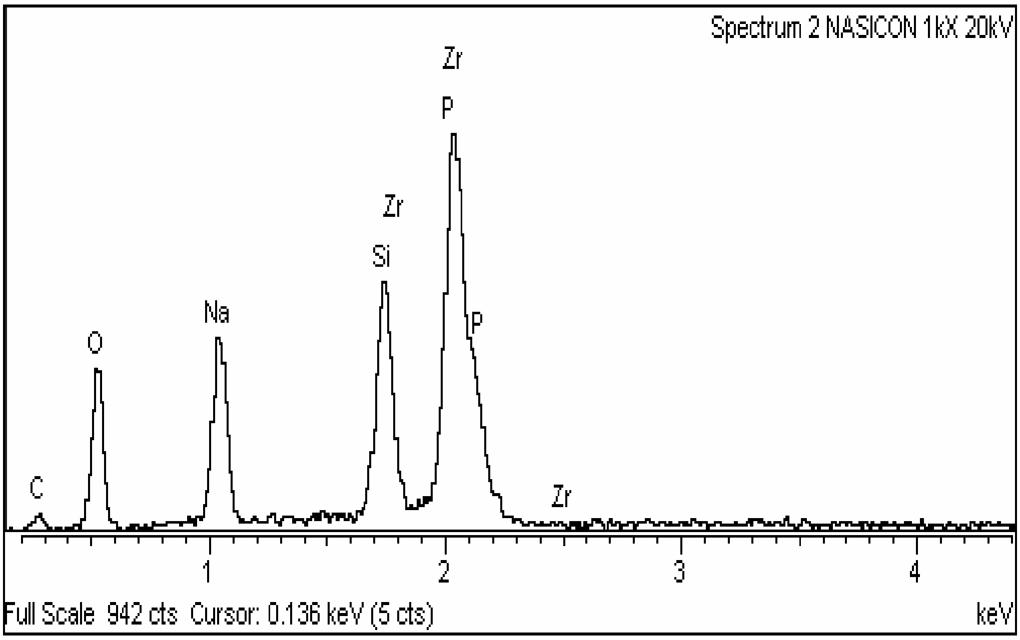

Fig. 3-6 EDS spectra for NASICON material

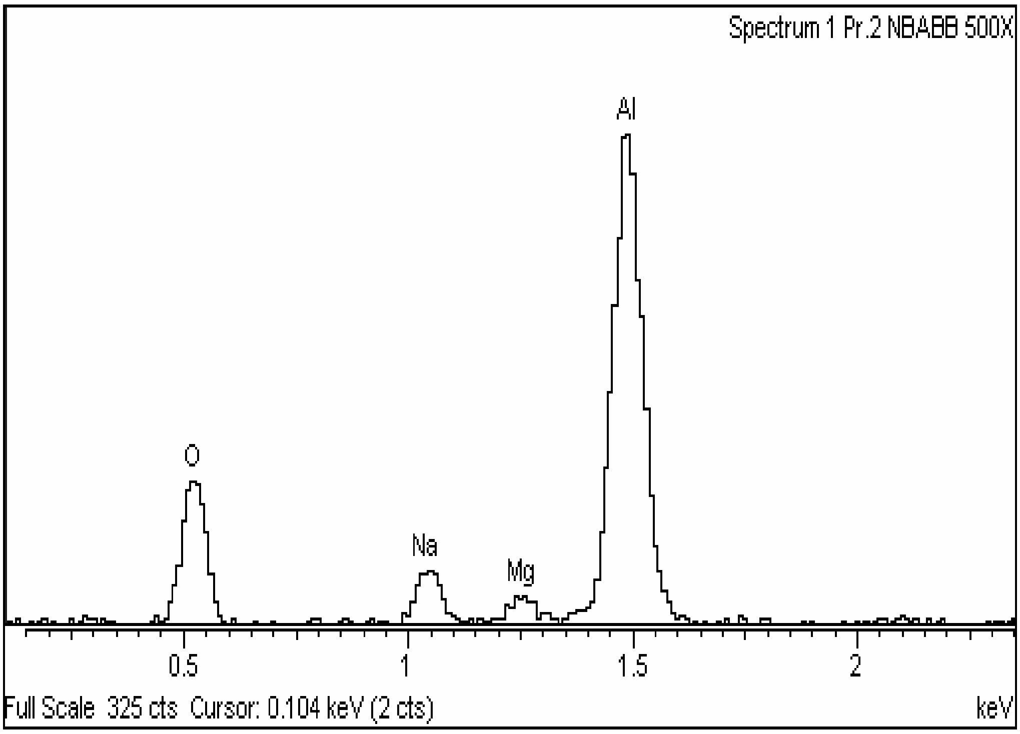

Fig. 3-7 EDS spectra for Na-beta-Al_2O_3 sample

3.3. Electrode preparation

Solid state electrochemical cells are usually constructed by combining a membrane of the solid electrolyte with a pair of electrodes.

3.3.1 Preparation of measuring electrode

The sensitive gas layer of the measuring electrode was manufactured by isostatically pressing (800 kN; 1 min) K_2CO_3 or Na_2CO_3 powder into a pellet of about 10mm in diameter and a thickness of 1-2 mm and sintering at 1023 K (K_2CO_3) and 923 K (Na_2CO_3). The gas mixture was established by successively diluting premixed O_2-CO_2 or CO_2-O_2-Ar gas mixtures with pure Ar (≤ 10 ppm impurities). For this purpose calibrated mass flow controllers (FC-2900; TYLAN General) were employed.
The premixed gases had the following compositions:
(1) Ar with 200 ppm O_2 and 200 ppm CO_2,
(2) Ar with 10^4 ppm O_2 and 10^4 ppm CO_2 and
(3) O_2 with 15 % CO_2.
The total gas flow through the sensor compartment was kept constant at a rate of 36 ml/min. For electrical resistance of the pellet to be less than 1 ohm, gold wires were statistically distributed within the pellet.

3.3.2 Preparation of the magnifer electrode

The magnifer electrode (Eq. 2-76 and Eq. 2-77), which was used as one of the reference electrodes, was prepared by encapsulating the solid electrolyte pellets into a FeNi (48) crucible (Krupp VDM GmbH) using a special solder glass [86]. The glass serves as a hermetical seal between the reference electrode side of the electrolyte and the gas in the

(b)

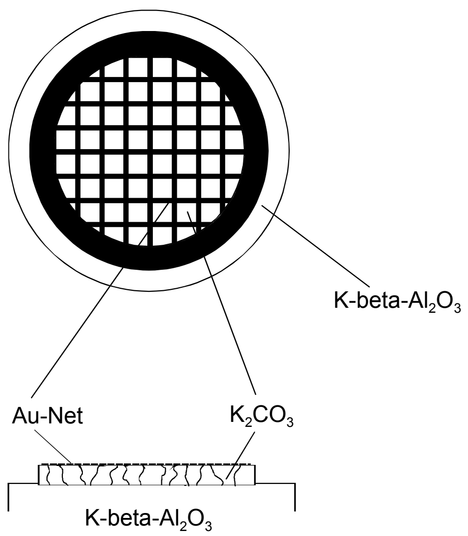

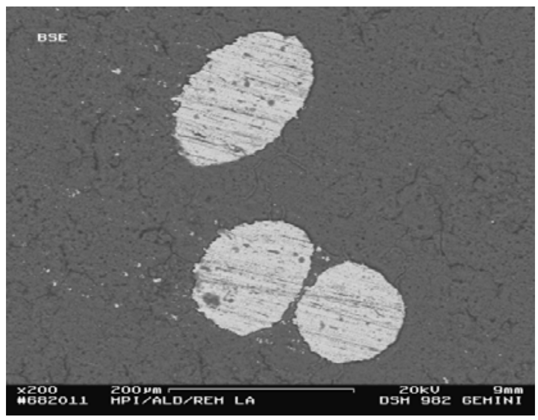

(a)

Fig 3-8 The carbonate electrode:
(a) Measuring electrode sketch
(b) SEM picture of K_2CO_3 with Au wire

ambience. By dissolving the oxides formed at the surface of the metallic crucible and by providing an intimate contact to the electrolyte and the metal, the glass simultaneously acts as the main component of the metal reference electrode.

3.3.3 Preparation of the silicate electrode

A mixture of a $KSi_xO_{2x+1/2}$ containing water glass and SiO_2 was used as reference electrode. The water glass was prepared by melting highly pure K_2CO_3 and SiO_2 in a molar ratio of about 1:3 at above 1673 K and dissolving the glass in pressurized water at 473 K. A layer of water glass was deposited on one side of the electrolyte pellet by dropping the solution and drying simultaneously adding particles of SiO_2 powder. The gold net along with platinum wires placed on this side of the sample served as part of the electrode for electrical contacts as shown in Fig 3-9. From the chemical analysis the composition of the water glass is $KSi_xO_{x+1/2}$ with x=1.5.

3.3.4 Preparation of two-phase $NaSbO_3$-$NaSb_{1.67}O_{4.33}$

3.3.4.1 Preparation of pure $NaSbO_3$

Pure $NaSbO_3$ was prepared by thoroughly mixing equimolar proportions of dried Na_2CO_3 and Sb_2O_4 in an agate mortar and firing the mixture at 1373 K for 8 h. The temperature of the mixture was increased to 1373 K in steps of 200 K for 10 h with intermittent cooling and mixing by regrinding. The mixture was subject to XRD after each cycle.

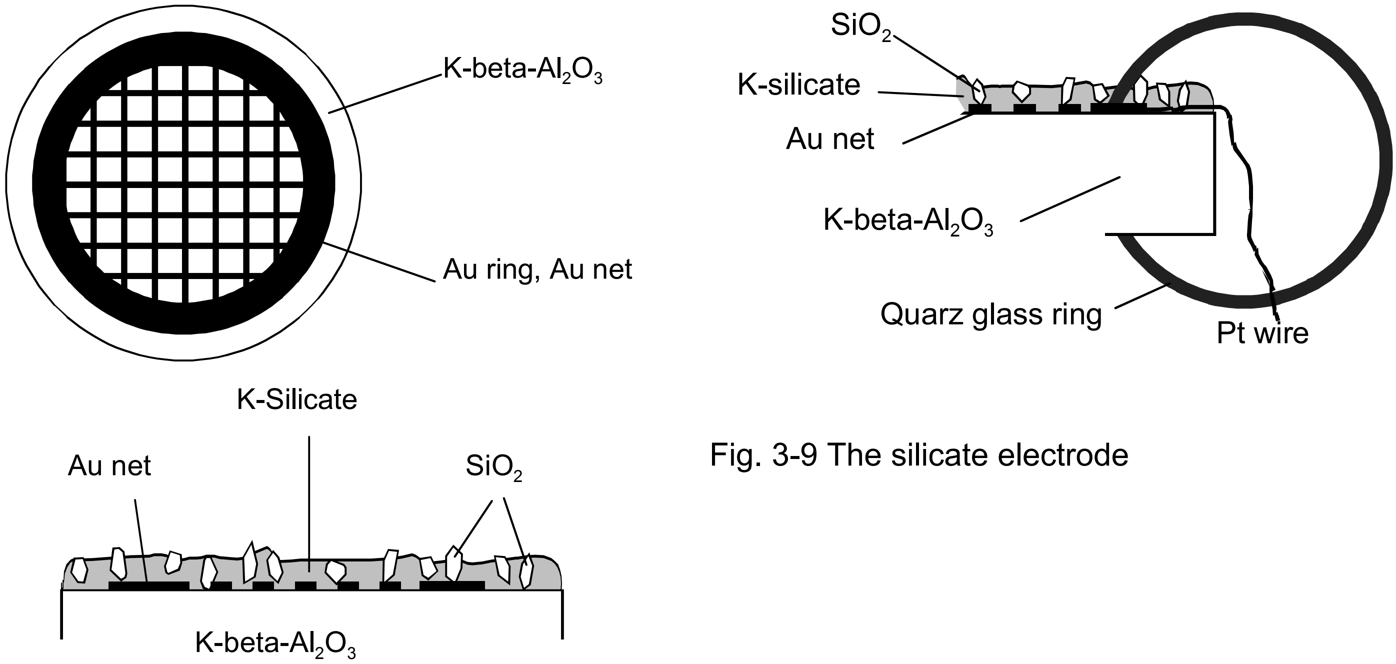

Fig. 3-9 The silicate electrode

3.3.4.2 Preparation of two-phase mixture of $NaSbO_3$ and $NaSb_{1.67}O_{4.33}$

The two-phase mixture of $NaSbO_3$ and $NaSb_{1.67}O_{4.33}$ was prepared by mixing 10 mol % α-Sb_2O_4 with 90 mol % $NaSbO_3$ within Pt wire, pelletizing the mixture and firing the pellet at 1373 K for 8 h. The heating procedure was similar as described in the above section. Gold wires were statistically distributed within the pellet for the same reason as described above for the carbonate pellet.

3.4. Galvanic cells

3.4.1 Isothermal condition

The system pellets were arranged to form a stacked assembly as shown for the respective cases in fig. 3-10 and 3-11. Pt wires along with Au nets served as electrical leads at the electrodes. The galvanic cell used to evaluate $a_{\oplus}$ was spring loaded (Fig. 3-12) and located in the uniform temperature zone of an inductively heated furnace. The whole set-up was flushed with CO_2-O_2-(Ar) gas mixtures of known compositions as given in section 3.3. The voltage was measured using high impedance electrometer (KEITHLEY 617, USA). Details of experimental apparatus are given in Fig. 3-13.

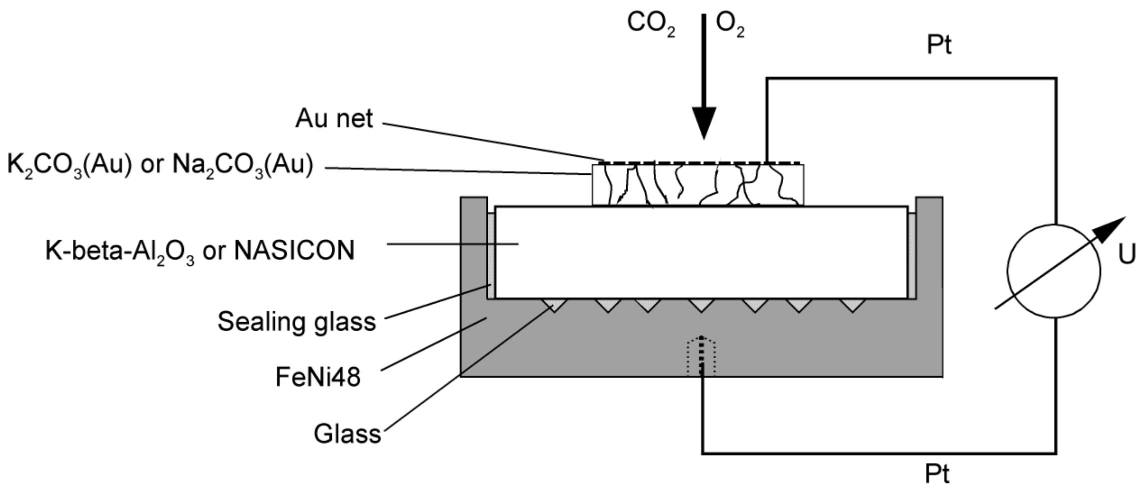

Fig. 3-10 Schematic set-up of galvanic cell I and cell III

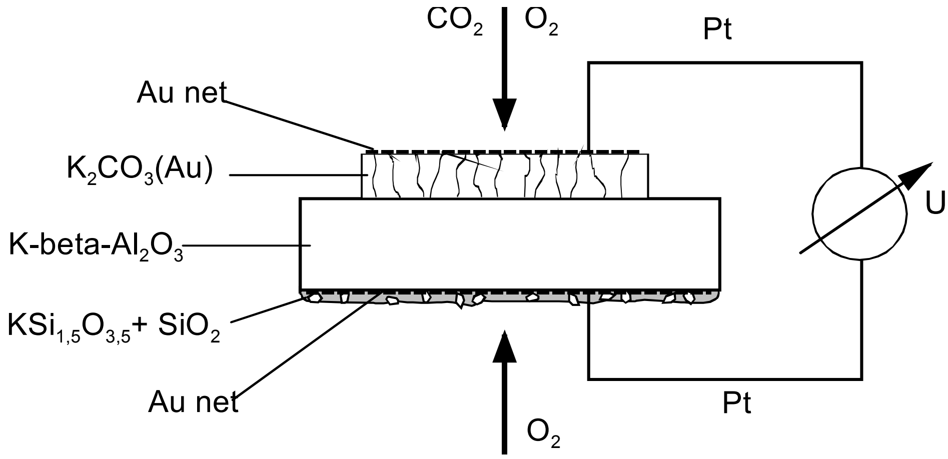

Fig. 3-11 Schematic set-up of galvanic cell II

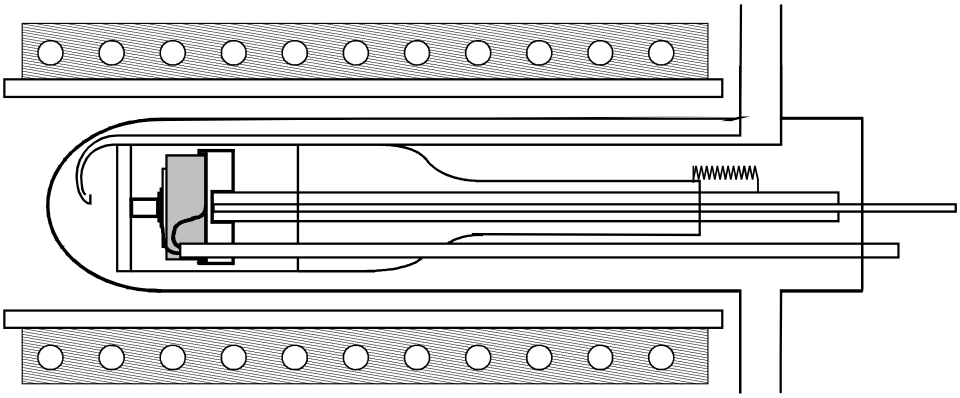

Fig. 3-12 Placement of the galvanic cell in an induction-heated furnace

3.4.2 Non-isothermal condition

The cell (V) was held in a position between two α-alumina blocks and the whole set-up was spring loaded. Two pre-calibrated Pt-10%Rh/Pt (type-S) thermocouples were used for the measurement of temperature. The whole assembly was placed in a vertical furnace, thus maintaining a linear temperature gradient across the two ends of the sample. The measurements were carried out at various CO_2-O_2 partial pressures as shown in section 3.2.1. Two Na_2CO_3 pellets were used as CO_2 sensitive layers.

3.4.3 Determination of thermodynamic stability of the material

The experimental set-up of the galvanic cell used to evaluate the thermodynamic stability of the two-phase material is schematically illustrated in Fig. 3-14 and 3-15. An yttria-stabilized zirconia (YSZ) pellet having the composition $Zr_{0.91}Y_{0.09}O_{1.955}$ (Friatec AG, Germany) with 10 mm diameter, 1 mm thickness and relative density greater than 99 % was used as the oxide-ion conductor.

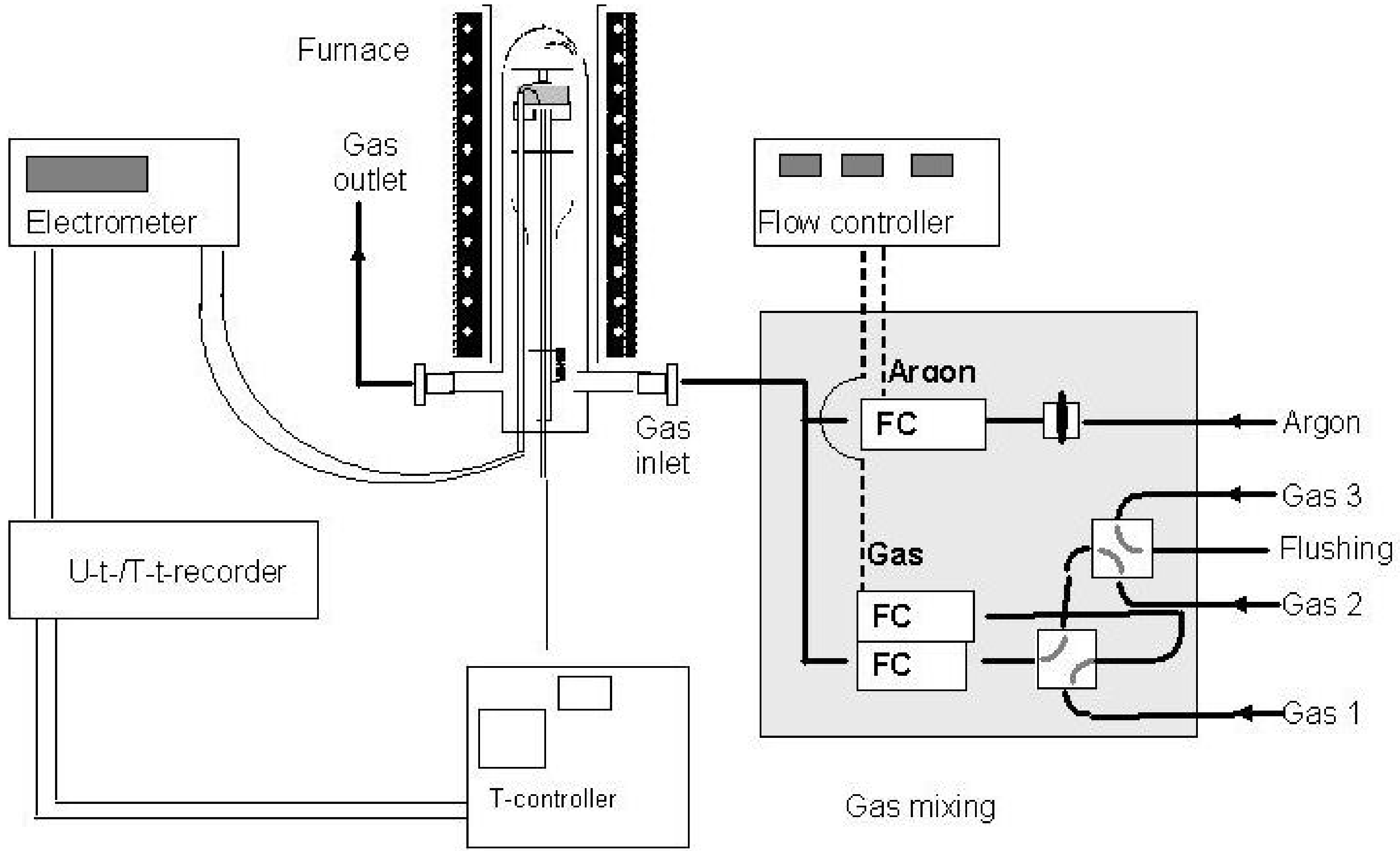

Fig. 3-13 Experimental apparatus

One of the parallel surfaces of the pellet was ground and polished in order to achieve a better contact with the two-phase pellet at the interface. The other surface of the YSZ pellet was painted with platinum paste (DEMETRON 308 A, Germany) which was fired in air at 1273 K to form an electrode reversible to O^{2-} ions. A sintered two-phase pellet (for detail information refer to the Table 3-3) with composition given in section 3.5 formed a part of the measuring electrode.

In order to electronically short-circuit the K-beta-Al_2O_3 disk, the sputtering method was used (see sputtering method). In case of the Na-Sb-O system, the gold wires were used within the pellet as shown for the carbonate pellet (cf. Fig. 3-14). The room temperature resistance of the electrode between the parallel surfaces was verified to be less than 1 Ω.

Table 3-3 Material under investigation

Material	Measuring electrode
K-β/β"-Al_2O_3	Pt; CO_2,O_2, K_2CO_3(Au) K-β/β"-Al_2O_3
$NaSb_{1.67}O_{4.33}$ +$NaSbO_3$	Pt; CO_2,O_2, Na_2CO_3(Au), $NaSb_{1.67}O_{4.33}$ +$NaSbO_3$

The three solids were arranged in the similar form illustrated in section 3.4.1.

3.4.3.1 Sputtering method

To obtain an electronically short circuit through the pellets an Au layer of about 300 nm thickness was sputtered on to the pellets. The sputtering layer is in the form of a ring as shown in Fig. 3-14. Hence, the interface of YSZ which is in contact with the KBA pellet is still reversible only to O^{2-}. The sputtering method is described in the Table 3-4.

Table 3-4 Sputtering conditions

Method	DC magnetron sputtering		
Target	Gold, 5 cm diameter		
Film thickness	300 nm		
Deposition conditions	0.02Torr Ar	20 W	25 °C
Post annealing	1 h at 350 °C in air		

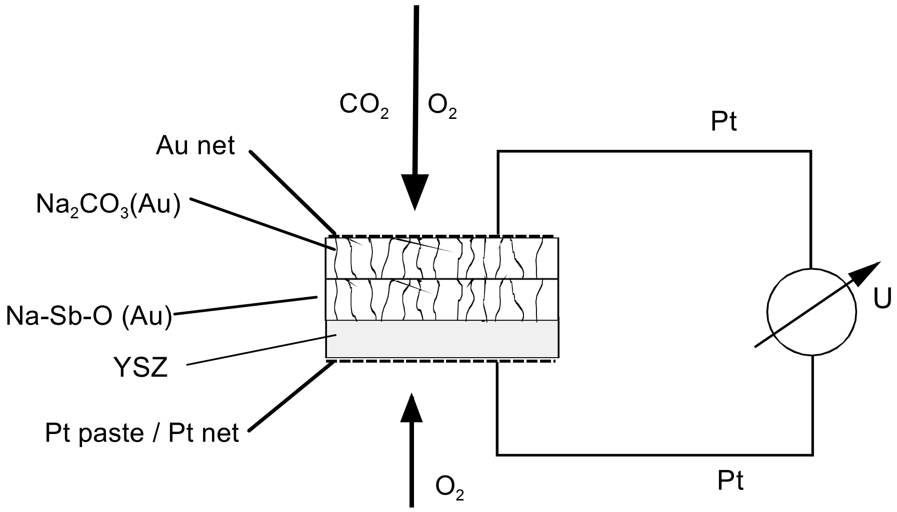

Fig. 3-14 Schematic sketch of galvanic cell used to evaluate thermodynamic stability of $NaSbO_3$-$NaSb_{1.67}O_{4.33}$ phase equilibria

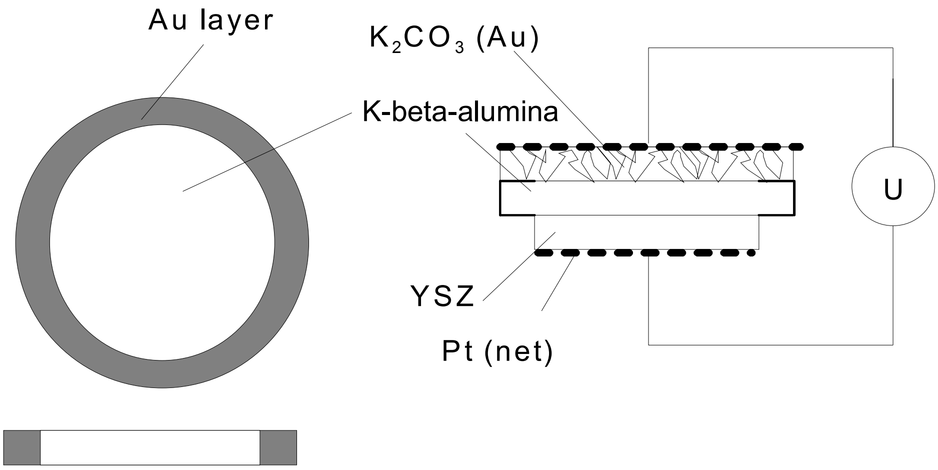

Fig. 3-15 Top and front view of the K-beta-Al_2O_3 disk sputtered with Au where the hatched area represents the Au layer together with schematic arrangement of galvanic cell VIII

3.4.4 Determination of the chemical potential of the reference electrode

The galvanic cells represented schematically in Table 2-8 were used to determine the potassium activity of the reference electrode. A pellet of YSZ (see section 3-2) was used as an oxide-ion conductor. Both of the parallel surfaces of the pellets were ground and polished in order to achieve a better contact to the K-β- and β''-Al_2O_3 phase at the interface. The sputtering method was used to obtain electronically short-circuit in K-beta-Al_2O_3 pellet (see sputtering method). The K-beta-Al_2O_3 in intimate contact with the electrodes used for the $a_{\oplus}$ evaluation as described above act as a part of the electrodes of the galvanic cell used for the determination of the chemical potential of the electrodes.

These cells shown in fig 3-16 and 3-17 are located in a similar way as the galvanic cells used for the $a_{\oplus}$ evaluation as described above.

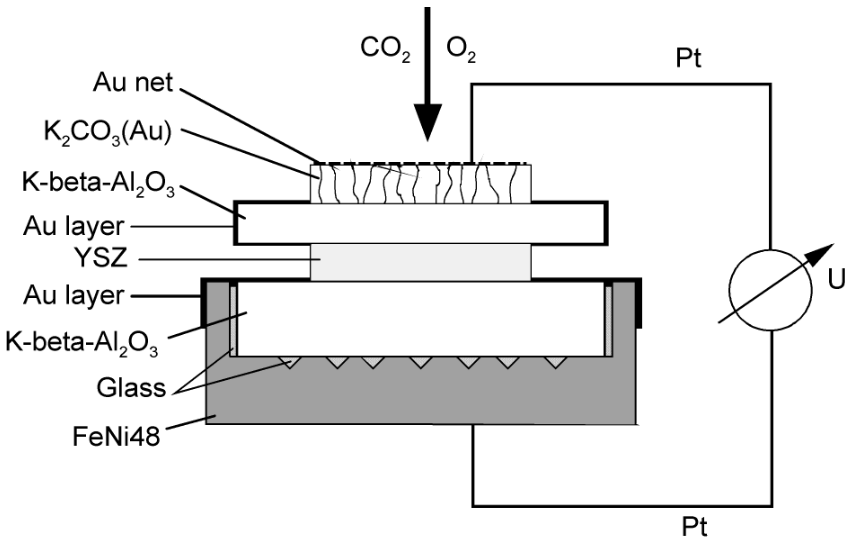

Fig. 3- 16 Schematic set-up of galvanic cell VI

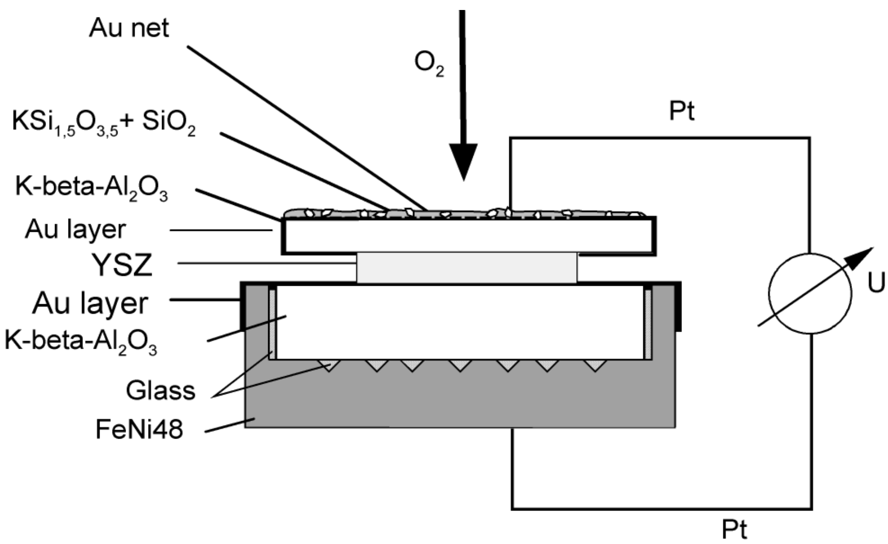

Fig. 3- 17 Schematic set-up of galvanic cell VII

4. Result and discussion

4.1 Thermodynamic stability of K-beta-Al_2O_3

The voltage of the cell VIII is related to the chemical potential of K_2O dissolved in K-beta-Al_2O_3 as well to CO_2 partial pressure in the ambient through the Eq. 2-100. The development of the voltage of cell VIII on changing the temperature or the gas composition usually takes a few minutes until a new stable value is established. The reversible voltage of the cell VIII at a particular gas composition (p_{CO_2}= 19.4 *10^{-6} [bar] and p_{O_2} = 19.7 *10^{-6} [bar]) is plotted as a function of temperature (Fig. 4-1). The voltage varies linearly with temperature, which indicates that the K_2O activity is constant within the potassium chemical potential interval (cf. eq. 2-100). By inserting the experimental values of the voltage obtained along with those of p_{CO_2} and the thermodynamic data for K_2CO_3 and CO_2 which were taken from JANAF [79] in Eq. 2-100, the a_{K_2O} for the β-β'' phase mixture can be calculated at different temperatures and varying potassium activities. The data points of a_{K_2O} are plotted as a function of potassium activity of the carbonate electrode (Fig. 4-2). It is visible from this figure that for various temperatures the potassium activity dependence of the potassium oxide activity appears to be a plateau.

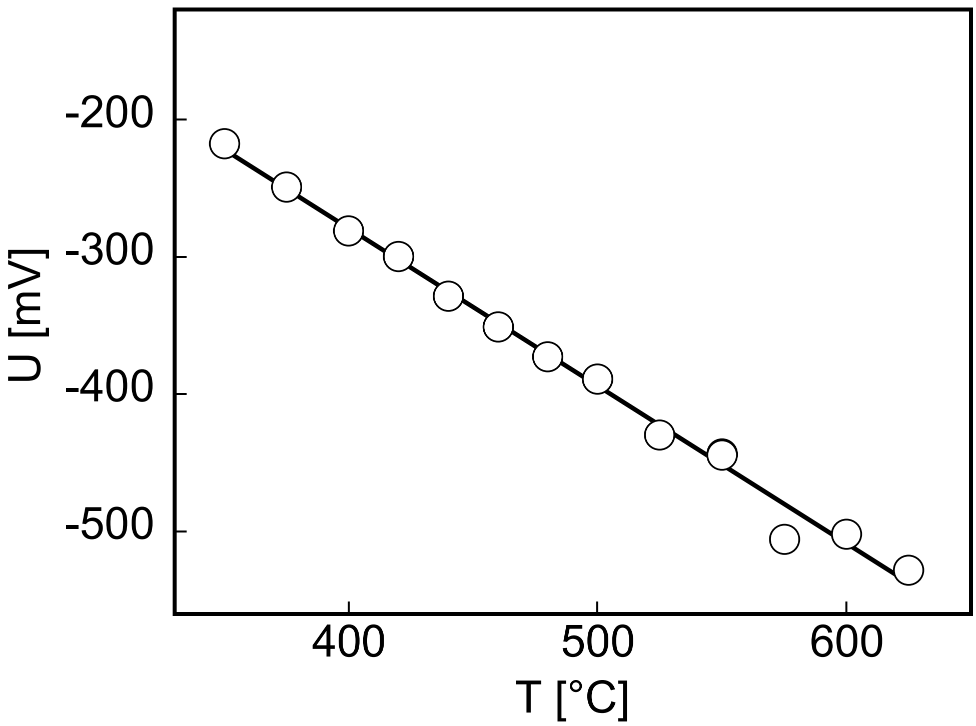

Fig. 4-1 Temperature dependence of voltage of the galvanic cell VIII at p_{CO_2}= 19.4 *10^{-6} [bar] and p_{O_2} = 19.7 *10^{-6} [bar]

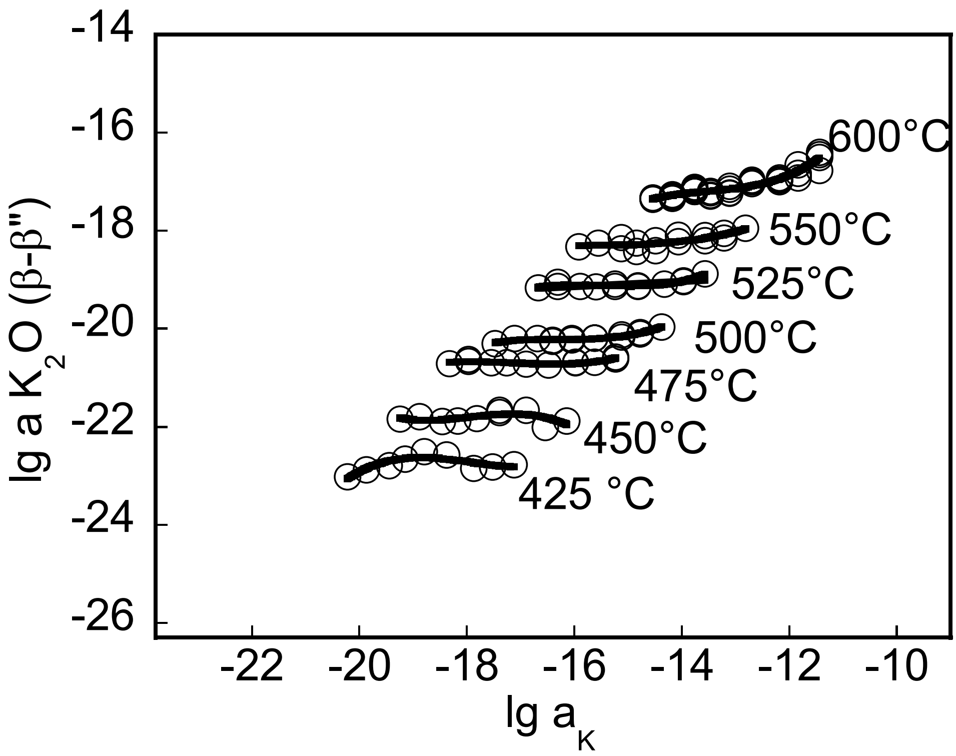

Fig. 4-2 Potassium oxide activities as a function of potassium chemical potential at various temperatures

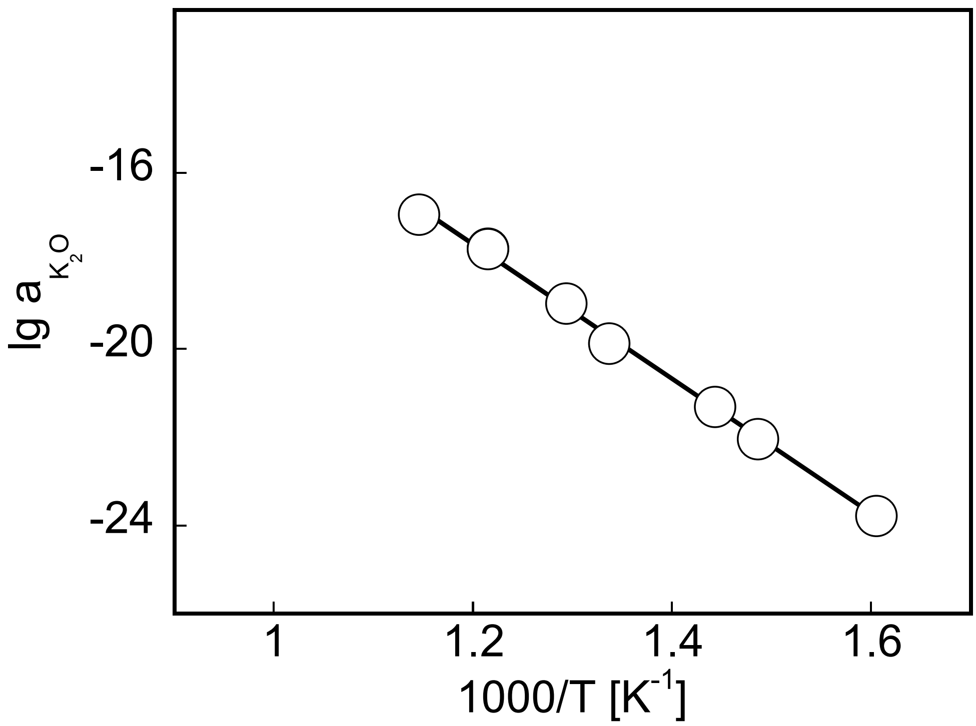

Fig. 4-3 Temperature dependence of the potassium oxide activity dissolved in K-β/β"-Al_2O_3

The plateau confirms that the a_{K_2O} in a two-phase mixture of K-β and -β''-Al_2O_3 is unambiguously fixed at a constant temperature by the Gibbs phase rule. At temperature above 600 °C, the potassium activity dependence on potassium oxide activity does not show anymore a plateau. At higher potassium activity, however, the equilibrium tends to shift to a β+$KAlO_2$ phase equilibrium.

The ordinates of plateaus of Fig. 4-2 are plotted against the inverse temperature as depicted in Fig. 4-3. The potassium oxide activity determined as a function of temperature can be represented by the following equation:

$$\lg a_{K_2O} = 0.638 - \frac{15{,}232.2}{T/K} \quad (350 \leq T \leq 625°C) \qquad \text{Eq. 4-1}$$

4.2 Chemical potential of reference electrodes

4.2.1 Potassium chemical potential of the magnifer electrode

In the Fig. 4-4 for six different temperatures, the voltage of cell VI (cf. Table 2-8) is plotted as a function of the potassium activity at the carbonate electrode used as measuring electrode. The potassium activity was adjusted by stepwise changing the CO_2 and O_2 partial pressure under isothermal conditions.

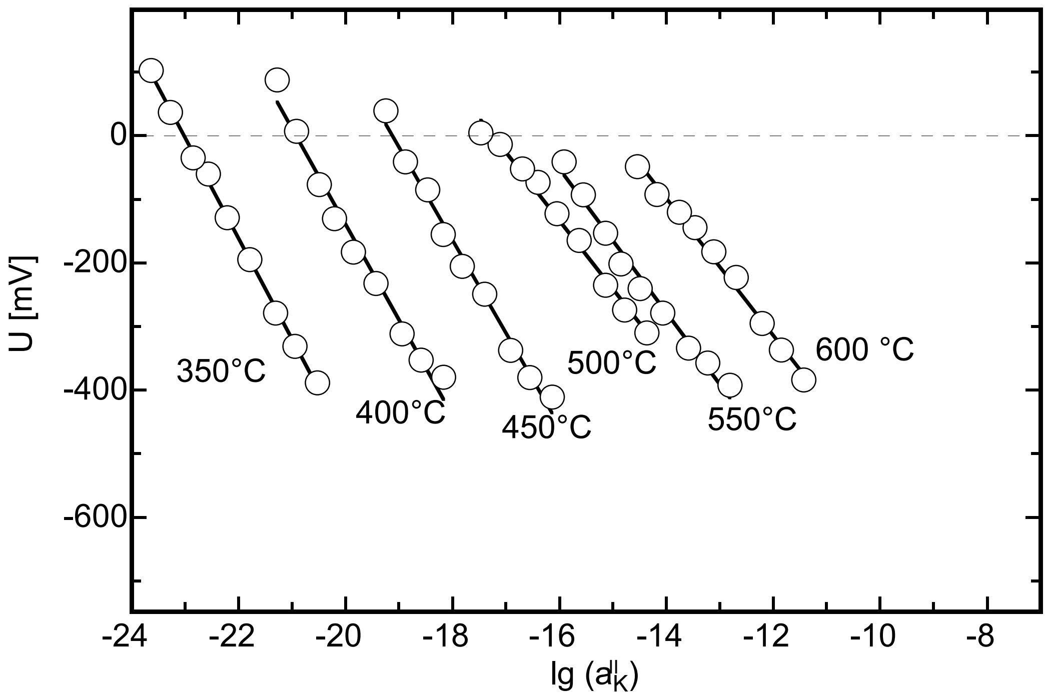

Fig 4-4 Voltage of cell (VI) as a function of the potassium activity of the measuring electrode at different temperatures

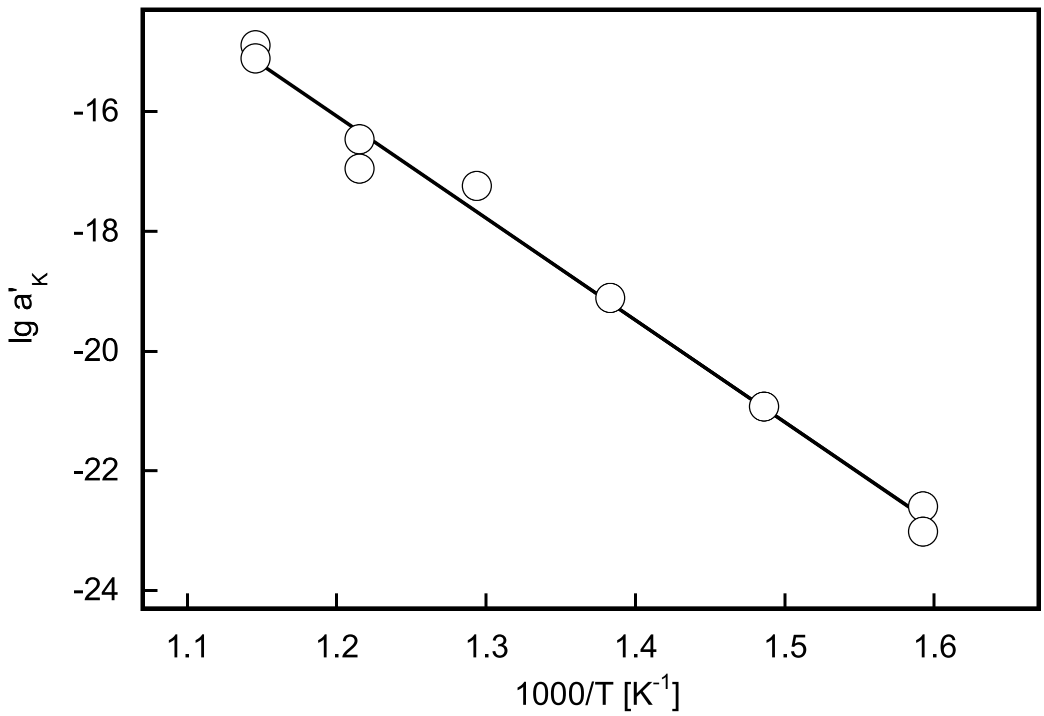

Fig. 4-5 Temperature dependence of the potassium activity at the magnifer electrode

As can be seen from Fig. 4-4, the data points either cross the zero line or closely approaches to it. In the latter case an extrapolation to zero can readily be done. Since the potassium activity of the magnifer (a'_K) is a real constant of the variable a''_K (cf. section 2.7.2) the abscissa at which the voltage is equal to zero corresponds to the unknown activity a'_K (cf. section 2.8.3) according to Eq. 2-96. The data a'_K obtained according to above procedure are plotted as a function of the inverse of temperature a straight line is achieved (Fig. 4-5), which can be described by the equation

$$\lg a'_K = 4.22 - \frac{16958}{T(K)}. \qquad \text{Eq. 4-2}$$

4.2.2 The potassium chemical potential of silicate electrode

At constant temperature the potassium activity at the magnifer electrode is used as a reference electrode in galvanic cell VII fixed according to the Eq. 4-2. Hence, the voltage of the cell varies by changing the gas composition. The voltage of cell VII (cf. Table 2-8) is plotted as a function of the O_2 partial pressure at different temperatures (Fig. 4-6). The changes in gas composition were undertaken in both directions, i.e. towards increasing as well as decreasing O_2 partial pressures.

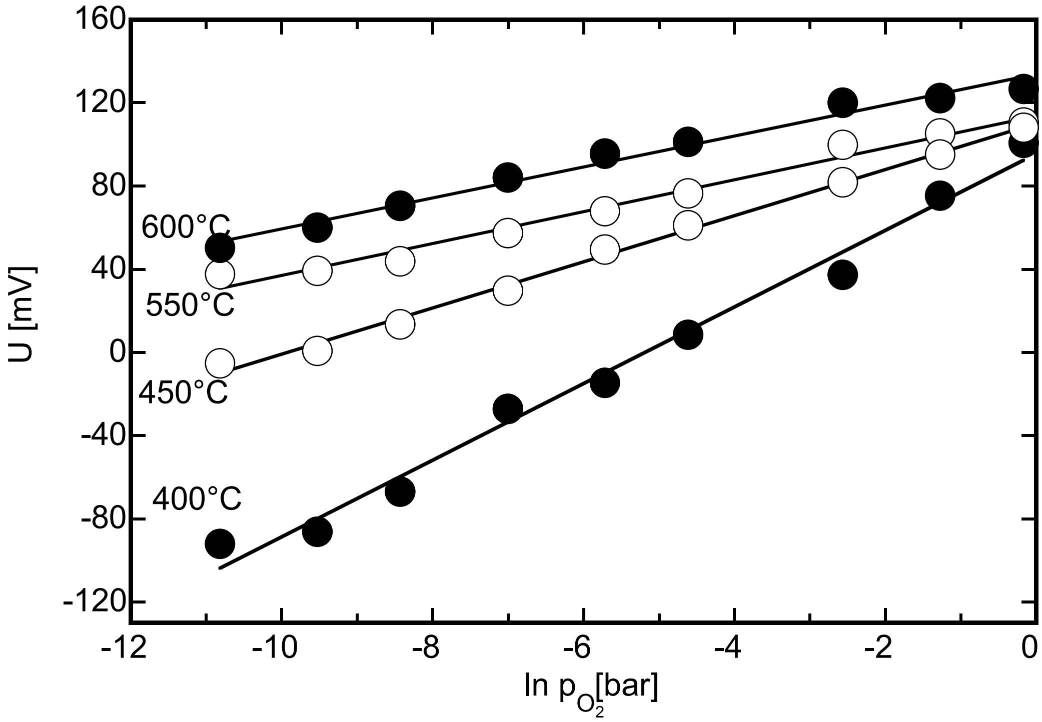

Fig. 4-6 Voltage of cell (VII) as a function of oxygen partial pressure at various temperatures

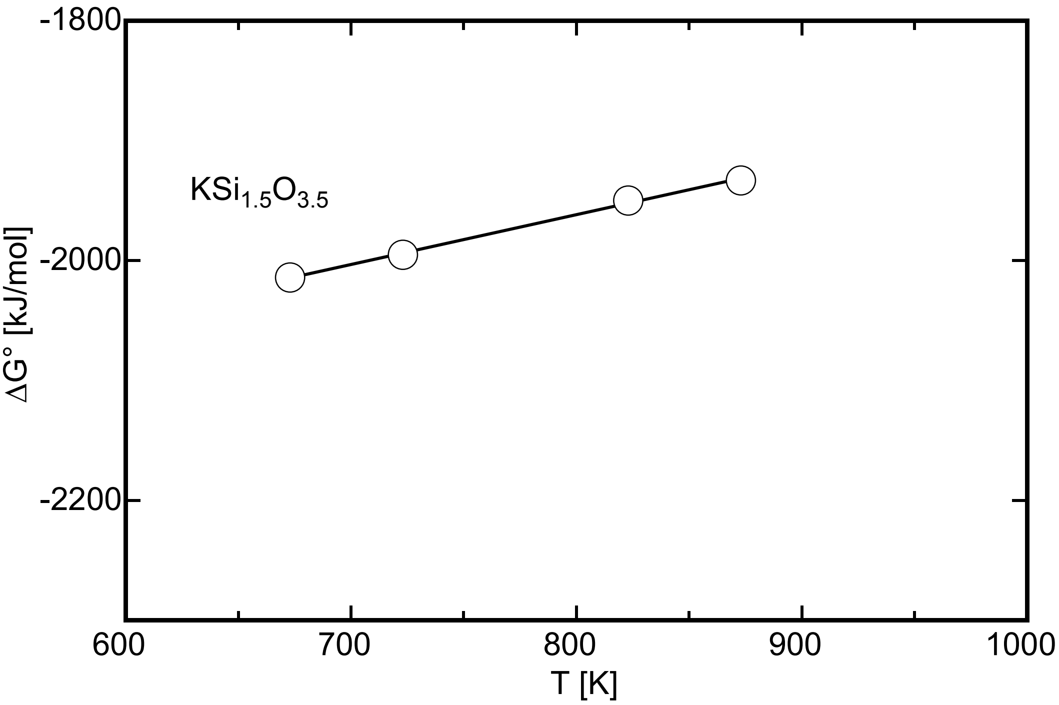

Fig. 4-7 Temperature dependence of the standard Gibbs energy of formation of $KSi_{1.5}O_{3.5}$

It is obvious from Fig 4-6 that, the data points approaches to the zero line. Since the potassium activity of silicate electrode (a''_K) varies with O_2 partial pressure the abscissa at which the voltage is equal to zero corresponds to the O_2 partial pressure where potassium activity at both electrodes are the same (cf. Eq. 2-96). For four different temperatures the data of O_2 partial pressure at zero voltage together with the potassium activity of silicate electrode are given in Table 4-1.

Table 4-1 The potassium activity of the silicate electrode as a function of T and ln p_{O_2}

T [K]	ln (p_{O_2} [bar])	lg a'_K (lg a''_K = lg a'_K)
873	-13.073	-15.205
823	-9.740	-16.385
723	-9.330	-19.235
673	-6.670	-20.978

The standard Gibbs energy of formation of $KSi_{1.5}O_{3.9}$ is evaluated using the Eq. 2-97 taking into account the result given in Table 4-1 {$\Delta G = f(T,\ p_{O_2},\ a''_K)$} and $\Delta G°_{SiO_2}$ from JANAF [79]. The standard Gibbs energy of formation of the silicate amounts to

$$\Delta_f G°_{KSi_{1.5}O_{3.5}}\left[\frac{kJ}{molK}\right] = -2292 + 0.414T(K)\,. \qquad \text{Eq. 4-3}$$

4.3 Determination of p-electronic conduction parameter ($a_\oplus$)

4.3.1 Potentiometric measurement using KBA and magnifer electrode

4.3.1.1 Potassium chemical potential dependence on the cell voltage

Fig. 4-8, 4-9 and 4-10 show how the cell voltage changes as a function of the potassium chemical potential of the carbonate electrode (a''_K) used as measuring electrode. A non-linear chemical potential dependence can be clearly seen. In the case of negligible electronic conductivity, the U vs. chemical potential relationship would represent a straight line with the slope -RT/F (cf. eq. (2-39)). By evaluating a field of experimental data U = f (T, a'_K, a''_K) the p-electronic conduction parameter ($a_\oplus$) can be determined by means of a non-linear procedure based on Eq. 2-47 (see chapter 2.3).

As seen from the solid lines in Figs. 4-8, 4-9 and 4-10, the experimental U vs. lg a''_K data are fitted fairly well according to Eq. 2-47. That means, the non-Nernstian slope of the quasi-linear part of the U vs. lg a''_K plots, as well as, the bending with decreasing lg a''_K can be quantified by taking into account the effect of the electron conduction parameter $a_\oplus$.

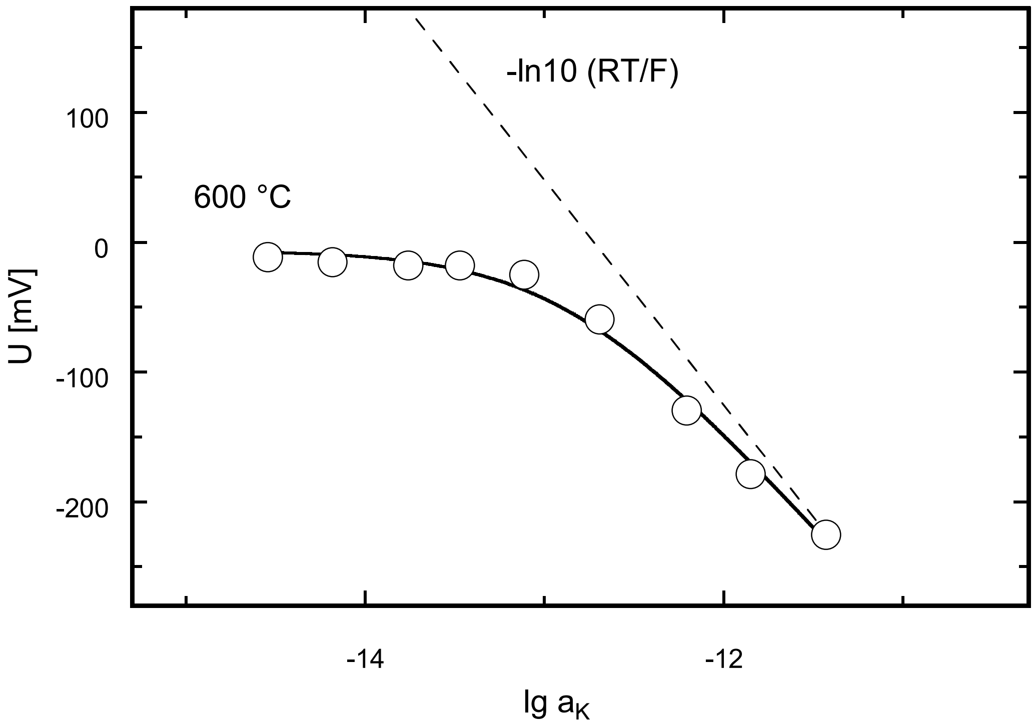

Fig. 4-8 Potassium chemical potential dependence of voltage at 600°C.

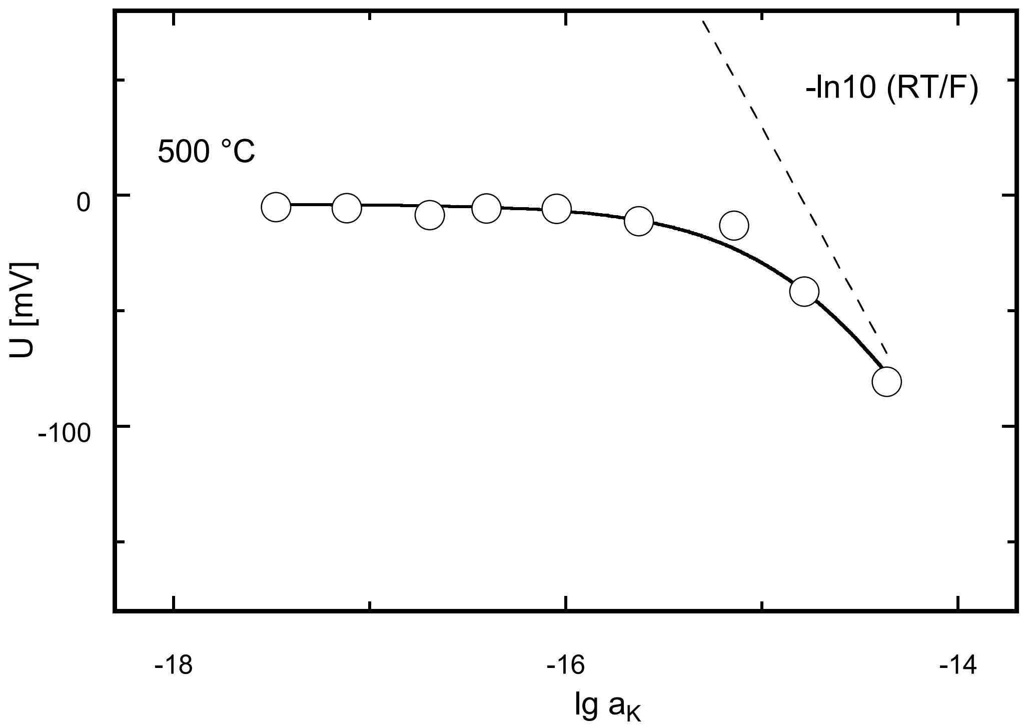

Fig. 4-9 The voltage of cell (I) as a function of potassium chemical potential of measuring electrode at 500 °C

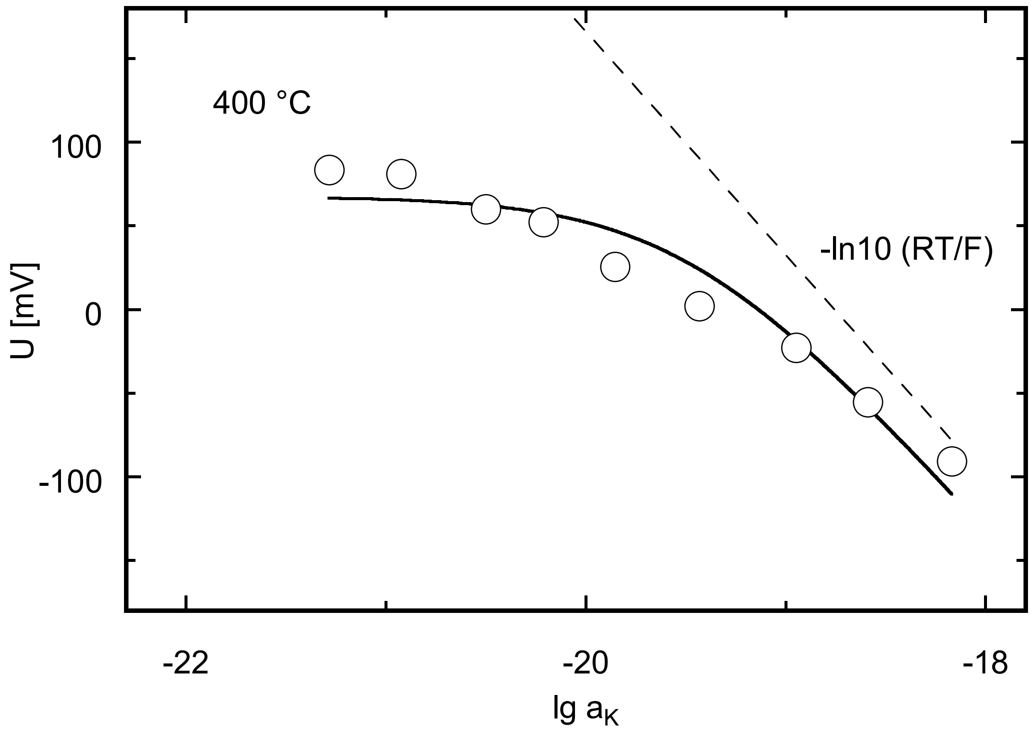

Fig. 4-10 Voltage of cell (I) as a function of the potassium chemical potential of the carbonate electrode at 400 °C

At the high potassium activity there is a comparatively small deviation from the Nernst behaviour, since $a_\oplus$ is, though not negligible, still very small compared with a''_K. Moving to the left of abscissa in Fig 4-8, 4-9 and 4-10 a'' decreases exponentially. That's why in Eq. 2-47 the summand $a_\oplus$ more and more prevails over a''_K, and the voltage becomes insensitive to a''_K.

4.3.1.2 Time dependence of the voltage

The impact of electronic conductivity becomes evident from the time dependent development of the cell voltage after stepwise changes in the potassium activity of the measuring electrode (a''_K) from one steady state level to another (Figs. 4-11 and 4-12).

Independent of whether the potassium activity is decreasing (Fig. 4-11) or increasing (Fig. 4-12), the voltage first responds in the direction as expected from the Nernst law, and after some time later does it more or less relax back. Note that this relaxation has no preferential direction towards rising or falling voltages. Regardless of which direction the potassium activity is changed, relaxation process always decreases the magnitude of the initial voltage response. Any permanent, i.e. irreversible, impact on the cell voltage is therefore excluded as a reason.

The reason of this behaviour is the interplay of two processes. At first, there is the response of the measuring electrode according to the Nernst equation. This is an interfacial process occurring at the measuring electrode and is therefore relatively faster. Secondly, as the electrolyte layers close to the measuring electrode get adapted to the new condition, the p-type conductivity begins to rise. As a result, the extent of the internal short-circuit through the cell increases and thus the voltage more and more breaks down and counteracts the effect of the first process.

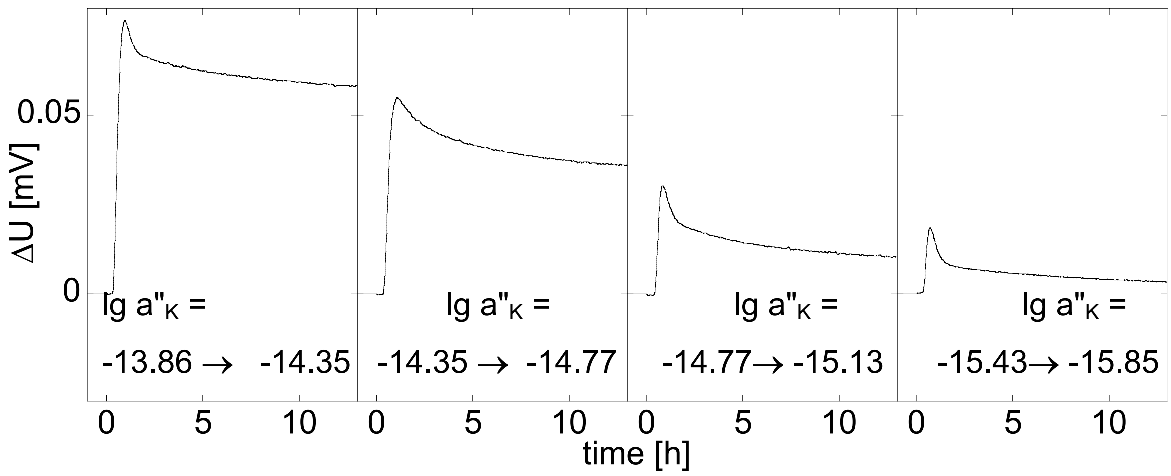

Fig. 4-10 Time dependence of the voltage of cell I with KBA as a solid electrolyte after stepwise decreasing the a''_K (measuring electrode) (T = 550°C)

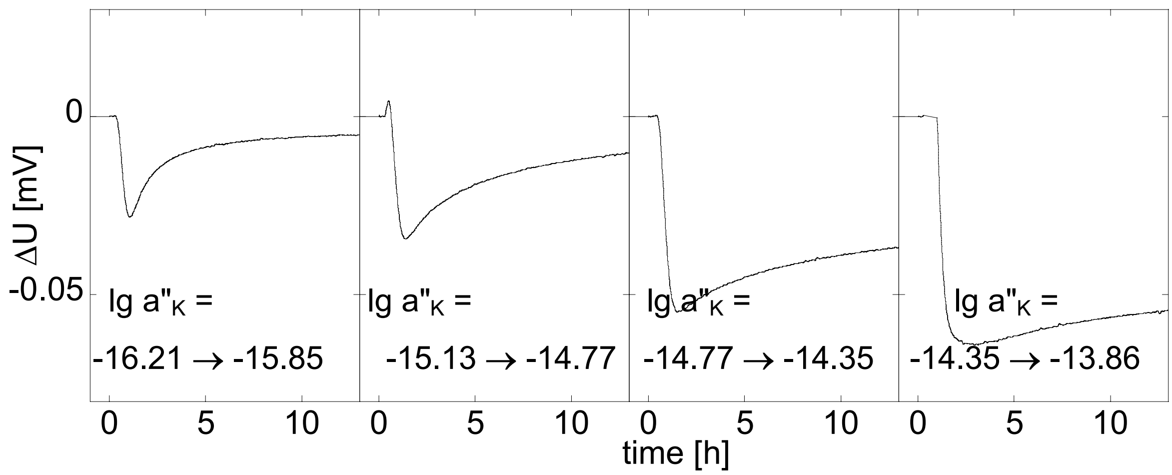

Fig. 4-11 Time dependence of the voltage of cell I with KBA as a solid electrolyte after stepwise increasing the a''_K (measuring electrode) (T = 550°C)

The magnitude of the short circuit is a function of the electronic conductivity of the electrolyte and, thus, a function of the potassium chemical potential distribution throughout the electrolyte [91]. The latter necessarily changes with the change of the potassium activity of the measuring electrode. Started from the measuring electrode side, this change progressively propagates throughout the whole electrolyte which needs time. Thus, the new steady-state level of the electronic conductivity is not immediately established and the counteracting second process is comparatively slower than the first one.

According to Eq. 2-20, after each of the downward potassium activity steps of Fig. 4-11, the magnitude of the total p-type conductivity rises compared to the situation before the step. As a result, the extent of the internal short-circuits through the cell increases, and the voltage tends to drop down each time. The magnitude of this voltage decay is, however, not constant. It becomes larger as the total level of the potassium activity falls illustrated by the different section of Fig 4-11. On the right-hand side, where the potassium activity level is the lowest, the voltage relaxation due to electronic transference is the largest after the activity step. That's why the initial Nernst response of the voltage is almost completely levelled out by the partial internal short circuit. In terms of Eq. 2-47, it means that a variation in a''_K causes the steady-state voltage to change to a lesser extent as the magnitude of a''_K is smaller compared to $a_\oplus$. In other words, any changes in a''_K are masked by the dominating impact of $a_\oplus$. This impact becomes smaller with an increasing level of the potassium activity (left side in Fig. 4-11). As a consequence, the voltage decays to a lesser extent from the right towards the left-hand side of Fig. 4-11.

In Fig. 4-12, where each potential step is due to a stepwise increase in the potassium activity, the extent of the electronic conductivity, according to Eq. 2-47, becomes smaller after each step. Whilst under the conditions prevailing in the left sections of Fig.4-12, the nominally high level of the electronic conductivity is not yet significantly reduced due to the activity steps it gradually recovers from left to right. Therefore the relaxation of the voltage against the direction of the Nernst response is the smallest in the outmost right section of the Fig. 4-12.

4.3.1.3 Temperature dependence of p-electronic conduction parameter

The $a_\oplus$ values that were obtained by applying the non-linear regression procedure to all sets of isothermal U vs. lg a''_K data point results in a lg $a_\oplus$ vs. 1/T dependence depicted in Fig. 4-13.

A comparison of the variation of the p-electron conduction parameter along with the logarithm of potassium activity at the working and reference electrodes is shown in Fig. 4-13. It is discernible from Fig. 4-13 that the position of the p-electronic conduction parameter is close to the potassium chemical potential of either electrode. In addition, the data points describe section of two straight lines with different slopes. The results on the characterization of the potassium activity of the magnifer electrode (cf. section 4.2) show that in high temperature region it is the reference electrode (magnifer electrode) that has the predominantly lower potassium chemical potential of the galvanic cell. The flatter plot section of the log $a_\oplus$ vs. 1/T dependence coincides with the temperature dependence of the potassium activity of the magnifer electrode in agreement with previous findings on sodium beta alumina [9, 13, 14].

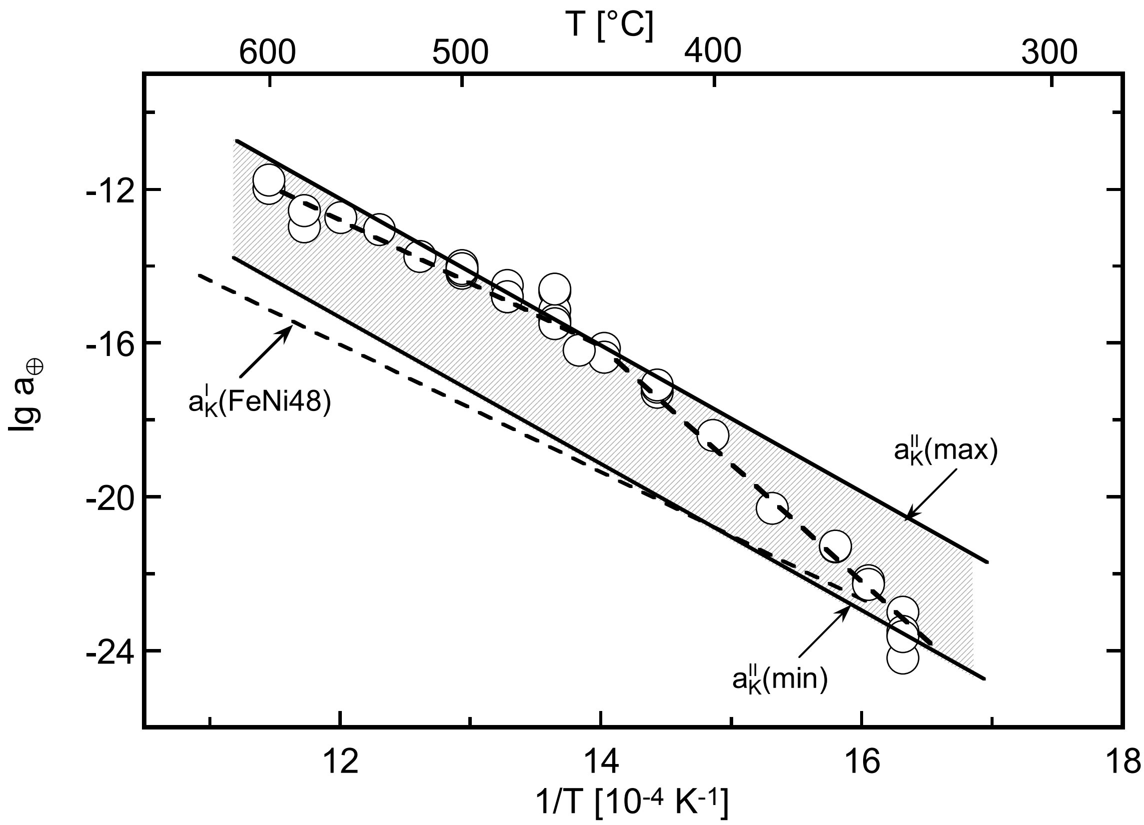

Figure 4-13 Temperature dependence of the logarithm of the p-electronic conduction parameter of KBA (Comparison with the logarithm of potassium activity at the carbonate (a''_K) and magnifer (a'_K) electrodes.

4.3.2 Potentiometric measurement using KBA and silicate electrode

4.3.2.1 Voltage as a function of the CO_2 partial pressure

Since the chemical potential of both electrodes is a function of O_2 and also because the oxygen gas atmosphere is common to both the electrodes of the cell II, the overall cell reaction involves CO_2. The voltage of the galvanic cell (II) was measured at various temperatures as a function of CO_2 partial pressure. The experimental data are shown in Fig. 4-14. The measured voltage changes linearly with the logarithm of p_{CO_2}. By inserting the values of the chemical potential of the carbonate and the silicate electrodes in Eq. 2-39, the Nernst voltage were calculated and depicted for T = 600 °C in Fig. 4-15. The experimental values of the voltages of cell II are more positive as compared to the Nernst voltage as revealed by the Fig. 4-15. The deviation from Nernst behaviour (Fig 4-15) is the result of electronic conductivity through solid electrolyte [13].

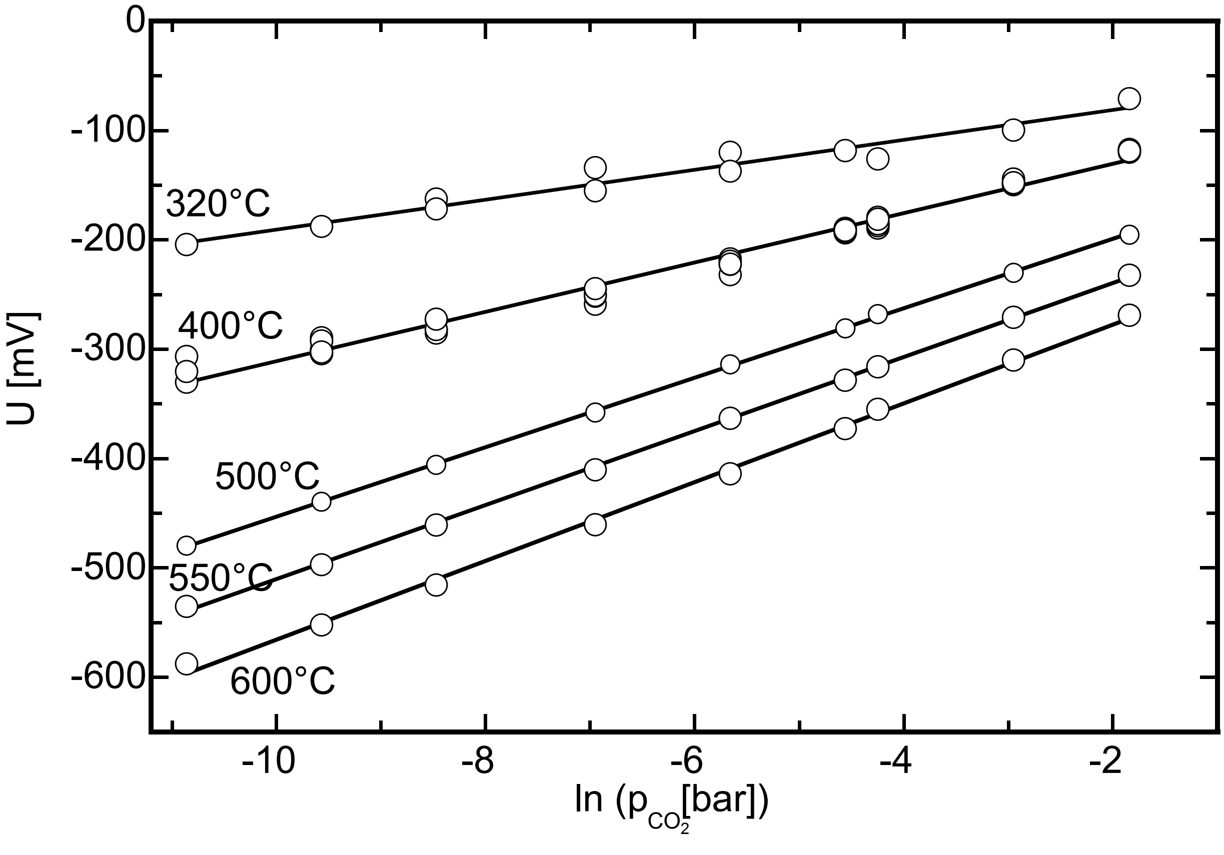

Fig. 4-14 Voltage of cell (II) as a function of the CO_2 partial pressure

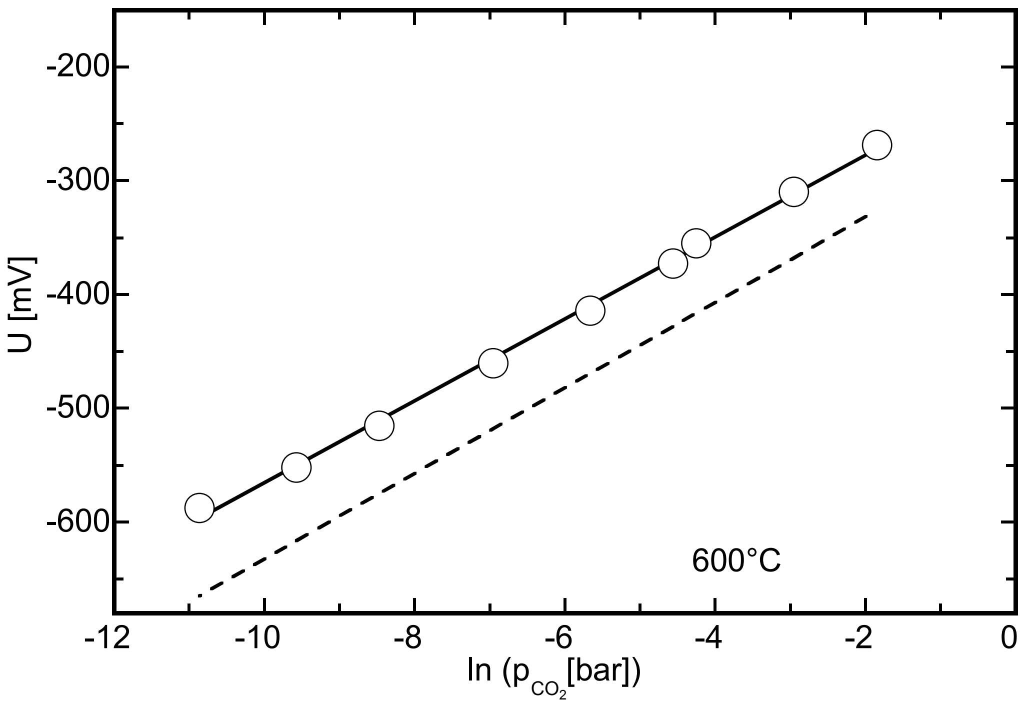

Fig. 4-15 Voltage of galvanic cell II as a function of CO_2 partial pressure at 600°C along with the Nernst voltage (Eq. 4-39 dotted line)

4.3.2.2 Evaluation of p-electronic conduction parameter ($a_\oplus$)

The substitution of Eq. 2-73 and 2-88 into Eq. 2-47 delivers a relationship that describes the voltage as a function of the CO_2 and O_2 partial pressure alone. This relationship has the following form:

$$U=\left[\begin{array}{l} -\dfrac{RT}{F}\ln\left(\dfrac{\exp\left(\dfrac{\Delta(\Delta G'')}{2RT}-\dfrac{1}{2}\ln p_{CO_2}\right)}{\exp\left(\dfrac{\Delta(\Delta G')}{RT}\right)}\right) \\ -\dfrac{RT}{F}\ln\left(1+\dfrac{a''_\oplus}{\exp\left(\dfrac{\Delta(\Delta G'')}{2RT}-\dfrac{1}{2}\ln p_{CO_2}-\dfrac{1}{4}\ln p_{O_2}\right)}\right) \\ +\dfrac{RT}{F}\ln\left(1+\dfrac{a'_\oplus}{\exp\left(\dfrac{\Delta(\Delta G')}{RT}-\dfrac{1}{4}\ln p_{O_2}\right)}\right) \end{array}\right] \qquad \text{Eq. 4-4}$$

where: $\Delta(\Delta G'')=\Delta_f G^\circ_{K_2CO_3}-\Delta_f G^\circ_{CO_2}$

$\Delta(\Delta G')=\Delta_f G^\circ_{KSi_{1.5}O_{3.5}}-1.5\Delta_f G^\circ_{SiO_2}$

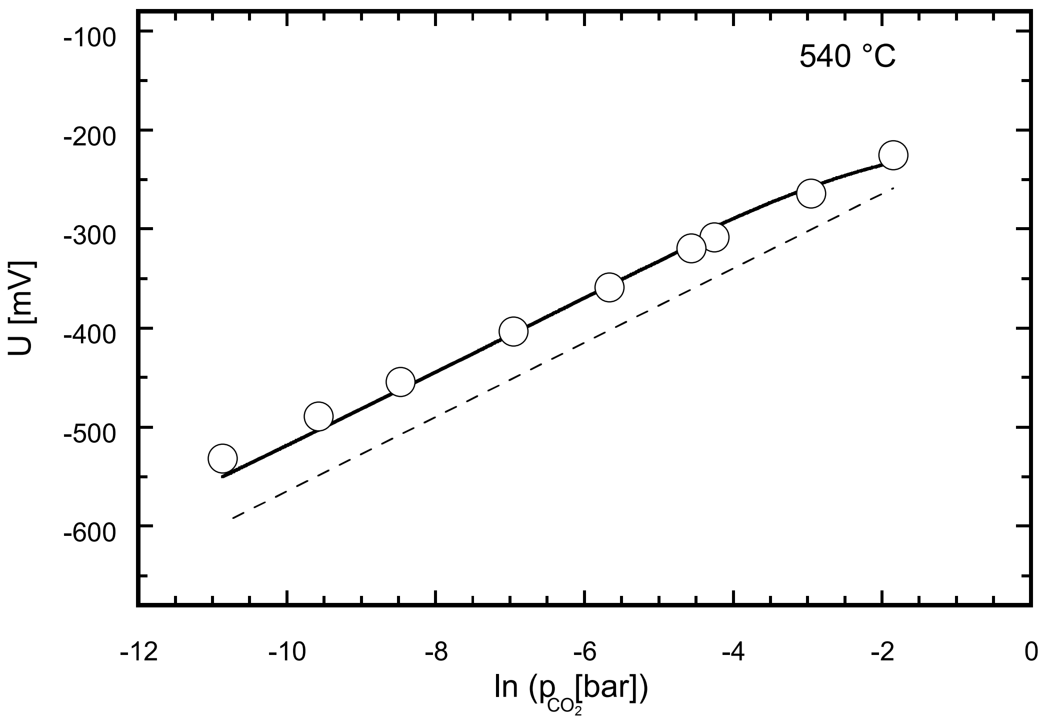

Fig. 4-16 Voltage as a function of CO_2 partial pressure at 540 °C (solid line curve fit according to Eq. 4-4 and dash line voltage according to Nernst law Eq. 4-39)

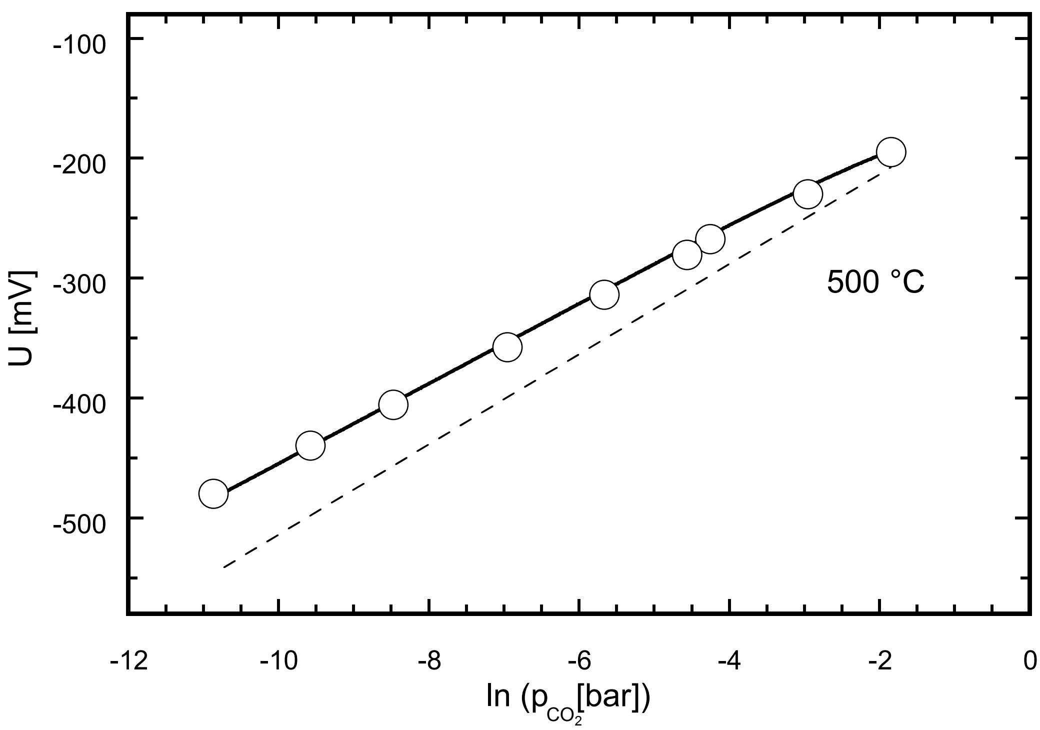

Fig. 4-17 CO_2 partial pressure dependence of the voltage at 500 °C (solid line curve fit according to Eq. 4-4 and dash line voltage according to Nernst law Eq. 4-39)

$\Delta_f G^\circ_{KSi_{1.5}O_{3.5}}$, $\Delta_f G^\circ_{K_2CO_3}$, $\Delta_f G^\circ_{CO_2}$ and $\Delta_f G^\circ_{SiO_2}$ are standard Gibbs energy of $KSi_{1.5}O_{3.9}$, K_2CO_3, CO_2 and SiO_2, respectively. The standard Gibbs energy of the silicate determined experimentally is represented by Eq. 4-3 (cf. chapter 4.3).

Based on the above equation the unknowns $a''_\oplus$ and $a'_\oplus$ can be extracted from multivariate non-linear regression of experimental data pairs of cell II U vs. ($\ln p_{CO_2}$; $\ln p_{O_2}$) by taking into account the known parameters R, T, F, $\Delta(\Delta G'')$ and $\Delta(\Delta G')$.

The solid line drawn through the data points of Fig. 4-15, 4-16 and 4-17 were computed on basis of Eq. 4-4 using the multivariate regression procedure.

4.3.2.3 Temperature dependence of $a_\oplus$

Simultaneously, numerical data for $a''_\oplus$ and $a'_\oplus$ are obtained which are plotted in Fig. 4-18 as a function of the inverse temperature. $a_\oplus$ established by various potassium chemical potential are different from each other (cf. Fig. 4-18). This fact supports the idea that the p-electronic conduction ($a_\oplus$) of K-beta-Al_2O_3 is not independent of chemical potential of surroundings.

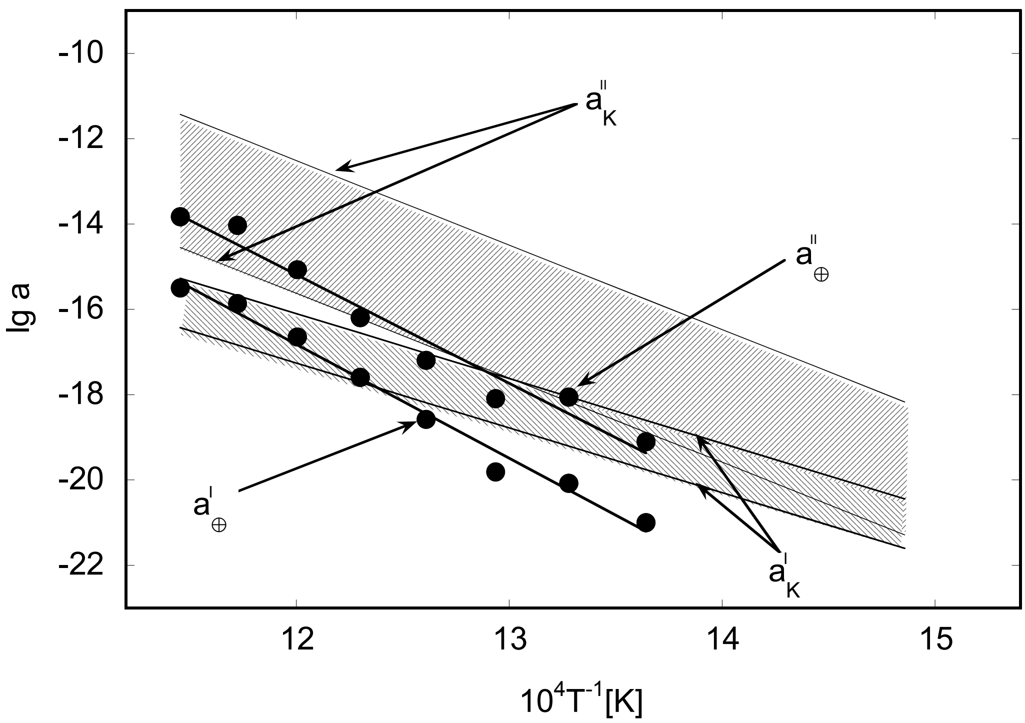

Fig. 4-18 Temperature dependence of the logarithm of the p-electronic conduction parameter in comparison with the potassium activity interval of the measuring electrode (a'') and reference electrode (a') (etched area)

4.3.3 p-electronic conduction parameter of K-beta-Al_2O_3

The variation of p-electronic conduction parameter of K-beta-Al_2O_3 with inverse of temperature is shown in Fig. 4-19. It is discernible from the Fig. 4-19 that the magnitude of $a_\oplus$ obtained using the silicate electrode (cell II) is 2-3 orders of magnitude lower compared with that using the magnifer electrode (cell I), although the same measuring electrode, carbonate system, and solid electrolyte material, potassium beta alumina, were used. This indicates that $a_\oplus$ is a function of the activity in the surroundings and not a constant. It means that the $a_\oplus$ value of K-beta-Al_2O_3 depends on the potassium activity and changes in accordance with the surrounding conditions fixed by the electrodes.

Since in the cell (I) and (II) different reference electrodes were used, the p-electronic conduction parameter $a_\oplus$ of K-beta-Al_2O_3, used as solid electrolyte in these cells, is influenced and adjusted according to the chemical potential of reference electrodes. As a consequence, the selection of the reference electrode which influences the mean $a_\oplus$ value of the solid electrolyte determines the conduction behaviour of the measuring electrode side of the solid electrolyte.

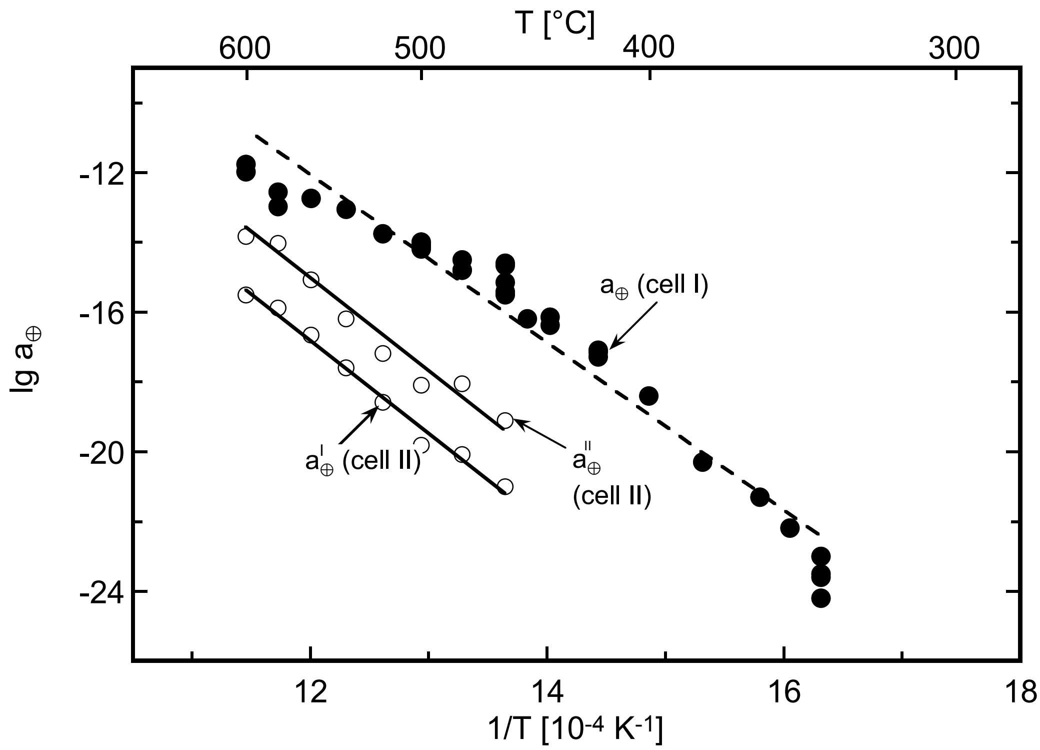

Fig. 4-19 The result of p-electronic conduction parameter on potassium beta alumina obtained using different reference electrode

Taking into account the results on p-electronic conduction parameter of K-beta-Al_2O_3 at T=500 °C, the schematic sketch of the conductivity as a function of chemical potential of carbonate system is simulated and depicted in Fig. 4-20. This figure shows schematically two different $a_\oplus$ values, potassium chemical potential of reference electrode employed in cell I ($a_\oplus$ (I)) and cell II ($a_\oplus$ (II)), and their influence on the p-electronic and ionic conductivity of potassium beta alumina. Additionally, the position of the electrode activities for cell (I) and (II) are given. The reference activity dependence of $a_\oplus$ manifests itself in a different extent of p-electronic transference at the measuring electrode side of the potassium beta alumina although the same measuring electrode and solid electrolyte material was used.

According to the definition of $a_\oplus$ (cf. section 2.3.2) the $a_\oplus/a_K$-ratio is equal to the σ_p/σ_i-ratio which defines the p-electronic conductivity σ_p in comparison to the ionic conduction σ_i at different potassium chemical potential in the ambient of the solid electrolyte (K-beta-Al_2O_3) (cf. Eq. 2-20).

Plotting the σ''_p/σ_i -ratio as a function of the inverse of temperature, the measuring electrode side of the solid electrolyte exhibits a strongly different electronic transference from the reference electrode (Fig. 4-21, 4-22 for cell I and cell II, respectively).

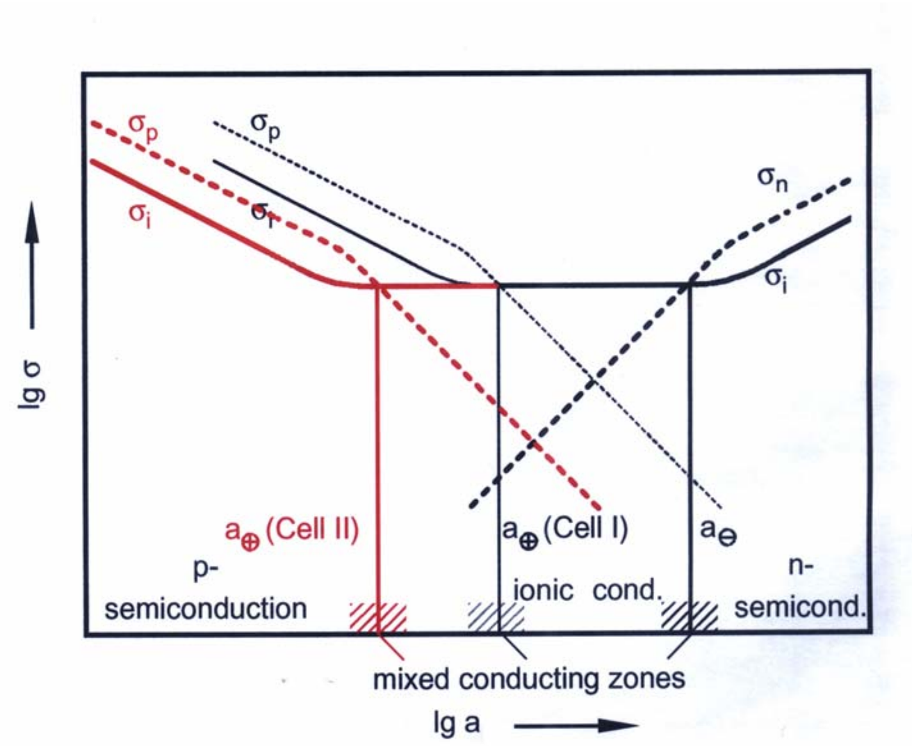

Fig. 4-20 Schematic sketch of conductivity diagram of K-beta-Al_2O_3 using two different reference electrode employing carbonate system as measuring electrode

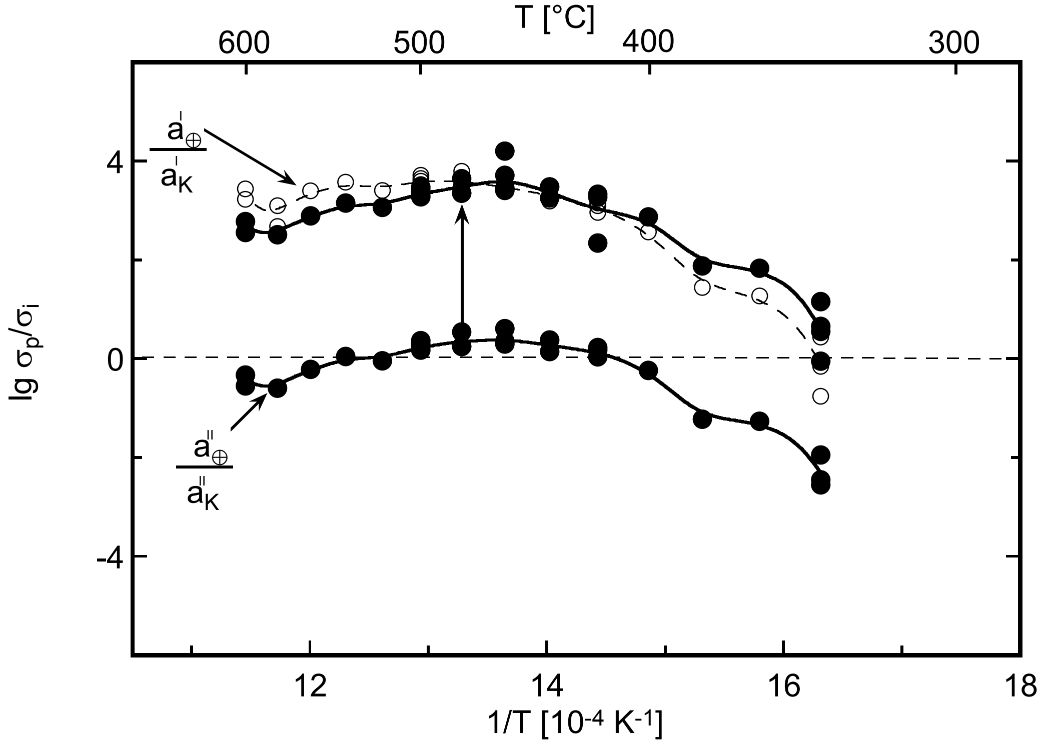

Fig. 4-21 Temperature dependence of logarithm of σ_p/σ_i ratio for cell I

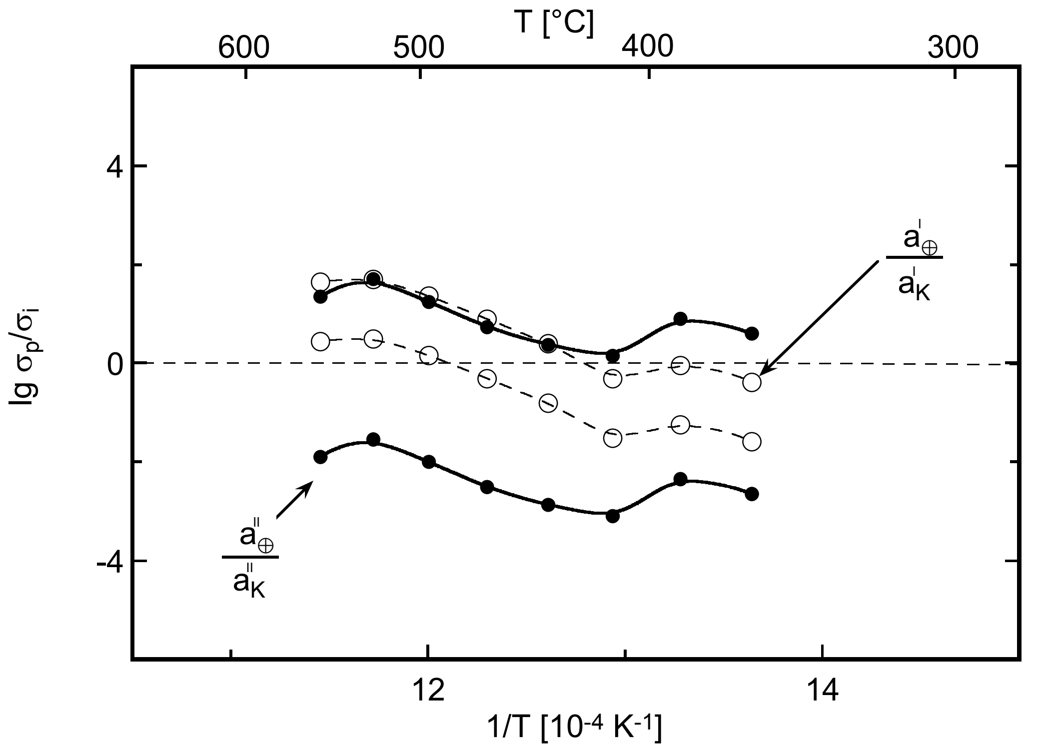

Fig. 4-22 Temperature dependence of logarithm of σ_p/σ_i ratio for cell II

Whereas in case of cell (I) the measuring electrode side shows p-electronic or ionic conductivity ($\sigma''_p/\sigma_i \gtrless 0$) depending on the measuring electrode activity, the measuring electrode side of cell (II) is predominately ionically conductive ($\sigma''_p/\sigma_i < 0$).

The reference electrode side of the solid electrolyte in cell I is predominantly p-conductive ($\sigma'_p/\sigma_i > 0$). For σ'_p/σ_i ratio of the reference electrode side of cell II, the situation appear to be more or less similar with that of cell I, although the position of the σ_p/σ_i-ratio is shifted more down, meaning that the properties of K-beta-Al_2O_3 respect to ionic conductor changes.

The fact that the electronic transference through the potassium beta alumina solid electrolyte depends on the surrounding potassium activity needs to be taken into consideration for the application of potassium beta alumina as a solid electrolyte in galvanic cells such as potentiometric CO_2 sensor. The $a_\oplus$ value and, therefore, the extent of the ionic domain which is the relevant area for sensor operation depends on the relative position of the electrode activities and is thus a function of the set-up of the sensor.

All these findings confirm the fact previously observed on sodium beta alumina [9-13], that $a_\oplus$ is not a constant but adapts to the chemical potential of neutral charge specie in the surroundings of the solid electrolyte.

4.3.4 Potentiometric measurement of NASICON

4.3.4.1 Voltage as a function of the sodium chemical potential

The voltage of the galvanic cell (III) is plotted as a function of the sodium activity of the measuring electrode at constant temperature (T = 550 °C) in Fig. 4-23.

From Fig. 4-23 it can be concluded that a non-linear chemical potential dependence is obtained. However, this dependence qualitatively follows the Nernst law, this means by decreasing sodium chemical potential at working electrode the voltage decreases. In case of a negligible electronic conductivity, the U vs. chemical potential would fullfill the Nernst equation and hence would represent straight lines with slope –RT/F (cf. Eq. 2-39)

The sodium chemical potential at reference electrode is fixed by a complex equilibrium (cf. chapter 3.7).

By evaluating a field of experimental data U = f (T, p_{CO_2}, p_{O_2}), $a_\oplus$ can be determined by means of the non-linear regression procedure based on Eq. 2-47 (see chapter 2.3) even though the sodium chemical potential at the reference electrode is unknown.

In the region of high sodium activity, there is a comparatively small deviation from the Nernst behaviour, since $a_\oplus$ though not negligible, still very small compared with a''_{Na}.

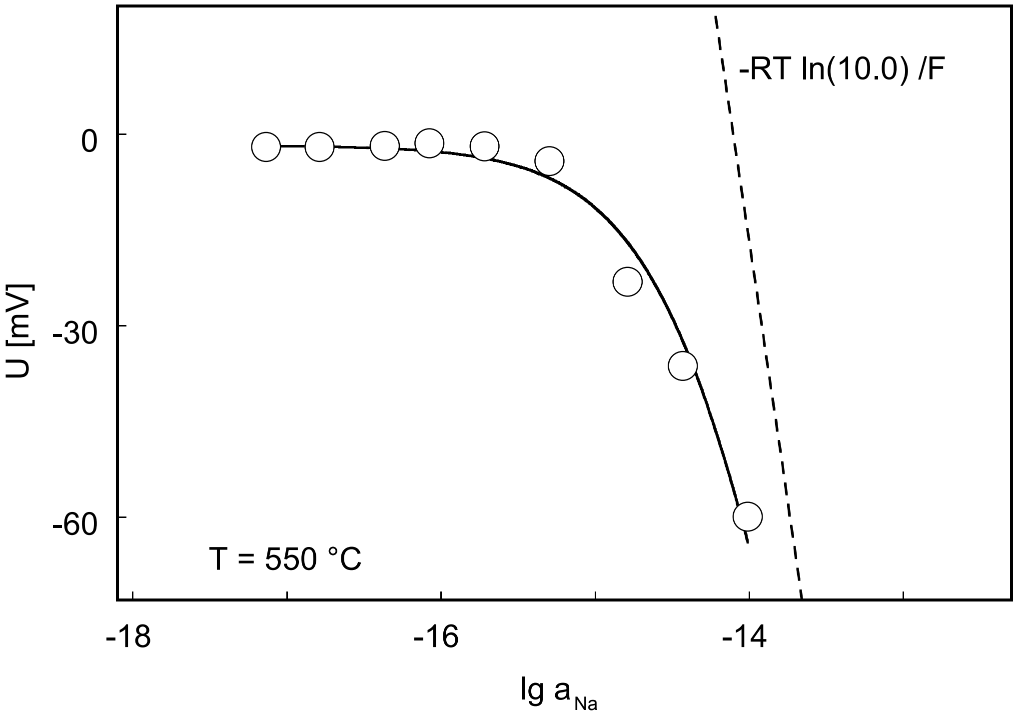

Fig. 4-23 The voltage vs. sodium activity of the carbonate electrode at T= 550 °C

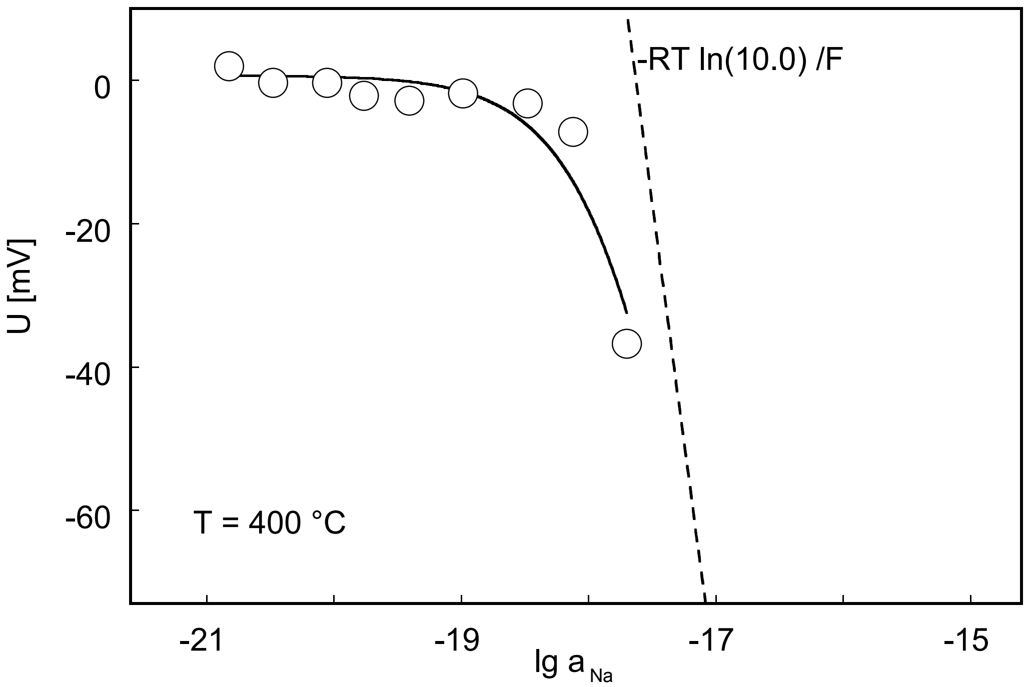

Fig 4-24 Voltage as a function of the sodium chemical potential at T= 400 °C;

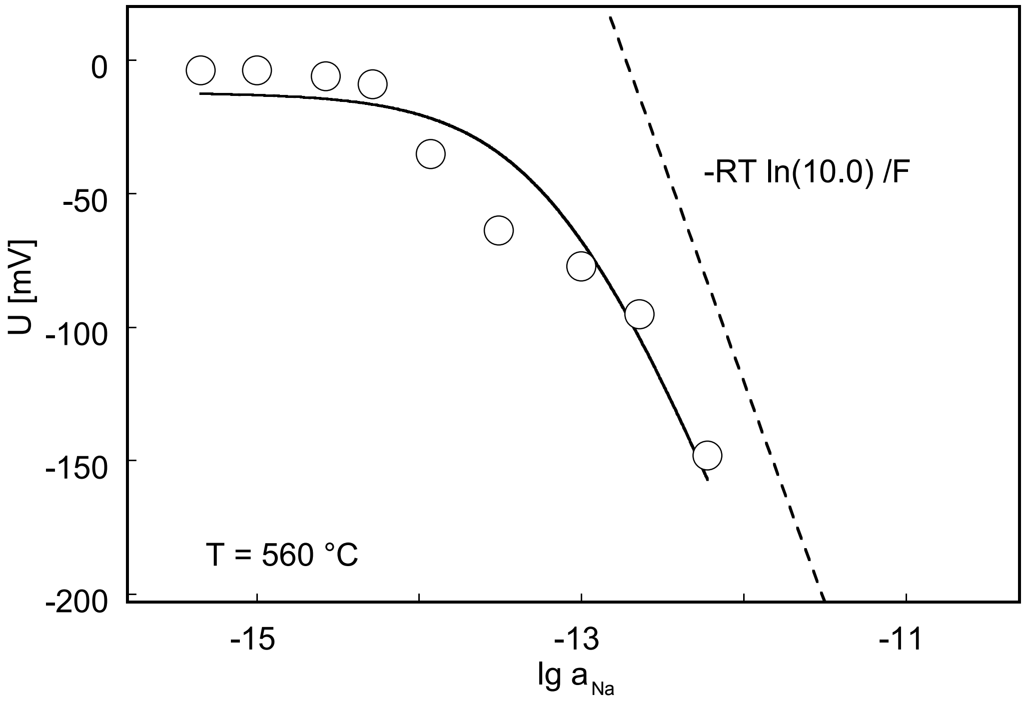

Fig 4-25 Voltage as a function of the sodium chemical potential at T = 560 °C.

Moving to the left of abscissa in Fig 4-23, 4-24 and 4-25 the a''_{Na} decreases exponentially and consequently the influence of p-electronic conduction parameter in Eq. 2-47 becomes higher which results in the bending of the plot.

4.3.4.2 p-electronic conduction parameter as a function of the temperature

The p-electronic conduction parameter determined according to the above procedure along with the sodium chemical potential of the carbonate electrode are depicted in Fig. 4-26 as a function of temperature.

It is visible from the Fig. 4-26 that the position of the p-electronic conduction parameter is close to that of the sodium activity of the carbonate electrode used as the measuring electrode. Hence, the influence of the electronic transference number (cf. Eq. 2-22) on the CO_2 sensor based on NASICON is not negligible. This is in contradiction to what is commonly stated in the literature about the use of NASICON as a solid electrolyte for monitoring the atmospheric pollution [92-101] and for the thermodynamic investigation [58, 70]. To overcome this contradiction, the conclusions for Na-beta-Al_2O_3 [13] can be supposed to be applicable for NASICON, according to which $a_{\oplus}$ of the solid electrolyte (NASICON) is a function of the chemical potential of the mobile species in ambience.

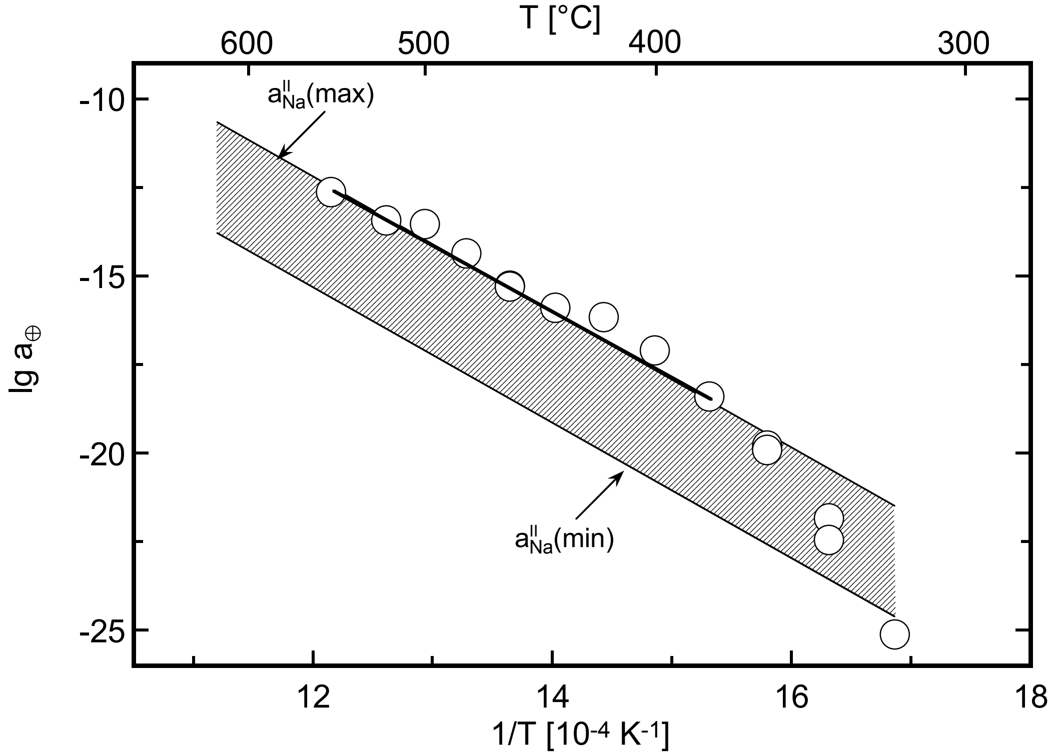

Fig. 4-26 Temperature dependence of $a_{\oplus}$ on NASICON in comparison with the sodium chemical potential of measuring electrode.

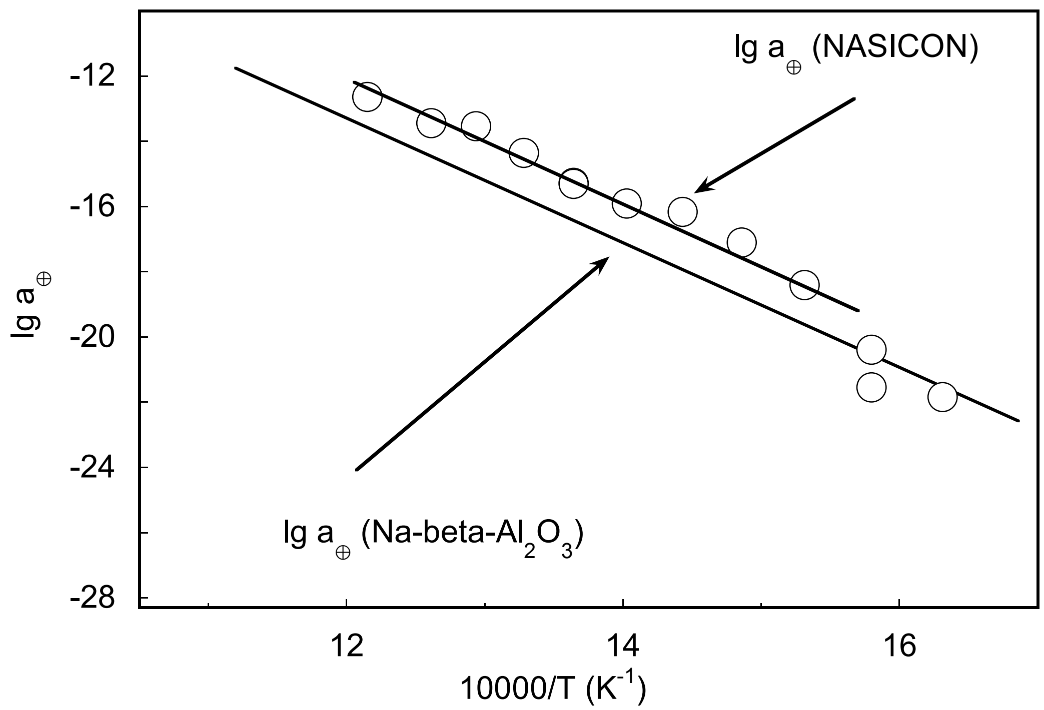

Figure 4-27 p-electronic conduction parameter of NASICON as a function of temperature compared with that for Na-beta-Al_2O_3 [13]

4.3.4.3 Conclusions

The sodium activities occurring at the measuring electrode of a CO_2 sensor with Na_2CO_3 as gas sensitive layer are compared with $a_\oplus$ data evaluated by potentiometric method on the electronic conductivity of NASICON electrolyte. This comparison indicates that the sodium potential of the measuring electrode is far away from the electrolytic domain of solid electrolyte by several orders. The numerical data of $a_\oplus$ is higher compared with sodium beta alumina data (cf. Fig. 4- 27).

The present results are in agreement with previous findings on Na-beta-Al_2O_3 [9-13]. That means the influence of p-electronic conductivity in CO_2 gas sensor cell is not negligible.

4.4 Non-isothermal measurement results on $a_\oplus$

4.4.1 Thermal voltage measurement

The non-isothermal voltage results vs. temperature gradient are plotted in Fig. 4-28 for various CO_2/O_2 partial pressures which are shown in the table attached to Fig. 4-28.

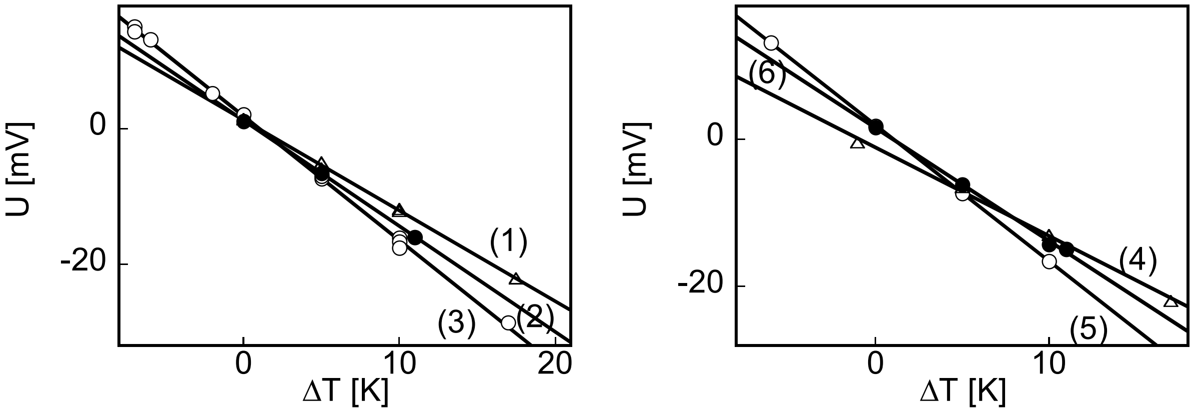

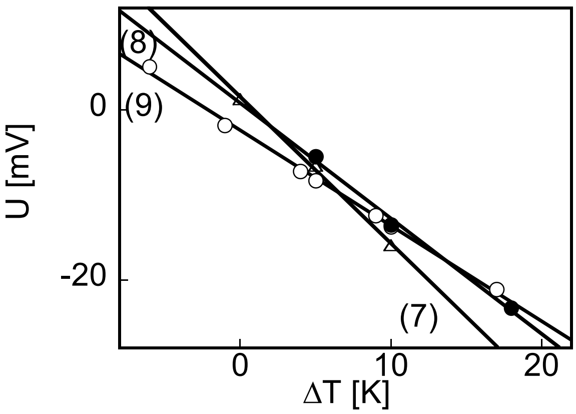

Plot	*p O_2 [bar]*	*p CO_2 [bar]*
(1)	$1.97*10^{-5}$	$1.94*10^{-5}$
(2)	$0.9079*10^{-3}$	$0.9103*10^{-3}$
(3)	0.07672	0.01423
(4)	$7.23*10^{-5}$	$7.10*10^{-5}$
(5)	$0.3296*10^{-2}$	$0.3338*10^{-2}$
(6)	0.27965	0.052185
(7)	$0.217*10^{-3}$	$0.213*10^{-3}$
(8)	0.0098849	0.010013
(9)	0.852	0.148

Fig. 4-28 Voltage vs. ΔT (T = 550 °C at reference electrode side)

The thermoelectric power of the cell IV is defined as a negative gradient of non-isothermal voltage with temperature. The thermoelectric power was evaluated as a function of sodium chemical potential as well as temperature of the reference electrode side of the solid electrolyte. The results of the thermoelectric power as a function of sodium activity at the reference electrode (cf. section 2.8.2) are shown in the Fig. 4-29. The chemical potential dependence of the thermoelectric power is not linear in accordance that solid electrolyte, Na-beta-Al_2O_3, behaves as a mixed conductor (cf. section 2.5).

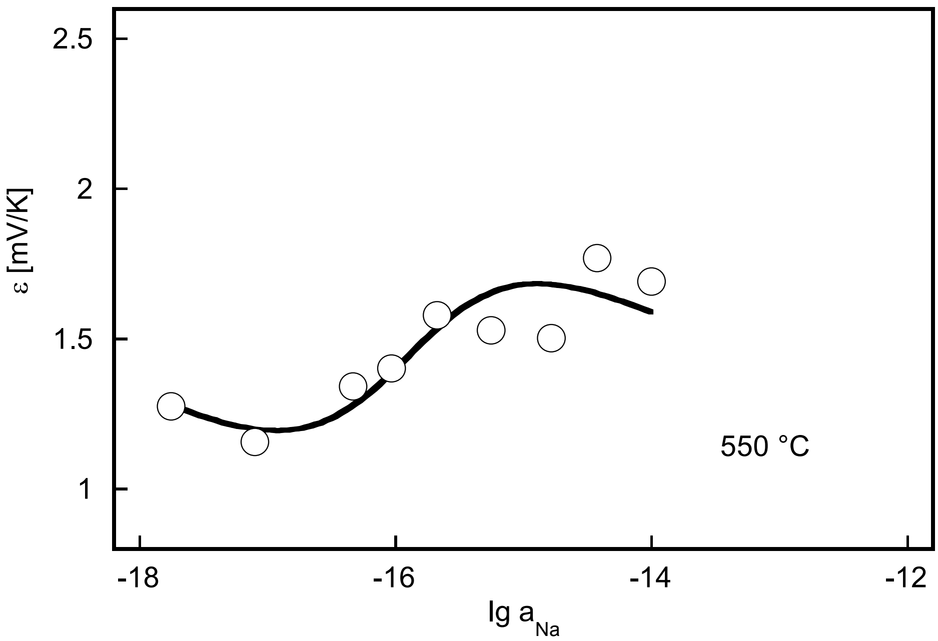

Fig. 4-29 Variation of the total thermoelectric power with the sodium chemical potential at T = 550 °C of the reference electrode

4.4.2 Sodium chemical potential dependence of the thermoelectric power

Variations of the thermoelectric power with sodium activity at different temperature of the reference electrode are shown in Fig. 4-28, 4-29 and 4-30. The data for thermoelectric power evaluated under wide range of sodium chemical potential are always positive.

The values of thermoelectric power measured under different sodium activity showed disagreement with theoretical behaviour (dotted line) when material is considered as pure ion conductor. Measured thermoelectric power as a function of sodium chemical potential at fixed temperature of the reference electrode are fitted by a non-linear regression procedure using Eq. 2-92 with $a_\oplus$, C_1, C_2 and C_3 (cf. 2.8.2) as a fitting parameters and are represented with solid line in the Fig. 4-30, 4-31 and 4-32.

The Fig. 4-30 4-31 and 4-32 reveal that at high sodium chemical potential the total thermoelectric tends to approach to pure ionic conductor behaviour (to upper dotted line in Fig. 4-30, 4-31 and 4-32).

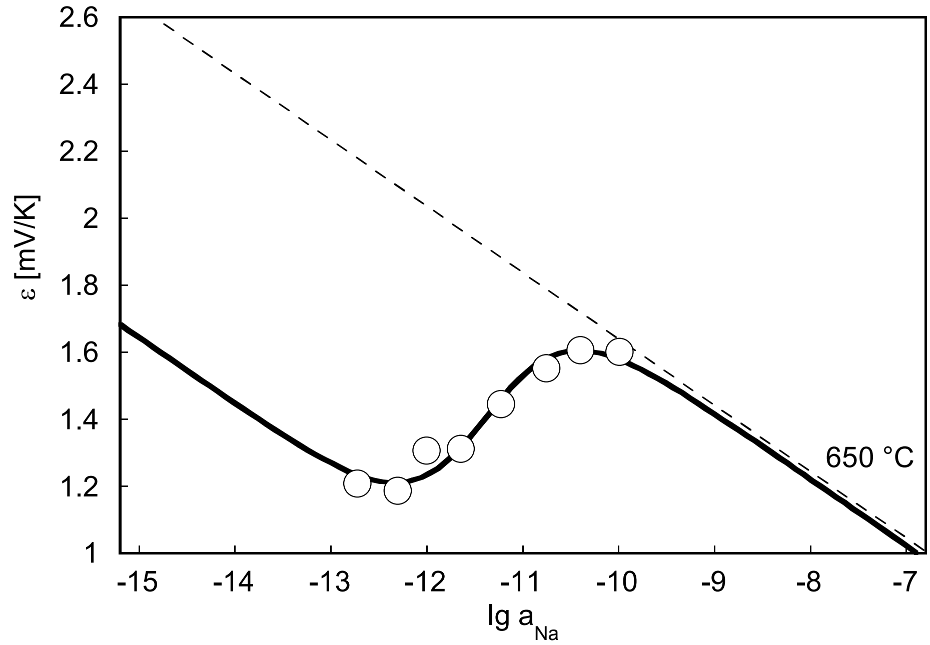

Fig. 4-30 Sodium chemical potential dependence of the thermoelectric power at T= 650°C (solid line curve fitting according to Eq. 2-92)

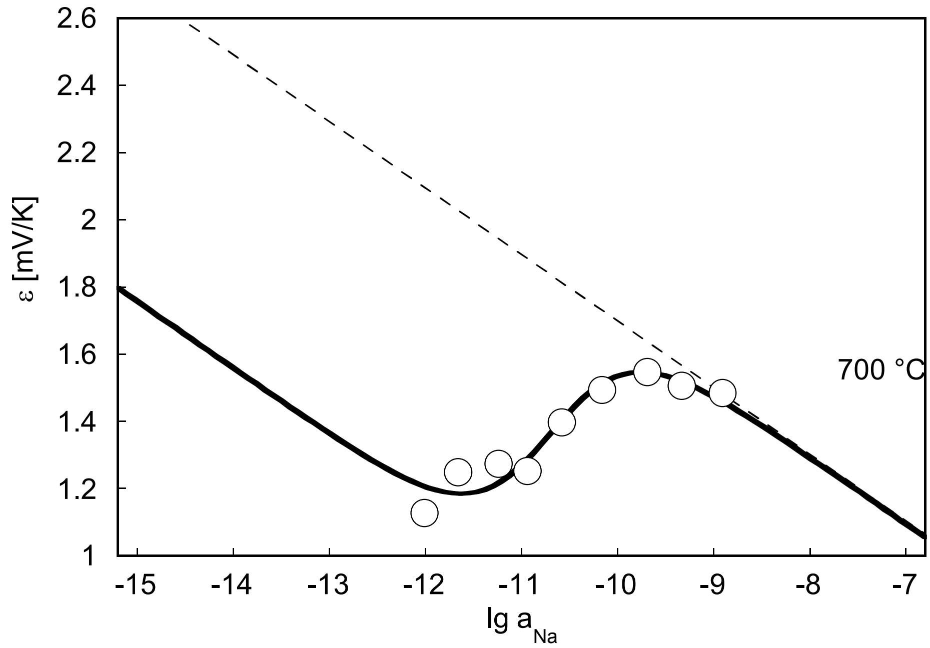

Fig. 4-31 The thermoelectric power as a function of the sodium activity at T= 700 °C (solid line curve fitting according to Eq. 2-92)

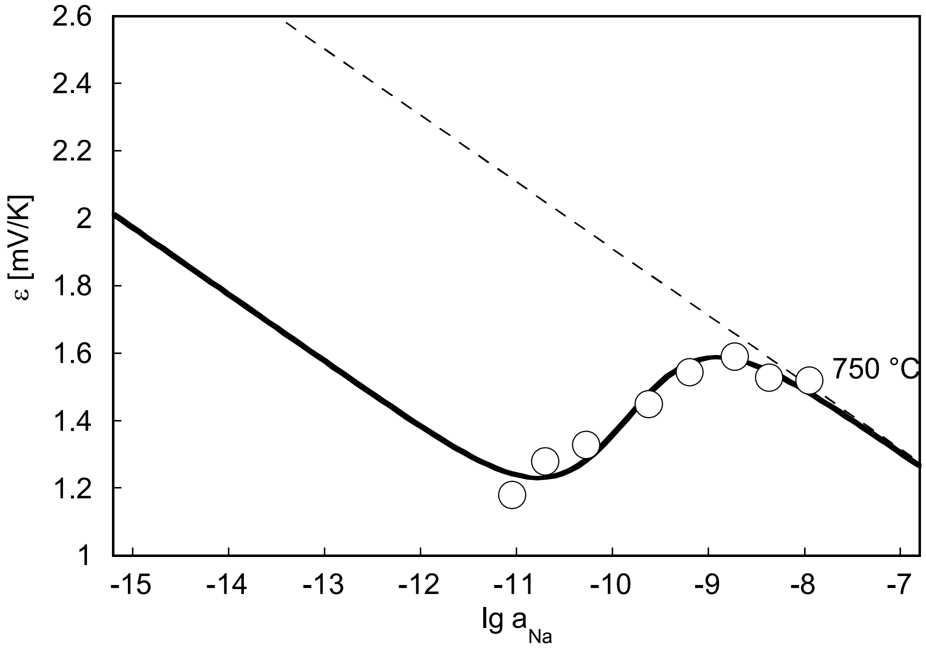

Fig. 4-32 The thermoelectric power as a function of the sodium activity at T= 750 °C (solid line curve fitting according to Eq. 2-92)

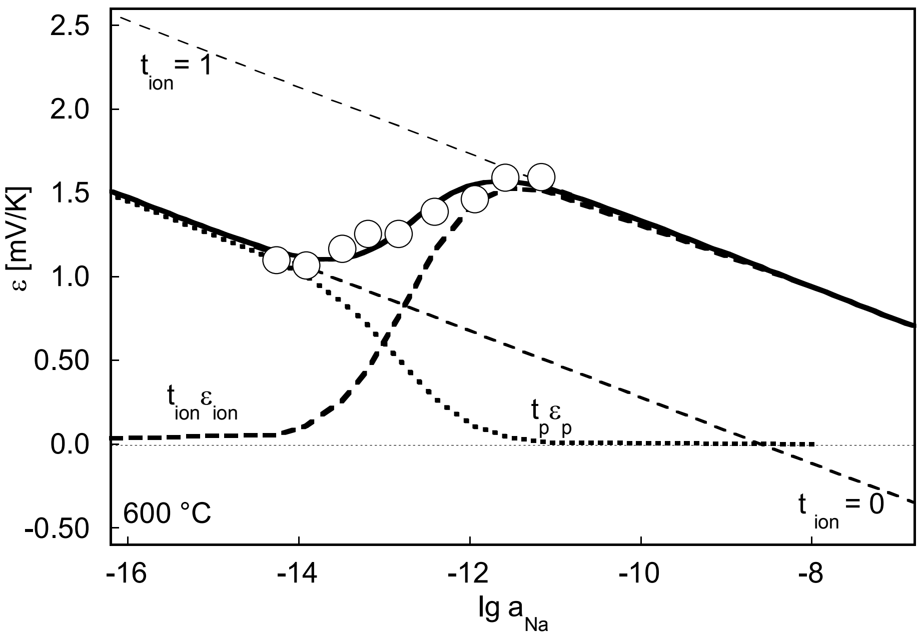

Fig. 4-33 Typical fitted results for the thermoelectric power ($\varepsilon = t_{ion}\varepsilon_{ion} + t_p\varepsilon_p$), illustrating the contribution of partial thermoelectric on total.

However, with decreasing the sodium chemical potential, the influence of electronic transference number on total thermoelectric power relationship increases. Hence, a drop on thermoelectric power takes place, and a new behaviour due to only hole electrons is established.

A typical fitting of the result at 600 °C is shown in the Fig. 4-33 to illustrate the contribution of partial thermoelectric power on total thermoelectric power. It is discernible that if the sodium activity is decreasing, the ionic contribution on thermoelectric power tend to vanish (the dash line is going to zero) and the profile of total thermoelectric power vs. sodium activity (bold line) becomes linear with slope equal to –R/F.

On the other hand, if the sodium chemical potential increases, the contribution of ions on thermoelectric power increases hence the contribution of p-electronic on thermoelectric power (dotted line) falls and becomes zero.

4.4.3 Temperature dependence of $a_\oplus$

The values of $a_\oplus$ at each temperature of the reference electrode side of the electrolyte calculated by non-linear regression procedure were plotted as a function of inverse temperature shown in Fig. 4-34. The data plot represents a straight line with relationship,

$$\lg a_\oplus = 8.596 - \frac{18692}{T/K} \qquad \text{Eq. 4-5}$$

The present data of p-electronic conduction parameter are in excellent agreement with that obtained by potentiometric technique [13].

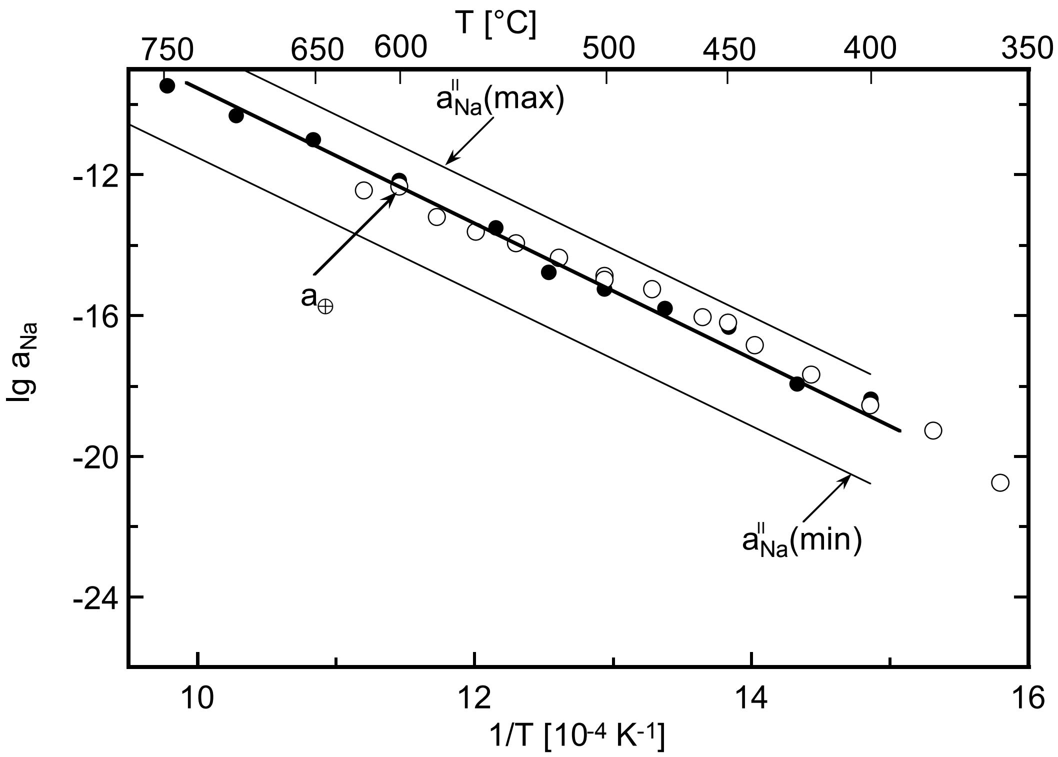

Fig 4-34 Temperature dependence of p-electronic conduction evaluated by thermoelectric power measurement (solid circle) compared with that taken using potentiometric measurement [13] (empty circle)

4.5 Influence of $a_{\oplus}$ on the thermodynamic data of $NaSb_{1.67}O_{4.33}$-$NaSbO_3$

4.5.1 The thermodynamic data of $NaSb_{1.67}O_{4.33}$ – $NaSbO_3$

Thermodynamic experiments and calculations on $NaSb_{1.67}O_{4.33}$ - $NaSbO_3$ were used to evaluate the impact of electronic conductivity on sodium beta alumina. The voltage produced by the cell (V) on changing the temperature or the gas composition usually takes few minutes until a new stable value is established. After completion of the experiment the cell was dismantled and examined by XRD and EDX and results without change as was in starting of the measurement. The variation of voltage of the cell V with sodium activity at T = 600°C, T = 550 °C and T = 500°C is shown in Fig. 4-35.

By inserting the experimental values of voltage obtained along with those of p_{CO_2}, p_{O_2} of the ambient and the thermodynamic data for Na_2CO_3 and CO_2 which were taken from JANAF [79] in Eq. 2-71, the sodium oxide activity for the $NaSb_{1.67}O_{4.33}$ – $NaSbO_3$ mixture can be derived for different temperatures and varying sodium activity. A plot of sodium oxide activity dependence on the sodium activity at T = 600 °C T = 550 °C and T = 500 °C are shown in Fig. 4-36, 4-37 and 4-38, respectively.

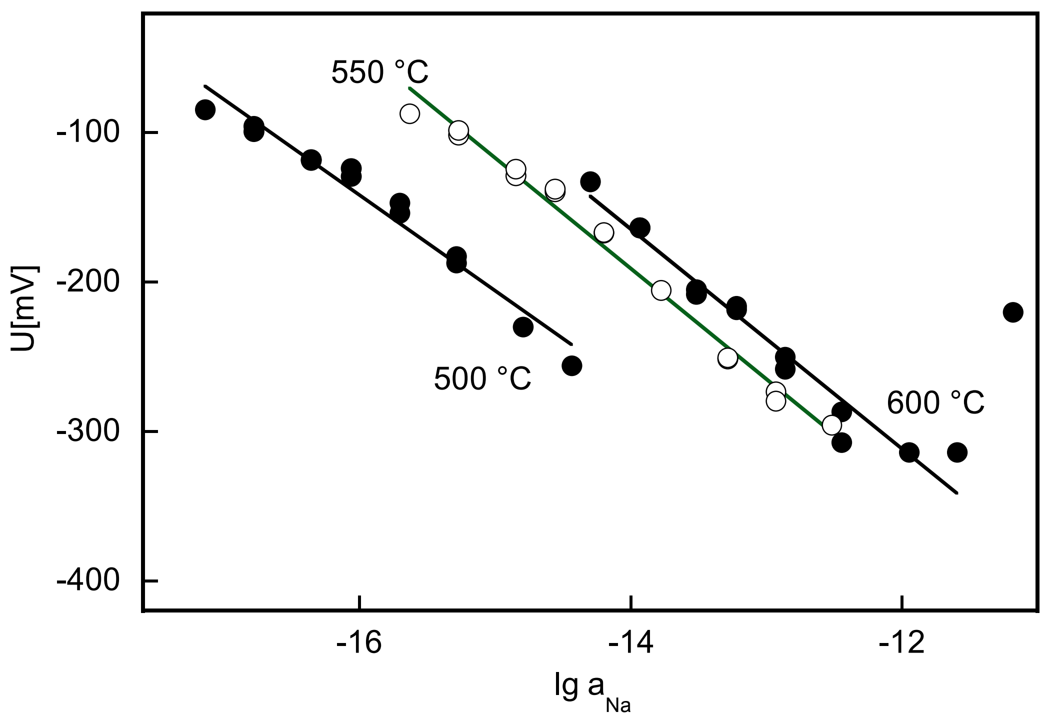

Fig. 4-35 Sodium chemical dependence of the voltage of the cell V

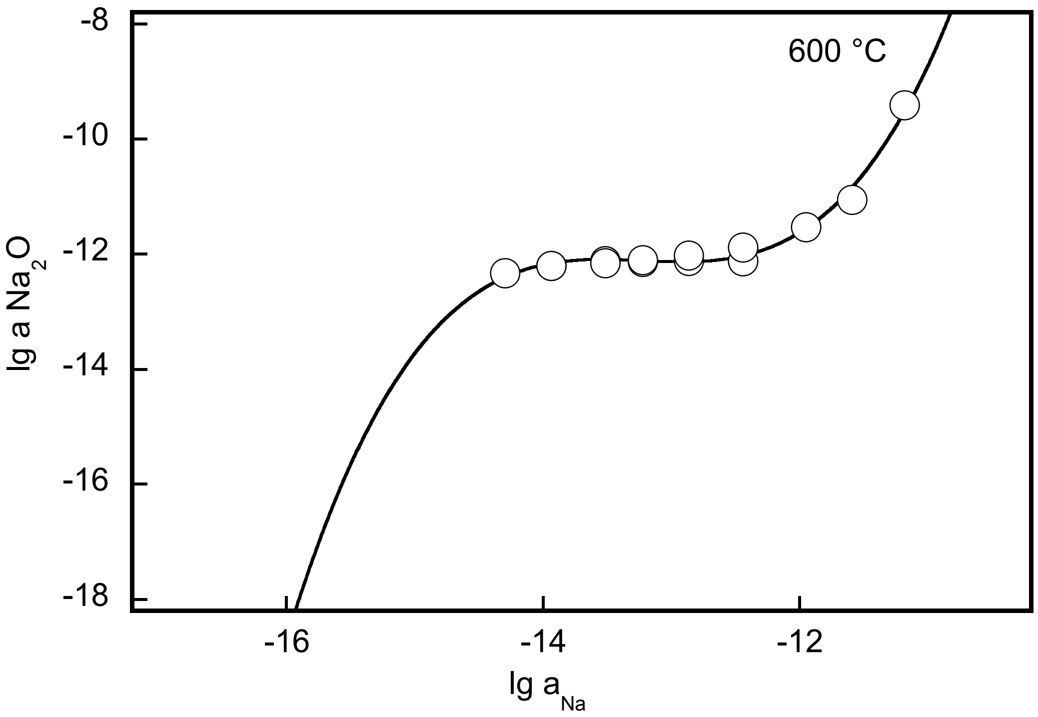

Figure 4-36 Sodium oxide activity established in $NaSb_{1.67}O_{4.33}$-$NaSbO_3$ phase equilibrium as a function of sodium activity at 600 °C

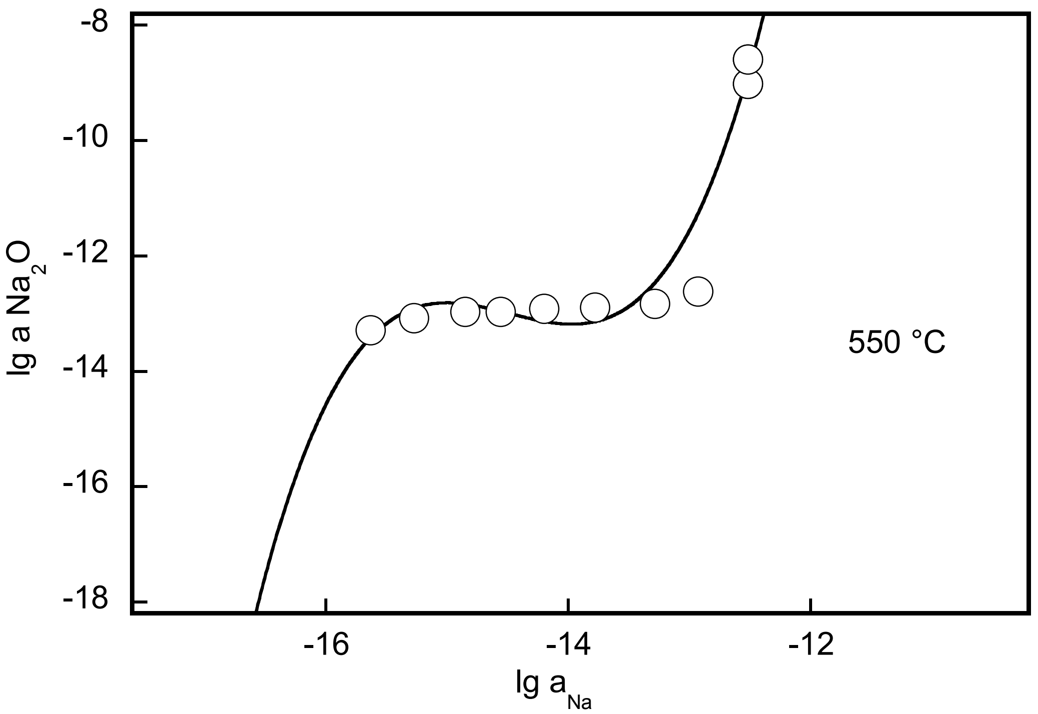

Fig. 4-37 Sodium oxide activity established in $NaSb_{1.67}O_{4.33}$-$NaSbO_3$ phase equilibrium as a function of sodium activity at 550 °C

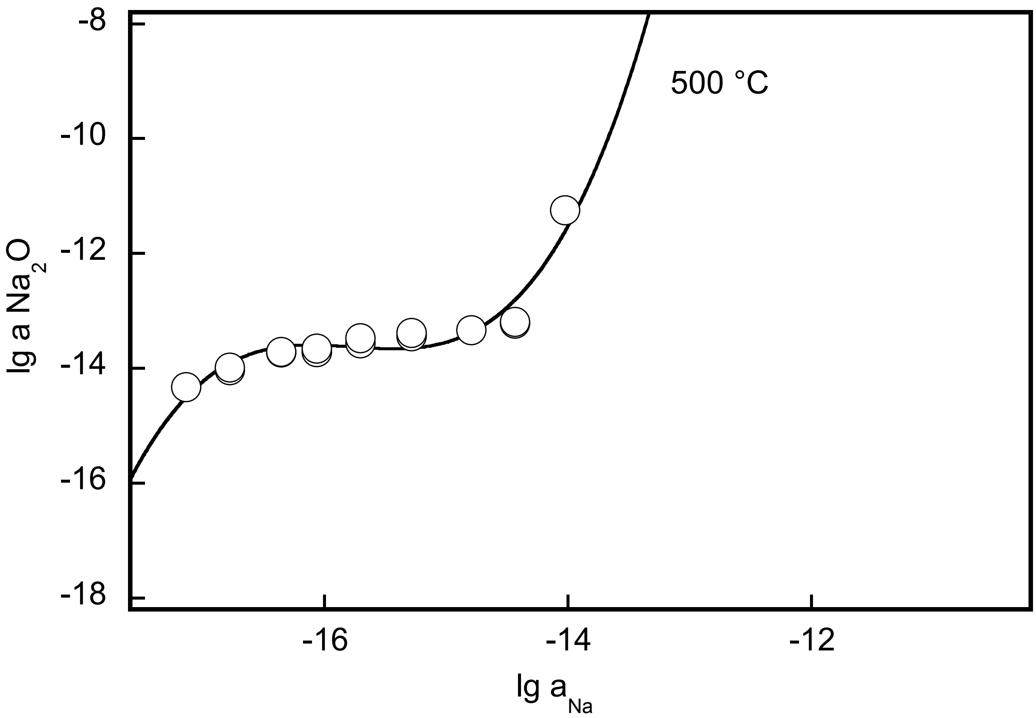

Figure 4-38 Sodium oxide activity established in $NaSb_{1.67}O_{4.33}$-$NaSbO_3$ phase equilibrium as a function of sodium activity at 500 °C

The invariance of sodium oxide activity against variation of sodium chemical potential which is the condition for the existence of two phase equilibrium as evident from the plateau of the plot (cf. Fig. 4-36, 4-37 and 4-38). The ordinates of the plateaus of Fig. 4-36, 4-37 and 4-38 as a function of the temperature are shown in Fig. 4-39.

4.5.2 Influence of $a_{\oplus}$ on thermodynamic stability data

The variation of the logarithm of sodium oxide activity with inverse of temperature in phase equilibrium under investigation along with the same obtained using galvanic cell employing Na-beta-Al_2O_3 as solid electrolyte reported in [72] is compared in Fig. 4-39.
The value of sodium oxide activity at this plateau determined as a function of temperature can be represented by the following equation:

$$\lg a_{Na_2O} = -0.2198 - \frac{10337}{T(K)} \qquad \text{Eq. 4-6}$$

Sodium activity in $NaSb_{1.67}O_{4.33}$ - $NaSbO_3$ reported by Kale et al. [72] has been measured by potentiometric measurement of the following solid state electrochemical cell

$$\text{Pt, air, } \alpha - Al_2O_3 + Na - \beta - Al_2O_3 \,|\, NBA \,|\, NaSb_{1.67}O_{4.33} - NaSbO_3\text{, air, Pt.}$$

It can be shown from the Fig. 4-39 that the data of the sodium oxide activity in the $NaSb_{1.67}O_{4.33}$-$NaSbO_3$ obtained using YSZ as solid electrolyte is lower by three to four orders of magnitude with that obtained using sodium beta alumina as solid electrolyte.

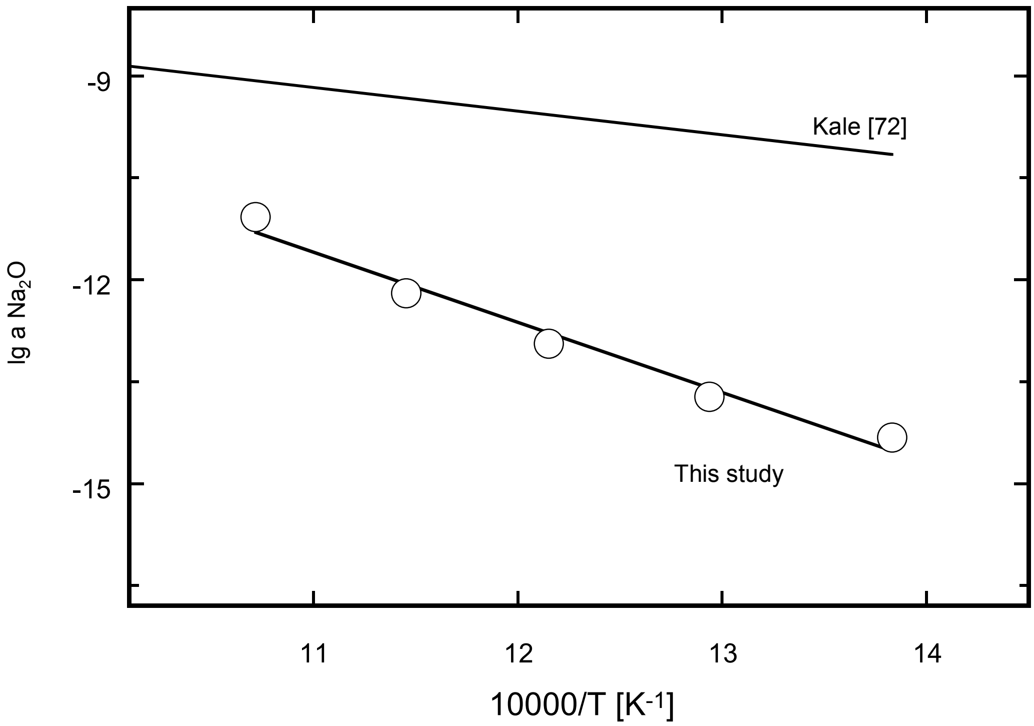

Figure 4-39 Comparison of the variation of sodium oxide activity dissolved in $NaSb_{1.67}O_{4.33}$-$NaSbO_3$ along with that reported by Kale [72].

The explanation of the above mentioned discrepancy using two different solid electrolytes is based on the influence of electronic conductivity of solid electrolytes.

The present data has been determined by a technique that definitely eliminates any falsifying effect of the electronic conduction. However, in case of Na-beta-Al_2O_3 as a solid electrolyte, the Na^+ transport number, t_{Na^+} is below unity [78].

Due to the influence of electronic conductivity on Na-beta-Al_2O_3 used as solid electrolyte the cell voltage shifts to positive values as compare to Nernst voltage [12] which is reflected in higher sodium oxide activity.

This conclusion is in well agreement with previous findings of impact of electronic conductivity on sodium beta alumina [9-13].

5. Conclusion and Outlook

The present results on p-electronic conduction parameter ($a_{\oplus}$) obtained by potentiometric technique of different solid electrolytes (K-beta-Al_2O_3, NASICON) demonstrate that the influence of the electronic transference through the solid electrolytes is not negligible.

The p-electronic conduction parameter of K-beta-Al_2O_3 is not a constant but a function of the chemical potential of the neutral potassium species in the surroundings of the electrolyte, and thus, a function of the setup of the galvanic cell. The same conclusion was drawn by Näfe et al. [13] for Na-beta-Al_2O_3.

The p-electronic conduction parameter obtained by thermoelectric power measurements on sodium beta alumina are in excellent agreement with that obtained using potentiometric technique.

The results on a_{Na_2O} for the $NaSb_{1.67}O_{4.33}$ – $NaSbO_3$ system achieved are nearly three orders of magnitude lower as data known from the literature on this system. These findings confirm that thermodynamic data obtained by electrochemical method using cation conductor as solid electrolyte may be erroneous due to non-negligible electronic conductivity through the solid electrolyte.

Further work is necessary in order to prove the consistency of electronic conductivity data for solid electrolyte using independent technique like Hebb-Wagner measurements.

To prove the consistence of these findings according to which the p-electronic conduction parameter changes if the activity of mobile species of the electrolyte is changed in the ambience, the study of electronic conductivity should be expanded to other material and to wider ranges of activity.

6. Zusammenfassung

6.1 Einleitung

Am Beispiel des Ionenleitermaterials Na-beta-Al_2O_3 konnte gezeigt werden, dass unter den Bedingungen eines potentiometrischen Gassensors in einem nicht zu vernachlässigenden Ausmaß p-elektronische Leitung im Festelektrolyten auftritt [1-10]. Zur Charakterisierung dieses Leitfähigkeitsanteils dient der p-Elektronenleitungsparameter $a_{\oplus}$, der sich zudem, und zwar entgegen seiner Definition, als eine von der Na-Aktivität in der Umgebung des Festelektrolyten abhängige Größe erweist. Diese Erkenntnisse kollidieren mit den konventionellen defektchemischen Zusammenhängen zur Beschreibung des Wechselspiels von Ionen- und Elektronenleitung in einem Festelektrolyten. Sie kollidieren ebenfalls, was ihre Bedeutung für die Gassensorik, insbesondere die CO_2-Gassensorik, anbelangt, mit der Mehrzahl der in der Literatur publizierten Arbeiten zur Anwendung solcher Sensoren. Darin spielt die elektronische Überführung als ein die Messeigenschaften beeinflussendes Phänomen keine Rolle, während ein solcher Einfluss an Na-beta-Al_2O_3 mehrfach und auf unterschiedliche Wiese belegt werden konnte. Wegen dieser Widersprüche und wegen der sich abzeichnenden grundlegenden Bedeutung der Erkenntnisse sind die bisherigen Aussagen mit Hilfe eines erweiterten Spektrums an experimentellen Untersuchungsmöglichkeiten zu verifizieren, und ihre Verallgemeinerungsfähigkeit ist anhand von Untersuchungen an ähnlichen Festelektrolytmaterialien nachzuweisen.

Zur Erfüllung des ersten Teils der Aufgabenstellung werden die bisher im Mittelpunkt stehenden Zellspannungsmessungen durch Messungen zur thermoelektrischen Kraft an Na-beta-Al_2O_3 und durch elektrochemische Messungen zur Bestimmung der thermodynamischen Stabilität eines ausgewählten heterogenen Phasengleichgewichtes ergänzt. Der zweite Aspekt der Aufgabenstellung betrifft Messungen zur Quantifizierung des p-Elektronenleitungsparameters an den alternativen Festelektrolytmaterialien K-beta-Al_2O_3 und NASICON. Für beide Materialien existieren bisher in der Literatur keinerlei Angaben zu den elektronischen Leitungseigenschaften.

Ziel der vorliegenden Arbeit ist es, die aus den alternativen experimentellen Ansätzen sich ergebenden Erkenntnisse zum Verhalten des Na-beta-Al_2O_3 mit dem bereits bekannten Wissen über dieses Material zu vergleichen und insbesondere die Leitungseigenschaften von K-beta-Al_2O_3 und NASICON an diesem Wissen zu messen.

6.2 Theoretischer Hintergrund

Die Spannung U einer galvanischen Zelle, an deren Elektroden die thermodynamischen Aktivitäten a' und a" der potenzialbestimmenden Spezies, im vorliegenden Fall Natrium oder Kalium, definiert sind, wird bei Vorliegen einer endlichen elektronischen Überführung im Festelektrolyten durch die Wagnersche Gleichung [11, 12] beschrieben. In der integrierten Form dieser Gleichung drückt sich das Ausmaß der elektronischen Leitfähigkeit quantitativ in den Elektronenleitungsparametern $a_\oplus$ und $a_\ominus$ aus [4]:

$$U = -\frac{RT}{F}\ln\left[\frac{(a'' + a_\oplus)(a' + a_\ominus)}{(a'' + a_\ominus)(a' + a_\oplus)}\right] \qquad \text{Gl. 6-1}$$

$a_\oplus$ und $a_\ominus$ sind definitionsgemäß die Metallaktivitäten, bei denen die elektronische Teilleitfähigkeit und die ionische Leitfähigkeit des Festelektrolyten identisch sind.
Werden die Aktivitäten a' und a" zu beiden Seiten des Festelektrolyten so gewählt, dass sie vernachlässigbar klein gegen den n-Leitungsparameter sind, was nach der bisherigen Kenntnis von $a_\ominus$ [10] der Fall ist, so gilt:

$$a', a'' \ll a_\ominus. \qquad \text{Gl. 6-2}$$

Unter diesen Bedingungen vereinfacht sich die verallgemeinerte Form der Wagnerschen Gleichung wie folgt [4]:

$$U = -\frac{RT}{F}\ln\frac{a''+a_\oplus}{a'+a_\oplus}\ . \qquad \text{Gl. 6-3}$$

Ist $a_\oplus$ vernachlässigbar klein im Vergleich zu den Metallaktivitäten, geht die Wagnersche in die Nernstsche Zellspannungsgleichung über:

$$U = -\frac{RT}{F}\ln\frac{a''}{a'} \qquad \text{Gl. 6-4}$$

Gl. 6-3 gestattet, aus Messdaten zur Zellspannung und der Temperatur bei Kenntnis von a' und a" die Unbekannte $a_\oplus$ zu ermitteln. Dieses Vorgehen entspricht dem Vergleich der Zellspannungen bei Vorliegen von elektronischer Überführung (Gl. 6-3) und ohne

elektronische Überführung (Gl. 6-4). Ist eine der Metallaktivitäten, im vorliegenden Fall a' nur unzulänglich oder gar nicht bekannt, so besteht alternativ die Möglichkeit, $a_\oplus$ aus der U-lg a''-Abhängigkeit zu bestimmen, was im vorliegenden Fall auf die Anwendung eines Algorithmus zur nichtlinearen Regression mit $a_\oplus$ als Optimierungsparameter hinausläuft.
Die galvanischen Zellen, die für die vorliegende Arbeit verwendet werden, haben folgenden Aufbau:

Pt, Au | CO_2, O_2, K_2CO_3(Au) | K-beta-Al_2O_3| FeO, NiO(Glas), FeNi48 | Pt, Zelle (I)
Pt, Au | CO_2, O_2, K_2CO_3(Au) | K-beta-Al_2O_3| $KSi_{1.5}O_{3.5}$, SiO_2 | O_2 | Au, Pt Zelle (II)
und
Pt, Au | CO_2, O_2, Na_2CO_3(Au) | NASICON | FeO, NiO(Glas), FeNi48 | Pt. Zelle (III)

Diese Zellen sind K- oder Na-Konzentrationsketten. Die chemische Aktivität der in den Zellsymbolen links stehenden Elektroden lässt sich durch folgende Gleichung beschreiben (M = Na, K):

$$\ln a''_M = \frac{\Delta_f G^\circ_{M_2CO_3} - \Delta_f G^\circ_{CO_2}}{2RT} - \frac{1}{2}\ln p_{CO_2} - \frac{1}{4}\ln p_{O_2} \qquad \text{Gl. 6-5}$$

Um zu garantieren, dass die an der Phasengrenze M_2CO_3/CO_2, O_2 sich einstellende Metallaktivität im gesamten Carbonat-Pellet gleich ist, ist dieses Pellet durch Au-Drähte im Innern des Festkörpers elektronisch kurzgeschlossen. Bei Vorliegen einer gewissen Natriumdiffusivität im Carbonat führt der Kurzschluss dazu, dass jeglicher Unterschied im Metall-Potenzial durch Diffusion von Metallionen ausgeglichen wird. Ähnliches bewirkt ein solcher bewusst herbeigeführter Kurzschluss auch an anderen Festkörpern.
Die Gleichgewichte, die das chemische Potenzial des jeweiligen Metalls in den rechts stehenden und als Referenzelektroden dienenden Phasensystemen der Zellen (I) – (III) definieren, sind zum Teil von komplexer Natur. In den Zellen (I) und (III) bestimmen die Oxide der zum Einsatz gelangenden FeNi-Ausdehnungslegierung (Magnifer), die während des Herstellungsprozesses an der Oberfläche der Legierung gebildet und in der angrenzenden Glasphase gelöst werden, ein Sauerstoffpotenzial, das seinerseits im Gleichgewicht mit dem im Festelektrolyten gelösten Natrium- bzw. Kaliumoxid die jeweilige Metallaktivität fixiert:

$$\ln a'_M = \frac{\Delta_f G^\circ_{M_2O}}{2RT} + \frac{1}{2} \ln a_{M_2O} - \frac{1}{4} \ln p_{O_2} \,. \qquad \text{Gl. 6-6}$$

Die Aktivität des Natrium- bzw. Kaliumoxids resultiert aus der thermodynamischen Stabilität des betreffenden Festelektrolytmaterials. Die Kenntnis dieser Größe und insbesondere die der in Gl. 6-6 eingehenden Aktivitäten der Legierungsbestandteile sowie deren Oxide ist die Voraussetzung für die Kenntnis des Referenzelektrodenpotenzials. Es kann mit Hilfe des weiter unten beschriebenen Messprinzips bestimmt werden.

Alternativ zu den bisher eingesetzten Untersuchungsmethoden zur Charakterisierung der elektronischen Leitfähigkeit wird in der vorliegenden Arbeit erstmalig die Messung der thermoelektrischen Kraft der Materialkombination Festelektrolyt/Platin praktiziert. Diese Größe ist wie folgt definiert:

$$\varepsilon = \frac{1}{F}\left[\left(1+\frac{a_\oplus}{a_{Na^+}}\right)^{-1}\left(-\frac{d\mu_{Na}}{dT} - \overline{S}_{Na^+} - \frac{Q^*_{Na+}}{T}\right) + \left(1+\frac{a_{Na^+}}{a_\oplus}\right)^{-1}\left(\overline{S}^\circ{}_p - R\ln a_{Na^+} + \frac{Q^*_p}{T}\right)\right] - \varepsilon^{(Pt)} \,. \qquad \text{Gl. 6-7}$$

Die Methode, die bisher lediglich für qualitative Aussagen, nicht aber zur Quantifizierung der elektronischen Leitfähigkeit von ionisch-elektronischen Mischleitern genutzt wurde, ist im Kontext der in der Literatur sich äußernden Konfusion um die Rolle der elektronischen Überführung von besonderer Bedeutung. Eine naheliegende Erklärung dafür könnte die Spezifik der in den unterschiedlichen Arbeiten verwendeten Referenzelektroden sein. Aus diesem Grund verspricht die Verwirklichung einer Methode, die gänzlich auf diese Spezifik verzichtet und die sich lediglich jener Materialien als Elektroden bedient, die nach gegenwärtigem Stand des Wissens alle potentiometrischen CO_2-Gassensoren auf der Basis kationenleitender Festelektrolyte gleichermassen kennzeichnen, einen wesentlichen Beitrag zur Erhellung der Konfusion. Die Messung thermoelektrischer Kräfte an einer galvanischen Zelle erfüllt diese Voraussetzungen in idealer Weise. Eine symmetrisch aufgebaute Zelle der Gestalt:

Pt, O_2, CO_2, Na_2CO_3 $(Au)_{T+\Delta T}$|Na-beta-Al_2O_3|$_T$ Na_2CO_3(Au), O_2, CO_2 Pt Zelle (IV)

mit dem zu charakterisierenden Festelektrolyten Na-beta-Al_2O_3 als Herzstück sowie identischen Elektroden auf beiden Seiten, bestehend aus der für CO_2-Sensoren typischen Phasenkombination Na_2CO_3, CO_2, O_2, liefert eine messbare Spannung, wenn der Festelektrolyt einem thermischen Gradienten ausgesetzt ist. Die zusätzliche Änderung der chemischen Umgebung des Festelektrolyten über einen möglichst großen Potenzialbereich hinweg erlaubt schließlich Aussagen über den Einfluss der elektronischen Ladungsträger auf den Messeffekt. Daraus lässt sich der Elektronenleitungsparameter quantitativ bestimmen.

Eine Möglichkeit, zu Aussagen über die elektronische Leitfähigkeit der betrachteten Festelektrolyte zu gelangen, die unabhängig von der Sensorthematik sind, bietet die kritische Analyse von in der Literatur publizierten Daten zur thermodynamischen Stabilität ausgewählter heterogener Phasengleichgewichte. Sind diese Daten mittels elektrochemischer Messungen unter Verwendung eben dieser Festelektrolyte gewonnen worden und befinden sich die von den Phasengleichgewichten realisierten Potenziale in einem Bereich, der nach den bisherigen Erkenntnissen eine merkliche elektronische Überführung erwarten läßt, dann sollten dieselben Daten verfälscht sein. Das heisst, sie sollten von denen abweichen, die auf eine Weise gewonnen wurden, bei der der Einfluss der elektronischen Überführung definitiv ausgeschlossen ist.

Die Schwierigkeit bei der Verwirklichung dieser Strategie besteht darin, einen Festelektrolyten zu finden, der hinsichtlich der elektronischen Leitungseigenschaften besser ist als der zuvor betrachtete. Im Falle eines Natrium-Ionenleiters gibt es diesbezüglich keinerlei Alternative zu Na-beta-Al_2O_3. Die Lösung des Problems gelingt mit einem Ansatz, der auf Näfe und Mitarbeiter [13] zurückgeht. Als ein für derartige Untersuchungen geeignetes Phasengleichgewicht wurde $NaSbO_3$-$NaSb_{1.67}O_{4.33}$ ausgewählt. Die galvanische Zelle hat die folgende Struktur:

$$\mathrm{Pt}\,|\,\mathrm{CO_2, O_2, Na_2CO_3 (Au)}\,|\,\mathrm{NaSb_{1.67}O_{4.33} - NaSbO_3}\underset{a'', p''_{O_2}}{|}\,\mathrm{YSZ}\underset{p'_{O_2}}{|}\,\mathrm{O_2}\,|\,\mathrm{Pt}\,. \qquad \text{Zelle (V)}$$

Zelle (V) ermöglicht die Bestimmung der thermodynamischen Stabilität von $NaSb_{1.67}O_{4.33}$ über die Bestimmung der sich in dem Gleichgewichtssystem einstellenden Aktivität des Na_2O durch Messen des Sauerstoffpotenzials an der Phasengrenze $NaSbO_3$-$NaSb_{1.67}O_{4.33}$/YSZ. Letzteres erfolgt mit Hilfe des Sauerstoffionenleiters YSZ ($Zr_{1-x}Y_xO_{2-x/2}$) nach Einstellen eines definierten Natriumpotenzials an der Phasengrenze Na_2CO_3, CO_2, O_2 und Transferieren dieses Potenzials zur Messstelle.

Vor ein ähnliches Problem wie das vorstehend beschriebene ist man gestellt, wenn die Natrium- bzw. Kaliumaktivität der Referenzelektroden jener Zellen, mit deren Hilfe die elektronische Leitfähigkeit der eingesetzten Elektrolyte ermittelt wurden, unabhängig von jeglichem Einfluss eines verfälschenden Elektronenleitungsanteils bestimmt werden soll. Dies ist die Voraussetzung zur Charakterisierung des Elektronenleitungsparameters auf konventionelle Art und Weise, das heisst über den Vergleich von Gl. 6-3 mit Gl. 6-4. Das Problem lässt sich mit Hilfe des von Näfe [14] beschriebenen Verfahrens lösen. Grundlage sind die folgenden galvanischen Zellen:

$$\text{Pt},\ \Big|\ CO_2, O_2,\ K_2CO_3(Au)_{a''_K}\ \Big|\ KBA(Au)\ \Big|\ YSZ\ \Big|\ KBA(Au)_{a'_K}\ \Big|\ \text{FeO, NiO(Glas), FeNi48}\ \Big|, \text{Pt} \qquad \text{(VI)}$$

und

$$\text{Pt},\ \Big|\ \text{FeNi48, NiO, FeO(Glas)}\ \underset{a'_K = f(T)}{|}\ KBA(Au)\ |\ YSZ\ |\ KBA(Au)\ \underset{a''_K}{|}\ KSi_{1.5}O_{3.5}, SiO_2, (Au)\ |\ O_2, \text{Pt}\text{. Zelle (VII)}$$

Die Zellen (VI) und (VII) sind Sauerstoffkonzentrationsketten, bei denen das zu bestimmende Natriumpotenzial auf thermodynamisch reproduzierbare Art und Weise in ein Sauerstoffpotential transformiert wird, dessen Messung ohne Beeinflussung durch elektronische Überführung gelingt. Die der Datenauswertung zugrunde liegende Gleichung lautet [14]:

$$U = -\frac{RT}{F}\ln\frac{a''_K}{a'_K} + \frac{RT}{2F}\ln\frac{a''_{K_2O}}{a'_{K_2O}}\,. \qquad \text{Gl. 6-8}$$

6.3 Experimentelle Durchführung

Als Festelektrolyte wurden kommerziell verfügbare und im Einzelfall speziell präparierte Materialien mit den in Tabelle 6.1 aufgeführten Zusammensetzungen verwendet.

Tabelle 6.1: Chemische Zusammensetzung der Festelektrolyte

	Oxidanteil [Gew. %]			
Festelektrolyte	M_2O (M = Na; K)	MgO	Li_2O	Al_2O_3
K-beta-Al_2O_3	11.58	-	0.73	87.69
Na-beta-Al_2O_3	9.7	2.52	-	87.78
NASICON	$Na_{1+x}Zr_2P_{3-x}Si_xO_{12}$ (x = 2)			

In den Zellen (V), (VI) und (VII) diente eine polierte ZrO_2-Tablette (Friatec AG, Mannheim D) mit 8 Gew.-% Y_2O_3 als Festelektrolyt. In der Thermozelle (IV) wurde zur Einstellung eines ausreichend großen Temperaturgradienten ein Sinterkörper von 25 mm Länge als Festelektrolyt eingesetzt.

Die Carbonat-Messelektroden wurden als etwa 1 mm starke Pellets durch isostatisches Pressen aus K_2CO_3- oder Na_2CO_3-Pulver hergestellt, oberflächlich bearbeitet und auf die jeweiligen Festelektrolyte per Federdruck aufgedrückt.

Zur Gewährleistung eines inneren elektronischen Kurzschlusses wurden beim Pressen Golddrähte in den Sinterkörper eingebracht. In den übrigen Fällen wurde der Kurzschluss durch Sputtern einer Au-Schicht auf die betreffenden Keramikoberflächen bewirkt.

Zur Herstellung von Zellen des Typs (I), (III) und (VI) wurde der in Pelletform vorliegende Festelektrolyt mit Hilfe eines Lotglases [16] in einen Metalltiegel aus einer Fe/Ni-Ausdehnungslegierung hermetisch eingefügt. Im Fall der Zellen (II) und (VII) erfolgte die Präparation der Referenzelektrode durch Auftragen einer dünnen Schicht aus speziell synthetisiertem $KSi_{1.5}O_{3.5}$-Wasserglas [17] auf die Oberfläche des K-beta-Al_2O_3-Sinterkörpers und anschließendes Verteilen eines grobkörnigen SiO_2-Pulvers über dieser Schicht.

$NaSbO_3$ und $NaSb_{1.67}O_{4.33}$ wurden durch Mischen der stöchiometrischen Mengen von Na_2CO_3 und Sb_2O_5 und durch Erhitzen auf 1373 K in Luft präpariert.

Alle Messzellen wurden in einen gasdichten Probenhalter aus Quarzglas montiert und in temperaturgeregelten Öfen auf die entsprechende Temperatur gebracht. Die Gasatmosphäre zur Fixierung der Metallaktivität nach Äquilibrierung mit M_2CO_3 wurde durch Verdünnen dreier unterschiedlicher, kommerziell verfügbarer CO_2-O_2-Ar-Gasmischungen (Tabelle 6.2) mit Ar eingestellt, so dass ein möglichst weiter Bereich der Gaspartialdrucke überstrichen werden konnte.

Tabelle 6.2: CO_2-O_2-(Ar)-Gase

Gas Nr.	Argon	p (O_2) [Pa]	p (CO_2) [Pa]
I	Ar 5.0 (≤ 2 ppm O_2)	20.27 (200 ppm)	20.27 (200 ppm)
II	Ar 5.0 (≤ 2 ppm O_2)	$1.01 * 10^3$ (10000 ppm)	$1.01 * 10^3$ (10000 ppm)
III	-	$85.11 * 10^3$ (84 vol-%)	$16.21 * 10^3$ (16 vol-%)

Die Spannung wurde mit Hilfe von hochohmigen Keithley-Elektrometern (Keithley Instr. Inc., USA) gemessen.

6.4 Ergebnisse und Diskussion

Das Ansprechen der Spannung von Zelle (I) auf die Änderung der K-Aktivität im untersuchten Temperaturbereich von 320 bis 620 °C ist qualitativ identisch mit dem Verhalten der entsprechenden, auf Na-beta-Al_2O_3 aufbauenden Zellen. Im Bereich großer K-Aktivitäten folgt das Messsignal zunächst der Tendenz des durch die Nernstsche Gleichung vorgegebenen Verhaltens. Mit kleiner werdender K-Aktivität aber wird der Anstieg der Zellspannung immer schwächer, bis die Zellen schließlich kaum noch auf die Änderung der äußeren Bedingungen reagieren. Die Steigung der U-lga_K-Kurven ist im gesamten über etwa drei Dekaden reichenden Aktivitätsintervall kleiner als der nach der Nernstschen Gleichung erwartete Wert.

Die experimentellen Daten können auf der Basis der Wagnerschen Gleichung (6-2) mit ausreichender Genauigkeit beschrieben werden, wobei sich der unbekannte Parameter $a_\oplus$ mit Hilfe eines Algorithmus zur nichtlinearen Regression quantitativ ermitteln lässt. Wird lg $a_\oplus$ über der inversen Temperatur aufgetragen, ergibt sich in Übereinstimmung mit den an Na-beta-Al_2O_3 gemachten Erfahrungen eine lineare Abhängigkeit.

Die Interpretation des beschriebenen Verhaltens als durch den Einfluss elektronischer Leitung im Elektrolyten verursacht, ist konsistent mit den Beobachtungen zur zeitabhängigen Entwicklung der Zellspannung bei schrittweiser Änderung der K-Aktivität der Messelektrode. Bei vergleichsweise hohen K-Aktivitäten zeigt die Zelle eine normale Reaktion, d.h. die Zellspannung ändert sich bei einem Gaswechsel schnell auf den neuen Wert. Wird das Niveau der K-Aktivität der Messelektrode kleiner, ändert sich auch die Zeitabhängigkeit der Spannung. Die Zellspannung steigt zunächst wie erwartet an, bricht aber anschließend partiell wieder zusammen. Die Ursache dafür ist das Ansteigen des Ausmasses des internen partiellen Kurzschlusses in der Zelle von großen zu kleineren K-Aktivitäten hin, verursacht durch das Ansteigen der p-elektronischen Leitfähigkeit im Festelektrolyten.

Auch das Messverhalten von Zelle (II) im Vergleich zu dem von Zelle (I) gleicht den vom Na-beta-Al_2O_3 her bekannten Beobachtungen. Allein die gegenüber Zelle (I) veränderte Referenzelektrode ist die Ursache dafür, dass die Spannung von Zelle (II) sich gänzlich anders verhält. Nunmehr reagiert das Messsignal nahezu in der vom Nernstschen Gesetz vorgeschriebenen Weise auf die Änderung der Bedingungen an der Messelektrode. Es lässt sich zeigen, dass dieses Verhalten nicht etwa auf das Ausbleiben jeglichen Einflusses von elektronischer Leitfähigkeit im Elektrolyten zurückzuführen ist. Vielmehr bewirkt das in Zelle (II) zu viel kleineren Werten hin verschobene K-Aktivitätsniveau, verursacht durch die Referenzelektrode, eine Verschiebung des Elektronenleitungsparameters zu noch kleineren Werten, als sie unter den Bedingungen von Zelle (I) sich einstellen konnten. Dadurch unterliegt die Messelektrode nicht mehr in solch starkem Maße dem Einfluss der Elektronenleitung wie im Fall von Zelle (I), woraus ein Ansprechen der Zellspannung in scheinbarer Übereinstimmung mit dem Nernstschen Gesetz vorgetäuscht wird. Dennoch bleibt die elektronische Leitfähigkeit für das Messverhalten von Zelle (II) insofern bestimmend, als sie nach wie vor die Referenzelektrodenseite beeinflusst und damit die Zellspannung unabhängig von dem Geschehen an der Messelektrode um einen nahezu konstanten Betrag erniedrigt. Das ergibt sich aus dem Vergleich der Ergebnisse von Zelle (II) mit denen von Zelle (VII). Wie sich diese Zusammenhänge in den jeweils ermittelten Werten für $a_\oplus$ niederschlagen, ist in Abb. 6-1 zusammengefasst.

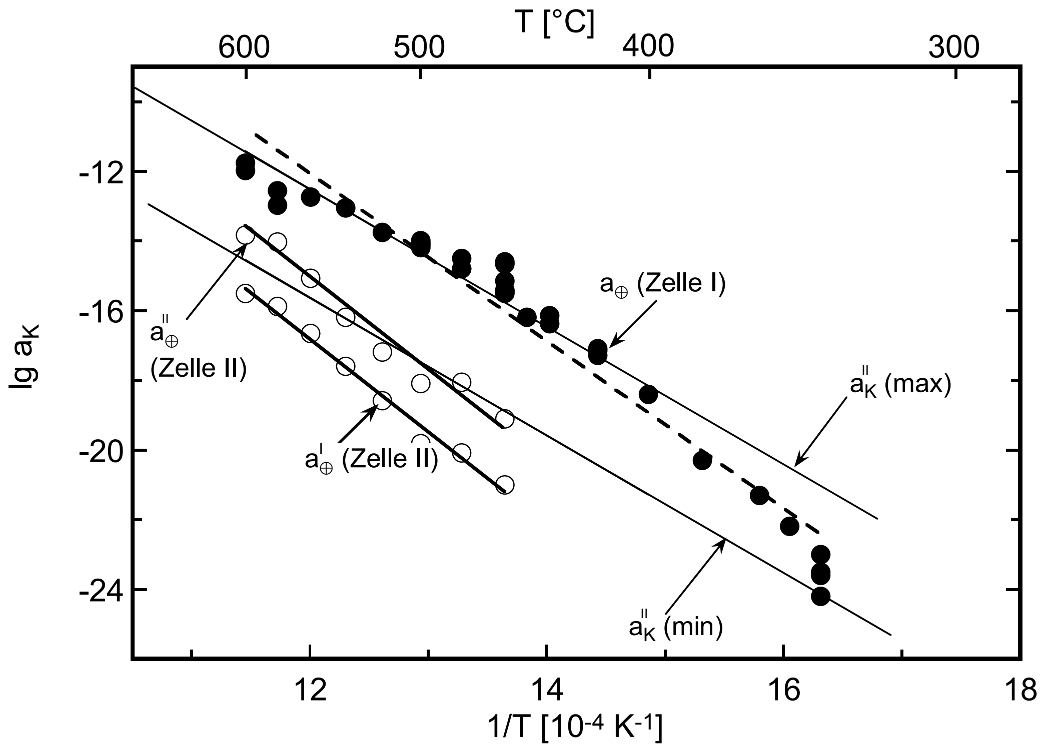

Abb. 6-1: Temperaturabhängigkeit des p-Elektronenleitungsparameters $a_\oplus$ für K-beta-Al_2O_3 im Vergleich mit dem oberen und unteren Kalium-Aktivitätsniveau an der Messelektrode von Zelle (I) und (II) ($a_\oplus$(I): Wert für Zelle I, $a_\oplus$(II): Wert für Zelle II).

Qualitativ ähnlich wie für Na-beta-Al_2O_3 und wie nach den hier gefundenen Ergebnissen auch für K-beta-Al_2O_3 liegen die Verhältnisse für NASICON. Es zeigt sich, dass NASICON hinsichtlich des Ausmaßes der elektronischen Überführung unter vergleichbaren Bedingungen keineswegs besser ist als Na-beta-Al_2O_3 (siehe Abb. 6-2). $a_\oplus$ ist sogar geringfügig größer als der Wert für Na-beta-Al_2O_3. Für die Temperaturabhängigkeit von $a_\oplus$ gilt:

$$\lg a_\oplus = 16.16 - \frac{23037}{T/K}. \qquad \text{Gl. 6-9}$$

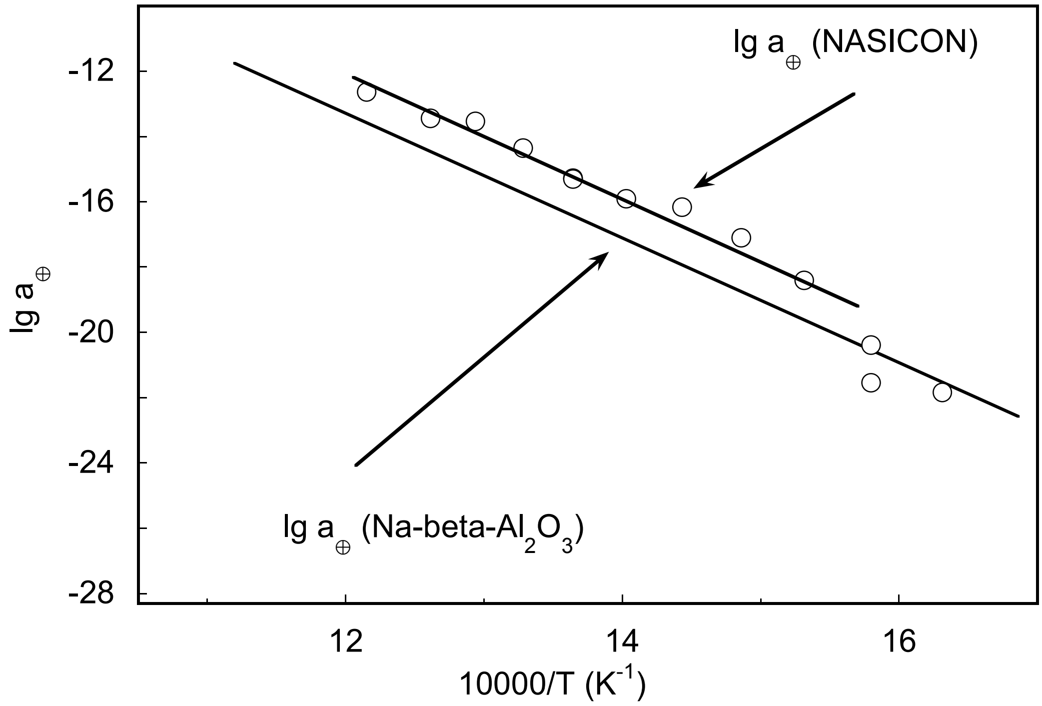

Abb. 6-2 Temperaturabhängigkeit des p-Elektronenleitungsparameters von NASICON im Vergleich zu der für Na-beta-Al_2O_3 [8].

Die Ergebnisse zur Messung der thermoelektrischen Kraft von Na-beta-Al_2O_3 als Funktion des Natrium-Potenzials in der Umgebung des Elektrolyten belegen schließlich, dass das Auftreten der Elektronenleitfähigkeit völlig unabhängig ist von der Natur der in den galvanischen Zellen zum Einsatz kommenden Referenzelektroden. Wie Abb. 6-3 verdeutlicht, sind die so erhaltenen Werte für $a_\oplus$ praktisch identisch mit denen auf konventionelle Weise für Na-beta-Al_2O_3 gewonnenen Daten. Entscheidend ist also nicht die Art der Elektrode, sondern lediglich das Niveau des von den Elektroden realisierten Potenzials der Metall-Aktivität. Demzufolge reicht das Natrium-Potenzial der in den üblichen CO_2-Sensoren einheitlich dienenden Messelektrode aus, um eine merkliche elektronische Leitung im Festelektrolyten Na-beta-Al_2O_3 zu induzieren. Dieses Ergebnis beweist, dass in allen potentiometrischen CO_2-Sensoren, die sich des hier praktizierten Messprinzips bedienen, eine mehr oder weniger große Elektronenleitung im Festelektrolyten auftreten muss. Erst dadurch, dass der Elektronenleitungsparameter, wie in der vorliegenden Arbeit erneut unter Beweis gestellt, die Eigenschaft besitzt, sich hinsichtlich seiner Größe an die äußeren Bedingungen zu einem gewissen Grade anzupassen, vermag sich der Einfluss der Elektronenleitung einer oberflächlichen Prüfung teilweise oder gänzlich zu entziehen. Das erklärt die bisherigen Widersprüche zu dieser Thematik in der Literatur.

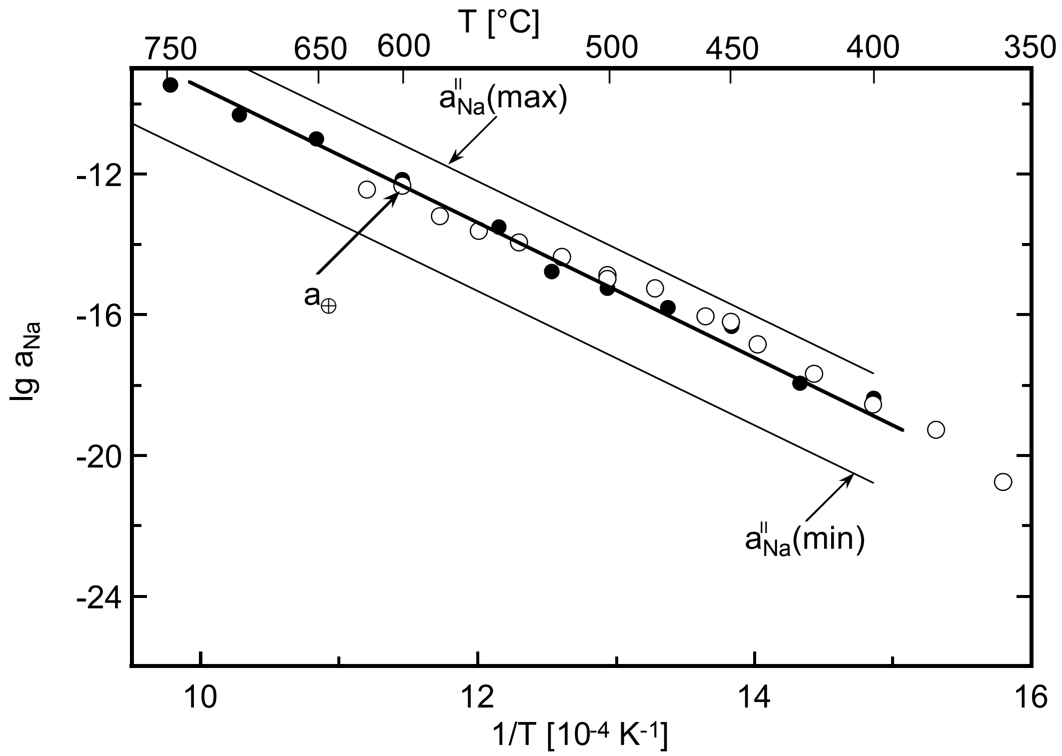

Abb. 6-3 Temperaturabhängigkeit des p-Elektronenleitungsparameters von Na-beta-Al_2O_3, ermittelt aus thermoelektrischen Messungen an der Zelle (IV), im Vergleich zu den aus isothermen Messungen an Zellen vom Typ (I) resultierenden Daten (aus [8]).

Die vorstehend erörterten Zusammenhänge werden durch die Messungen zur thermodynamischen Stabilität des $NaSbO_3$-$NaSb_{1.67}O_{4.33}$-Systems gänzlich bestätigt.. Die von Kale [18] an diesem System mit Na-beta-Al_2O_3 als Festelektrolyt ermittelte Na_2O-Aktivität unterscheidet sich den Messungen mit Zelle (V) zufolge, also bei definitivem Ausschluss jeglicher elektronischer Überführung, von den hier erhaltenen Ergebnissen um mehrere Größenordnungen (Abb. 6-4). Das bestätigt, daß unter den von Kale praktizierten Bedingungen für die Autoren unbemerkt, aber in guter Übereinstimmung mit den hier erörterten Daten zum Elektronenleitungsparameter $a_{\oplus}$, der Messwert in seiner Größe durch elektronische Leitung verfälscht wurde.

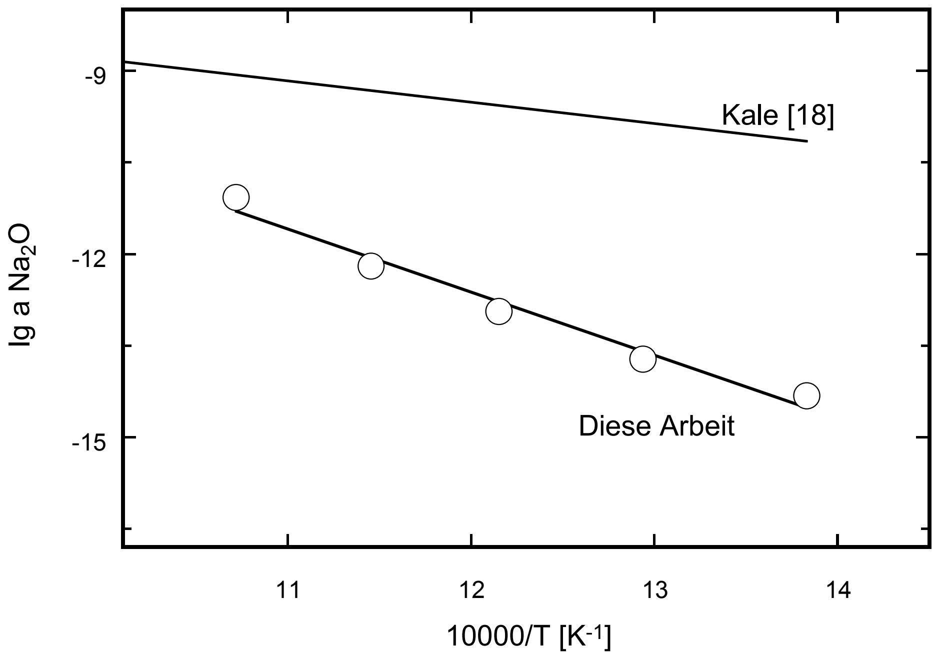

Abb. 6-4 Temperaturabhängigkeit der Na_2O-Aktivität im heterogenen Phasensystem $NaSbO_3$-$NaSb_{1.67}O_{4.33}$.

Die in vorliegender Arbeit durchgeführten Untersuchungen an Na-beta-Al_2O_3, K-beta-Al_2O_3 und NASICON bestätigen voll und ganz die für Na-beta-Al_2O_3 bereits bekannten Zusammenhänge. Sie unterstreichen den verallgemeinerungswürdigen Charakter der beobachteten Phänomene.

6.5 Literatur

[1] H. Näfe, Solid State Ionics **68** (1994) 249

[2] H. Näfe, M. Fritz und W. J. Lorenz, Solid State Ionics **74** (1994) 275

[3] H. Näfe, C. Sun, Solid State Ionics **86-88** (1996) 773

[4] H. Näfe, Solid State Ionics **113-115** (1998) 205

[5] H. Näfe, J. Electrochem. Soc. **143** (1996) 943

[6] H. Näfe, Sensors and Actuators **B 21** (1994) 79

[7] H. Näfe, S. Gollhofer and F. Aldinger, Mater. Res. Soc. Symp. Proc. **548** (1999) 521

[8] H. Näfe, S. Gollhofer and F. Aldinger, J. Electrochem. Soc. **149** (2002) E311

[9] H. Näfe, M. Steinbrück, J. Electrochem. Soc. **141** (1994) 2779

[10] S. Gollhofer, Dissertation, Max-Planck-Institut für Metallforschung Stuttgart, Stuttgart 2002

[11] M. Steinbrück, H. Näfe, Solid State Ionics **67** (1994) 271

[12] C. Wagner, Z. Phys. Chem. **B 21** (1933) 25

[13] C. Wagner, in: Advances in Electrochemistry and Electrochemical Engineering, Bd. 4, Hrsg. P. Delahay, Wiley-Interscience New York (1966) 1

[14] H. Näfe, F. Meyer und F. Aldinger, Electrochim. Acta **45** (1999) 1631

[15] H. Näfe, J. Electrochem. Soc., submitted

[16] H. Näfe, J. Nucl. Mat. **173** (1990) 67

[17] H. Näfe, J. Electrochem. Soc. **144** (1997) 915

[18] G. M. Kale and S. Srikanth, J. Am. Ceram. Soc. **82** (1999) 2161

7. References

[1] N. Weber, Energy Conv. **14** (1974) 1

[2] L. C. De Jonghe, L. Feldman and A. Beuchele, J. Mater. Sci. **16** (1981) 780

[3] L. C. De Jonghe, J. Electrochem. Soc. Techn. **129** (1982) 752

[4] A. V. Virkar, J. Mater. Sci. **20** (1985) 552

[5] C. Sun, Z. Guo, Guisuanyan Xuebao **9** (1981) 444

[6] O. Takikawa, A. Imai und M. Harata, Solid State Ionics **7** (1982) 101

[7] M. Fritz, M. R. Barbosa, G. Staikov, W. J. Lorenz, M. Steinbrück and R. Knödler, Solid State Ionics **62** (1993) 273

[8] M. Steinbrück, H. Näfe, Solid State Ionics **67** (1994) 271

[9] H. Näfe, Solid State Ionics **68** (1994) 249

[10] H. Näfe, M. Fritz and W. J. Lorenz, Solid State Ionics **74** (1994) 275

[11] H. Näfe, C. Sun, Solid State Ionics **86-88** (1996) 773

[12] H. Näfe, Solid State Ionics **113-115** (1998) 205

[13] H. Näfe, S. Golllhofer and F. Aldinger, J. Electrochem. Soc. **149** (2002) E311

[14] H. Näfe, Sensor Actuators **B 21** (1994) 79

[15] M. Itoh, E. Sugimoto and Z. Kozuka, Trans. Jap. Inst. Met. **25** (1984) 504

[16] T. Maruyama, S. Sasaki and Y. Saito, Solid State Ionics **23** (1987) 107

[17] R. Akila and K. T. Jacob, Sensor Actuators **16** (1989) 311

[18] J. Liu and W. Weppner, Eur. J. Solid State Inorg. Chem. **28** (1991) 1151

[19] H. –H. Möbius, P. Shuk and W. Zastrow, Fresenius J. Anal. Chem. **356** (1996) 221

[20] H. Y-P. Hong, Mat. Res. Bull. **11** (1976) 173

[21] J. B. Goodenough, et al., Mat. Res. Bull. **11** (1976) 203

[22] C. A. Beevers, S. Brohult, Z. Krist. **95** (1937) 59

[23] M. Bettman, L.L. Terner, Inorg. Chem. **10** (1971) 1442

[24] J. Felsche, Naturwissenschaften **54** (1967) 612

[25] C. R. Peters, H. Bettman, J. W. Moore, M. D. Glick, Acta Cryst. B**27** (1971) 1826

[26] P. D. Dernier, J. P. Remeika, J. Solid State Chem. **17** (1976) 245

[27] T. Kodama, G. Muto, J. Solid State Chem. **17** (1976) 61

[28] W.L. Roth, J. Solid State Chem. **4** (1972) 60

[29] F. A. Kröger, H. J. Vink, Solid State Physics, Vol. **3**, 307, ed. by F. Seitz, D. Turnbull, Academic Press, New York 1956

[30] F. A. Kröger, H. J. Vink, J. Phys. Chem. Solids, **5** (1958) 208

[31] H. Näfe, M. Steinbrück, J. Electrochem. Soc. **141 [10]** (1994) 2779

[32] W. L. Worrell, Solid Electrolytes, ed. by S. Geller, Spring-Verlag, Berlin-Heidelberg-New York 1977, pp. 146

[33] K. S. Goto, Solid state electrochemistry and its applications to sensors and electronic devices, Material Science Monographs 45, Elsevier, Amsterdam-Oxford-New York-Tokyo 1988, pp 12.

[34] J. L. Briant and G. C. Farrington, J. Solid State Chemistry **33** (1980) 385

[35] W.L. Roth, R.E. Benenson, V.K. Tikku, J.L. Briant and B. Dunn; Solid State Ionics **5** (1981) 163

[36] A. P. de Kroon, F. Gstrein, G.W. Schäfer, F. Aldinger; Solid State Ionics **133** (2002) 107

[37] Takashi, K. Kuwabara, H. Ohyanagi, J of Applied Electrochemistry **11** (1981) 77

[38] M. Williams, A. Kisor, and M. A. Ryan, J. Electrochem. Soc. **142**, No. 12 (1995) 4246

[39] M. Williams, B.J. Nakamura, M.L. Underwood, M.A. Ryan, D. O'Connor, and S. Kikkert, Solid State Ionics **53-56** (1992) 806

[40] N. Baffier, J.C. Badon, Ph. Colomban, Mat. Res. Bull. **16** (1981) 259

[41] H. Engstrom, J. B. Bates and J. C. Wang, Solid State Commun. **35** (1980) 543

[42] J. B. Bates, H. Engstrom, J. C. Wang, B. C. Larson, N. J. Dudney and W. E. Brundage, Solid State Ionics **5** (1981) 159

[43] I. W. Jones, L. J. Miles, Proc. Brit. Ceram. Soc. **19** (1971) 161

[44] A. Imai, M. Harata, Electrochem. Soc. Meeting, Abst. 277, May 1970

[45] J. H. Kennedy, A. F. Sammells, J. Electrochem. Soc. **119** (1972) 1609

[46] Y. F. Y. Yao, J. T. Kummer, J. Inorg. Nucl. Chem. **29** (1967) 2453

[47] L. C. De Jonghe, EPRI Rept. 252, July 1975

[48] R. L. Cohen, J. P. Remeika, K. W. West, J. Phys. (Paris), Collod. **6** (1974) 513

[49] D.B. McWhan, S. J. Allen, Jr., J. P. Remeika, P. D. Dernier, Phys. Rev. Letters **35** (1975) 953

[50] W. L. Roth, Trans. Am. Cryst. Assoc. **11** (1975) 51

[51] H. Rickert, C. Wagner, Ber. Bunsenges. Phys. Chem. **67** (1971) 621

[52] J. T. Kummer, Prog. Solid State Chem., **7** (1972) 141

[53] N. S. Choudhury, J. Electrochem. Soc., **120** (1973) 1663

[54] D. J. Fray, Met. Trans., **8B** (1977) 153

[55] A. Dubreuil, M. Malenfant, and A. D. Pelton, J. Electrochem. Soc., **128** (1981) 2006

[56] F. A. Elrefaie and W. W. Smeltzer, J. Electrochem. Soc., **128** (1981) 1443

[57] S. Yamaguchi, A. Imai, and K.S. Goto, Scand. J. Metall. **11** (1982) 263

[58] R. J. Brisley and D. J. Fray, Met. Trans., **14B** (1983) 435

[59] G. Rog, S. Kozinski, and A. Kozlowska-Rog, Electrochim. Acta, **28** (1983) 43

[60] W. Dai, S. Seetharaman, and L.-I. Staffansson, Scand. J. Metall. **13[1]** (1984) 32

[61] F.A. Elrefaie and W.W. Smeltzer, Solid State Ionics, **12** (1984) 517

[62] M. Itoh, K. Kimura, and Z. Kozuka, Met. Trans. Jpn. Inst. Met., **26** (1985) 353

[63] N. S. Choudhury, J. Electrochem. Soc., **133** (1986) 425

[64] S. Yamaguchi, Y. Kaneko and Y. Iguchi, Trans. Jpn. Inst. Met. **28[1]** (1987) 986

[65] M. Itoh and Z. Kozuka, J. Am. Ceram. Soc., **71[1]** (1988) C36

[66] A. Petric, A.D. Pelton, and M. Saboungi, J. Chem. Phys. **89[8]** (1988) 5070

[67] G.M. Kale and K.T. Jacob, Met. Trans., **20B** (1989) 687

[68] K.T. Jacob, K. Swaminathan, and O.M. Sreedharan, Electrochim. Acta, **36** (1991) 791

[69] G. Rog, A. Kozlowska-Rog, and K. Zakula, J. Chem. Thermodyn. **24** (1992) 41

[70] L. Zhang, D. J. Fray, J. C. Dekeyser, and F. de Schutter, Met. Trans., **27B** (1996) 794

[71] T. Mathews, D. Krishnamurthy, and T. Gnanasekaran, J. Nucl. Mater. **247** (1997) 280

[72] G. M. Kale and S. Srikanth, J. Am. Ceram. Soc. **82 [8]** (1999) 2161

[73] S. Dum, R.V. Kumar, and D.J. Fray; Solid State Ionics, **128** (2000) 141

[74] G.M. Kale and S. Srikanth, J. Am. Ceram. Soc. **83 [1]** (2000) 175

[75] R. Subasri, T. Mathews, K. Swaminathan, and O.M. Sreedharan, J. Nucl. Mater. **300** (2002) 237

[76] R. Pankajavalli, O.M. Sreedharan, and J.B. Gnanamoorthy, J. Nucl. Mater. **250** (1997) 53

[77] H. Näfe, F. Meyer, and F. Aldinger, Electrochim. Acta **45** (2000) 1631

[78] H. Näfe, Solid State Ion. **93** (1997) 117

[79] NIST-JANAF Thermochemical Tables, 4th Edition, National Institute of Standards and Technology, New York (1998)

[80] Y. Saito, T. Maruyama, Y. Matsumoto, and Y. Yano, Anal. Chem. Symp. Ser., **17** (Chem. Sens.) (1983) 326

[81] T. Maruyama, S. Sasari, Y. Saito, Solid State Ionics **23** (1987) 107

[82] R. Akila, K. T. Jacob, Journal of Applied Electrochemistry **18** (1988) 245

[83] F. Mauvy, E. Siebert, P. Fabry, Talanta **48** (1999) 293

[84] H. Kohler, H. Schultz, Solid State Ionics, **9/10** (1983) 795

[85] O. Knacke, et al. Thermochemical Properties of Inorganic Substances, Springer-Verlag/Verlag Stahleisen, Berlin-Düsseldorf (1991)

[86] J. L. Waring, R. S. Roth, H. S. Parker and W. S. Brower, J. Res. Natl. Bur. Stand., Sect. A, **80A [5-6]** (1976) 761

[87] H. Näfe, J. Nucl. Mater. **175** (1990) 67

[88] H. Näfe, J. Electrochem. Soc., submitted

[89] D. W. Johnson, S. M. Grundstaff and W. W. Rhodes, Bull. Am. Ceram. Soc. **58** [9] (1979) 849

[90] G. E. Youngblood, A. V. Virkar, W. R. Cannon and R. S. Gordon, Am. Ceram. Soc. Bulletin, **56** [1] (1977) 206

[91] H. Näfe, J. Electrochem. Soc. **144 [11]** (1997) 3922

[92] T. Maruyama, X. Y. Ye, Y. Saito, Solid State Ionics **23** (1987) 113

[93] F. Salam, S. Bredikhin, P. Birke, W. Weppner, Solid State Ionics **110** (1988) 319

[94] T. Maruyama, Materials Science and Engineering, **A146** (1991) 81

[95] S. Yao, Y. Shimizu, N. Miura and N. Yamazoe, J. Electrochem. Soc. **139** (1992) 1384

[96] N. Miura, S. Yao, Y. Shimizu and N. Yamazoe, Sensor and Actuators B **13** (1993) 387

[97] N. Miura, S. Yao, Y. Shimizu and N. Yamazoe, Solid State Ionics **70-71** (1994) 572

[98] G.M. Kale, A.J. Davidson and D.J. Fray, Solid State Ionics **86-88** (1996) 1107

[99] S. –D. Choi, W.-Y. Chung, D.-D. Lee, Sensor and Actuators B **35-36** (1996) 263

[100] M. A.-Porta, R.V. Kumar, Sensor and Actuators B **71** (2000) 173

[101] Y. Shimizu and N. Yamashita, Sensor and Actuators B **64** (2000) 102

[102] K. Kaneyasu, K. Otsuka, Y. Setoguchi, S. Sonoda, T. Nakahara, I. Aso and N. Nakagaichi, Sensor and Actuators B **66** (2000) 56

CURRICULUM-VITAE

Family name:	Shqau
First name:	Krenar
Date of birth:	16/12/1971
Place of birth:	Tirana, Albania
Nationality:	Albanian
Sex:	Male
Marital status:	Single

Education and working experiences:

09.1978 – 06.1982	Primary School, Tirana, Albania
09.1982 – 06.1986	Secondary School, Tirana, Albania
09.1986 – 06.1990	High School, Tirana, Albania
09.1990 – 06.1995	Diploma Chemistry
Thesis:	*Determination of heavy metals (Cu, Pb, Zn, Cd, Hg) using Anodic Stripping Voltametry (ASV)technique*
09.1995 – 10.1999	Working in Faculty of Natural Science (Department of Chemistry), Tirana University, Tirana, Albania
08.11.1999 – Now	Pursuing Ph.D. (Material Science) at Max-Planck-Institute for Metals Research affiliated to University of Stuttgart, Stuttgart, Germany.

Topic of Ph.D. Thesis*: “Characterization of the electronic conduction parameter of cation conducting solid electrolytes“*